Effects of the model-data integration on the carbon cycle simulation of terrestrial ecosystems

陸域生態系炭素循環におけるモデル―データ融合の効果

Ph.D Thesis

Masayuki Kondo

(近藤　雅征)

Graduate School of Agriculture

Hokkaido University

2015

Contents

List of Tables

List of Figures

Chapter 1

General Introduction

1.1. Terrestrial carbon cycle

Terrestrial carbon cycle is the biogeochemical process of which carbon is transported among reservoirs (i.e., atmosphere, vegetation, and soil) by a sequence of carbon uptake and release processes such as photosynthesis, respiration, decomposition, and fire emission. Understanding the mechanism of carbon cycle is important because of its close association with climate change (Joos et al., 2001; Houghton et al. 2001; Friedlingstein et al., 2006). In conjunction with raising atmospheric CO_2 concentration and temperature during the past decades, carbon cycle has a critical role of forming a feedback loop (Friedlingstein et al., 2006). There have been studies suggesting that terrestrial biosphere acts as a positive feedback to climate change in the 21st century; specifically, carbons are lost from the terrestrial biosphere to the atmosphere under global warming, leading to an increase of atmospheric CO_2 concentrations (Friedlingstein, et al., 2006; Sitch et al., 2008). However, this positive feedback under climate change accompanies large uncertainty, especially in estimates of future projection. For example, an increase in atmospheric CO_2 level by the end of 21st century largely varies from 20 to 200 ppm in estimates of eleven coupled climate-carbon cycle models, and the corresponding increase in temperature varies from 0.1 to 1.5 ˚C (Friedlingstein, et al., 2006; IPCC 2007). This large model uncertainty is still persistent in estimates reported in the most recent IPCC assessment report (IPCC AR5: IPCC 2013). Thus, the dynamics of terrestrial carbon cycle need to be evaluated further for better understanding of the future projection of climate change effect.

1.2. Carbon cycle modelling

Terrestrial carbon cycle has most frequently been analyzed with terrestrial ecosystem models, which simulate dynamics of carbon cycle (i.e., carbon fluxes in and out of reservoirs and carbon accumulations of reservoirs) by a prescribed climate and atmospheric CO_2 variability. Terrestrial ecosystem models proved effective in carbon cycle studies because of a wide range of applicability in temporal and spatial scales, supplementing limitations of direct observation techniques, e.g., eddy-covariance measurements are sparse and often short term, and remote sensing measurements provide only indirect proxy of carbon variables (Piao et al., 2013). During the past decades, a number of terrestrial ecosystem models were introduced for the purpose of studying aspects of terrestrial ecosystems, such as terrestrial carbon, nitrogen, and water cycles, and evaluated at various world's biomes with in-situ observations (e.g., Sitch et al., 2003; Krinner et al., 2005; Beer et al., 2006; Jung et al., 2007; Bonan et al., 2011; Keenan et al., 2012). At the same time, the research community has been mindful of agreement between performances of ecosystem model simulation. To date, a number of multi-model synthesis studies were conducted to understand the status of model performance (Pan et al., 1998; Cramer et al., 1999 and 2001; Schimel et al., 2000; Friedlingstein et al., 2006;). Yet, a common notion from these studies was that there were still variations in estimations of carbon flux among ecosystem models (Sitch et al., 2008; Schwalm et al., 2010; Huntzinger et al., 2012).

1.3. The role of model-data integration

The model-data integration is an effective approach for reducing uncertainties in carbon cycle simulation. This modelling scheme takes advantage of available observation data by integrating them to simulation processes with the aim of minimizing differences between simulations and observations. In the study of carbon cycle, the model-data integration has been

used in two different approaches: bottom-up and top-down approaches. The top-down approach integrates atmospheric CO_2 concentration measurements into forward simulation of an atmospheric transport model with the aim of estimating terrestrial carbon exchange that is optimally consistent with atmospheric CO_2 concentration (e.g., Taguchi, 1996; Chevallier et al., 2005; Peters et al., 2007; Maksyutov et al., 2008). The bottom-up approach seeks improvement of process-based ecosystem model simulation by integrating various ecological observations such as eddy covariance measurements of net ecosystem exchange (NEE), chamber-based measurements of soil respiration (SR), ancillary measurements of leaf area index (LAI), litterfall, and woody biomass and soil carbon increments (Raupach et al., 2005; Wang et al, 2009; Richarson et al., 2010; Keenan et al., 2011, 2012). While the top-down approach is confined with the improvement of net carbon exchange, the bottom-up approach allows to improve components of carbon cycle (i.e., photosynthetic and respiration processes, net productivity of vegetation, biomass accumulation, etc.) depending on observations used as constraints. Thus, various aspects of carbon cycle can be experimented with the bottom-up approach.

1.4. Objectives

This analysis takes advantage of the model-data integration to explore the current and future states of terrestrial carbon cycle. Specifically, the analysis is aimed at (1) identifying effects of data constraints (i.e., eddy flux and biometric observations) in estimates of a future projection of carbon cycle, (2) identifying behaviors of multiple carbon fluxes under anomalous climate conditions using multi-data integration, and (3) evaluating the current CO_2 budget by comparing estimates from the top-down and bottom-up data integration approaches. For these objectives, three studies were conducted as follows (Fig. 1.1).

First, using eddy covariance and biomass observations for constraints of the

model-data integration, reproducibility of carbon fluxes and woody biomass at four ecological research sites in East Asia was tested with a process model, Biome-BGC (Thornton et al., 2002). Furthermore, this study evaluated the impact of eddy covariance and biomass observations on the future projection of net carbon exchange using three different data integration schemes (i.e., integrations with eddy covariance data only, biomass data only, and both data).

Having tested the model-data integration with carbon flux and biomass, the second study experimented an extension of the model-data integration with multivariable such as GPP, foliage NPP, above-ground and below-ground woody NPPs, recruitment, mortality, and litterfall, observed at the Takayama research forest for eight consecutive years. In this application, multiple data constraints were designed to provide plausible annual variations of fine root production that is difficult to infer from observation. Using the estimated fine root production in conjunction with multiple observations of carbon fluxes, this study evaluated how components of forest production vary under contrasting anomalous climate years.

As an extension from site scale applications conducted in the first and second studies, the third study extended the application of the model-data integration to the global scale; specifically, global net carbon exchanges estimated by two data integration approaches (i.e., top-down and bottom-up approaches) were analyzed. Unlike the site scale studies, reliable global carbon flux estimation cannot be expected from a process-based ecosystem model even with the data integration because constrainable observation data have substantially limited global coverages. Instead, empirically upscale eddy flux observation was used as net carbon exchange estimation from the bottom-up approach. Using the two data integration approaches, this study examined the status of the current regional and global CO_2 budgets.

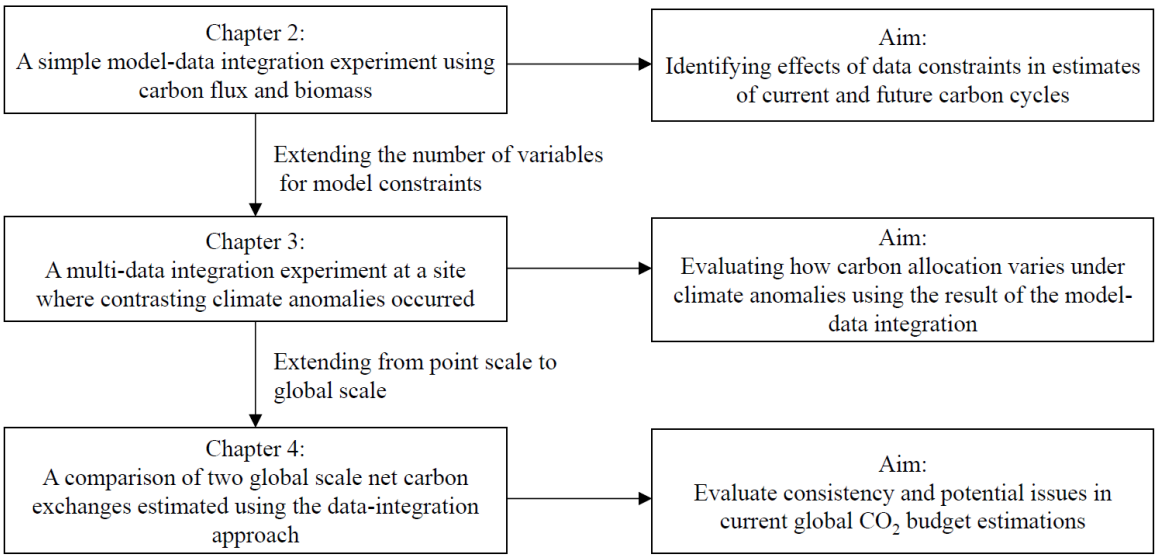

Figure 1.1. Short descriptions and aims of this study.

Chapter 2

The role of carbon flux and biometric observations in constraining a terrestrial ecosystem model: a case study in disturbed forests in East Asia

Abstract

This study demonstrates the importance of carbon flux and biometric observation in constraining a terrestrial ecosystem model with a simple optimization scheme. At the selected sites from AsiaFlux network, a simultaneous optimization scheme for both carbon flux and biomass was compared with carbon flux-oriented and biomass-oriented optimization schemes using the Biome-BGC model. The optimization scheme oriented to either carbon flux or biomass provided simulation results that were consistent with observations, but with reduced performance in unconstrained variables. The simultaneous optimization scheme yielded results that were consistent with observations for both carbon flux and biomass. Correspondingly, long-term projections simulated by three schemes showed a large difference. In the scheme oriented to carbon fluxes, misrepresented biomass caused a larger projection of carbon exchange than other two schemes. The scheme oriented to biomass yielded a projection of carbon exchange similar to the simultaneous scheme; however, projections of photosynthesis and ecosystem respiration were largely different from those of the simultaneous scheme. From these experiments, we found that (1) a process model like Biome-BGC is capable of reproducing both carbon flux and biomass within acceptable proximity, (2) constraining biomass is importance not just because it is one of carbon cycle components, but also it significantly affects future projections of carbon exchange. Thus, it is important to invest more efforts to improve simulation of biomass as well as carbon flux.

(Based on: Kondo M., Ichii K., Ueyama M., Hirata R., Mizoguchi Y., Saigusa N. (2013) Role of carbon flux and pool observations to constrain terrestrial ecosystem model: a case study in disturbed forests in East Asia. Ecological Research, 28(5), 893-905)

2.1. Introduction

Terrestrial ecosystem models (Cox et al. 2001; Thornton et al. 2002; Sitch et al. 2003; Ito 2008; Sato et al. 2007) have been major tools to predict the future terrestrial carbon budget. Although these models are designed in such a way to express the same eco-physiological aspects of nature, there are substantial uncertainties in their predictions due to differences in their approaches and assumptions (e.g., Friedlingstein et al. 2006; Ichii et al. 2010; Ise et al. 2010; Ito et al. 2010; Schwalm et al. 2010; Wang et al. 2011a, 2011b). For this reason, terrestrial ecosystem modeling is still considered as being in a developmental stage, and further studies are required to identify specific aspects for refinement or modification. With the current state of performance, it is often the case that models need to be calibrated by adjusting predefined parameters to achieve agreement with the observations (e.g., Chiesi et al. 2007; Ichii et al. 2010; Ueyama et al. 2010, 2011).

For a better estimation of the carbon cycle, model optimization techniques have been introduced and tested with terrestrial ecosystem models (Santaren et al. 2007; Wang et al. 2009; Mitchell et al. 2009, 2011). Although such techniques are powerful, when applied only to particular aspects of an ecosystem, the resulting model parameters may have inherent biases and may therefore not reflect the true characteristics of a study site. In practice, a number of model-based analyses have focused solely on terrestrial carbon flux and have often neglected carbon storage, such as forest biomass, implying that the resulting model parameters are inevitably oriented toward carbon flux. Even studies addressing disturbance events have often focused only on carbon flux and neglected forest regrowth (Thornton et al. 2002; Ito et al. 2005; Mitchell et al. 2009, 2011). Such approach is insufficient to fully reduce the uncertainties

about future terrestrial carbon cycle and climate change.

A potentially effective approach to resolve this issue is to establish an enhanced data-model fusion: a combination of biometric and micrometeorological observations and terrestrial ecosystem modeling with a disturbance scheme. This combination would help to establish more accurate terrestrial ecosystem modeling, thereby leading to a better estimation of the time evolution of biomass and carbon flux. Although attempts have been made to refine carbon flux and biomass simulations at specific observation sites (Law et al. 2001; Pietsch et al. 2005; Chiesi et al. 2011; Ueyama et al. 2011), a successful adaptation of an explicit and robust methodology has not yet been reported.

With a goal of more sophisticated ecosystem modeling, this study explores the potentiality of a terrestrial ecosystem model to reproduce both observed carbon flux and biomass. An experiment was performed with a widely used model, Biome-BGC (Thornton et al. 2002), the parameter sensitivity of which has been explored in detail by White et al. (2000), Tatarinov et al. (2009), Mitchell et al. (2009), and Mitchell et al. (2011). The methods applied are (1) iterative least square-based optimization for carbon flux and (2) biomass constraint using inventory data for the below- and above-ground biomass. In the experiment, results from the simultaneous optimization for carbon flux and biomass were examined with optimizations oriented toward either carbon fluxes or biomass. Additionally, we demonstrate how long-term simulations of carbon fluxes and biomass would differ if both carbon flux and biomass were not included in explicit optimization targets.

2.2. Materials and Methods

2.2.1. Terrestrial biosphere model: Biome-BGC

Biome-BGC is a prognostic terrestrial biogeochemical model driven by daily surface meteorological data (daytime, minimum, and maximum air temperatures, precipitation, vapor

pressure deficit (VPD), and shortwave radiation) and plant eco-physiological parameters for described vegetation types. The model is designed to simulate the carbon, nitrogen, and water cycles. The model includes the following compartments (1) four vegetation compartments - leaf, stem (live and dead), fine root, and coarse root (live and dead); (2) four litter compartments - labile, unshielded and shielded cellulose, and lignin; and (3) four soil compartments - fast, medium, and slow microbial and recalcitrant soil organic matter.

Carbon enters the system through the photosynthetic fixation of atmospheric carbon dioxide (CO_2), and the carbon fixed by photosynthesis can either be deposited as new growth in any plant tissue or respired and returned to the atmosphere. Nitrogen enters the system through the deposition of mineral nitrogen from the atmosphere into the soil. Soil mineral nitrogen can be incorporated into organic matter through the action of soil microorganisms. Nitrogen can be taken up by vegetation for incorporation into new tissues. It can be accumulated into soil by mineralization through litter and soil decompositions or it can be leached from the soil through outflow.

The photosynthetic mechanism is based on the Farquhar biochemical photosynthesis model (Farquhar et al. 1980). The gross primary productivity (GPP) is calculated as the sum of photosynthesis from leaves under the two types of light environment: illuminated and shaded. Autotrophic respiration (AR) is treated as the sum of maintenance and growth respiration: the former is driven by the nitrogen content in the living tissue, with a temperature dependency (Q_{10} model), and the latter depends on the predefined carbon allocation proportions allotted to the vegetation components. Heterotrophic respiration (HR) is driven by the nitrogen content in each litter and soil organic matter pool, with a rate constant and a product of two scalar potentials: the Lloyd-Taylor type temperature scalar potential (Lloyd and Taylor, 1994) and the Andren-Paustian type water scalar potential (Andren and Paustian, 1987). The total ecosystem respiration (RE), by definition, is the sum of AR and HR. The net primary productivity (NPP)

and the net ecosystem productivity (NEP) are calculated as the difference between GPP and AR, and GPP and RE, respectively. Biomass, litter, and soil carbon are treated as cumulative compartments of the leftovers from the daily allocated carbon and nitrogen transfer.

The “harvest and replanting” disturbance scheme introduced in Thornton et al. (2002) is adopted to construct a time series of the disturbance effects. In this process, a prescribed harvested fraction from the above-ground live and dead carbon and nitrogen pools are removed from the site. The same fraction from the leaf and fine root carbon and nitrogen pools and the below-ground live and dead carbon and nitrogen pools is transferred to the fine litter and coarse woody debris (CWD) pools, respectively.

2.2.2. Data

Among the eddy flux observation sites in the AsiaFlux network, the present analysis focused on four sites with well-known ecological histories. The study sites consisted of three from Japan, the Tomakomai flux research site (TMK), the Takayama deciduous broadleaf forest site (TKY), and the Fujiyoshida forest meteorology research site (FJY), and one from China, the Laoshan flux site (LSH). The locations and details for each site are provided in Figure 2.1 and Table 2.1, respectively.

The daily meteorological data for the model input were generated with NCEP (National Centers for Environmental Prediction)/NCAR (The National Center for Atmospheric Research) reanalysis (Kalnay et al. 1996), CRU-TS3.1 (Climate Research Unit - Time Series) (Mitchell and Jones, 2005), ISCCP-FD (International Satellite Cloud Climatology Project - Finite Differences) (Zhang et al. 2004), and tower meteorological observations. Each meteorological data was extracted from a grid corresponding to site location. The daily air temperature and VPD were generated by the merging of NCEP/NCAR reanalysis and CRU-TS3.1: the daily variations were based on NCEP/NCAR reanalysis data, and the monthly averages were adjusted to fit the

CRU TS3.1 data. The 1948 NCEP/NCAR reanalysis data were used for the period of 1901-1947 because NCEP/NCAR reanalysis data were not available for this period. The merged data were then linearly fitted by adding a location-specific constant such that the monthly mean was reasonably close to the tower meteorological observations. Precipitation and solar radiation data were similarly generated from the NCEP/NCAR reanalysis, CRU-TS3.1 precipitation data, ISCCP-FD solar radiation data, and site observations. The daily meteorological model input used in this study is the same as the one used in Ichii et al. (2013).

The temporal coverage of the eddy flux observations were 2001-2003 for TMK, 2001-2004 for TKY and FJY, and 2004 for LSH, and the methods of gap-filling and flux-partitioning are based on those of Ueyama et al. (2012). Although the input drivers were generated with the temporal coverage of 1901 to 2005 for each site, the initial year for simulation was set to the approximate year of forest establishment: 1901 for FJY, 1955 for TMK and TKY, and 1970 for LSH.

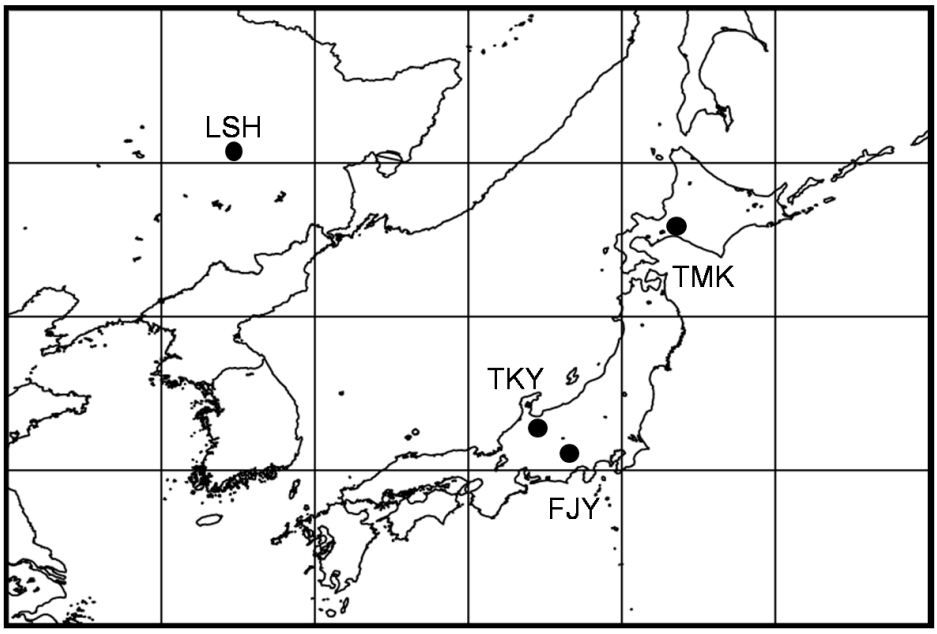

Figure 2.1. Locations of the four eddy flux observation sites used in this study.

2.2.3. Optimization of the Biome-BGC model

Biome-BGC requires a set of static eco-physiological parameters, including turnover fractions, carbon allocation proportions, and carbon-nitrogen ratios, and a combination of eco-physiological parameters define the vegetation type of the area for simulation. In the present study, type-specific average values from the literature (White et al. 2000) were used as the default parameter sets. For each study site, the vegetation type occupying the major fraction of the basal area was considered representative of the site, specifically, evergreen needleleaf forest parameters for FJY, deciduous broadleaf forest parameters for TKY, and deciduous needleleaf forest parameters for TMK and LSH. Other model parameters, such as parameters for the disturbance sub-model, the removed fraction and replanted biomass, were held constant at 95% and 10 gC m^{-2}, respectively. Based on these parameters, a disturbance effect was simulated in the approximate year of forest emergence (see Table 2.1).

Table 2.1. Descriptions of four eddy flux observation sites. *Abbreviations for vegetation classes: Evergreen Needleleaf Forest (ENF), Deciduous Broadleaf Forest (DBF), and Deciduous Needleleaf Forest (DNF).

	TMK	TKY	FJY	LSH
Site name	Tomakomai flux research site	Takayama deciduous broadleaf forest site	Fujiyoshida forest meteorology research site	Laoshan experiment site
Location	42º 44'N, 141º 31'E	36º 08'N, 137º 25'E	35º 27'N, 138º 46'E	45º 20'N, 127º 34'E
Vegetation class*	DNF	DBF	ENF	DNF
Dominant species	Larch (*Larix kaempferi*)	Birch (*Betula ermanii*) Oak (*Quercus crispula*)	Red Pine (*Pinus densiflora*)	Larch (*Larix gmelinii*)
Observation period	2001-2003	2001-2003	2001-2003	2004
Maximum LAI	5.6	3.5	5	2.5
Elevation (m)	140	1420	1030	370
Mean annual temperature (ºC)	6.0	7.0	10.0	5.0
Annual precipitation (mm)	1040	2030	2060	640
Stand age (years)	50	50	90	36
Biomass (kg C m^{-2})	Above: 3.3 Below: 0.9	Above: 6.1 Below: 1.5	Above: 8.9 Below: 3.4	Above: 6.9 Below: 2.1
References	Hirata et al. (2007), Yone et al. (2005)	Ohtsuka et al. (2009), Saigusa et al. (2002)	Mizoguchi et al. (2011), Tanabe et al. (2003)	Wang et al. (2005), Wang et al. (2008)

Using the eco-physiological parameters, optimization was conducted in four steps. (I) A parameter representing the stem-to-root carbon allocation proportion was constrained using the below to above-ground biomass ratio from the observations. (II) A parameter representing the leaf-to-stem allocation proportion was optimized with respect to the magnitude of the below- and above- ground biomasses. (III) Parameters having strong sensitivities to GPP were optimized with respect to eddy flux observation. (IV) When necessary, (II) and (III) were repeated until a balance between GPP and biomass was established. The following steps were performed at each site.

Step (I): The below- to above-ground biomass ratio from observation was used to fix the allocation proportion of coarse root carbon to stem carbon (CRC:SC). In Biome-BGC, bole and stem are treated as a single compartment, namely the stem carbon, and coarse roots are the dominant constituent of below-ground carbon (the contribution from fine root carbon is small). Thus, CRC:SC roughly corresponds to the below- to above-ground biomass ratio. The ratio calculated using the observed biomasses (Table 2.1) was used to constrain CRC:SC.

Step (II): Once the ratio was fixed, the magnitude of biomass was optimized using the allocation proportion of stem carbon to leaf carbon (SC:LC). Photosynthetically fixed carbon is transferred to stem carbon according to the proportion defined by SC:LC. This new stem carbon is then transferred to the coarse root carbon according to the proportion defined by CRC:SC (fixed in step (I)). Because the stem carbon and coarse root carbon essentially correspond to the above-ground and below-ground biomasses in Biome-BGC (the fine root

biomass is negligible), SC:LC is the primary parameter controlling the magnitude of biomass.

The optimization for biomass (step (II)) was conducted as follows. Simulations were iteratively performed with independently varying SC:LC values for the range of 10 to 200%, with 10% increments from the default values. At each end of the model run, the difference with respect to the observation (Δbiomass = |biomass$_{sim}$- biomass$_{obs}$|) was calculated, and the value of SC:LC corresponding to the minimum Δbiomass was stored as the optimized parameter.

Step (III): Using the sensitivity studies performed by White et al. (2000), Tatarinov et al. (2006), and Mitchell et al. (2009) as a guideline, the parameters known to be strongly sensitive to GPP were selected for optimization: they are the allocation proportion of new fine root carbon to new leaf carbon ratio (FRC:LC), the C:N ratio of leaves (C:N$_{leaf}$), C:N ratio of fine roots (C:N$_{fr}$), maximum stomatal conductance ($g_{s,max}$), and the proportion of leaf nitrogen content in Rubisco (PLNR). Other parameters were used for minor adjustments. Because of the high correlation between GPP and RE, optimization was performed only for GPP, and no explicit attempt was made to calibrate against RE. Because some of the parameters used for optimizing GPP also affect biomass production, particularly FRC:LC and PLNR, a final adjustment was necessary to preserve a balance between carbon flux and biomass (step (IV)).

Specifically, the optimization for GPP (step (III)) was performed by χ^2 minimization:

$$\chi^2 = \sum_{i=1}^{n} \frac{(X_{sim,i} - X_{obs,i})^2}{X_{sim,i}} \quad (1)$$

where X_{sim} and X_{obs} are the simulated and observed variables of the corresponding month and n is the number of months in the observation period, respectively. The minimization was conducted as follows: a simulation was performed independently for each selected parameter in the range of 10 – 200%, with 10% increments from the default value. At the end of each run, χ^2 of the simulated and observed GPP was calculated. This process was repeated for each sensitive parameter, and the value corresponding to the minimum χ^2 was stored as the optimized parameter. Throughout the optimization, adjustments were attempted to prevent exceeding the observation boundary, the maximum and minimum observed values listed in White et al. (2000).

2.2.4. Experiment

We evaluated the potential impact of constraining carbon flux and biomass in ecosystem modeling for two different durations. In short-term simulations, model results with three optimization schemes were compared with observations in order to evaluate the simultaneous reproducibility of constraining both carbon flux and biomass. Along with the optimized eco-physiological parameter set (OPT), which was prepared as described in Section 2.2.3, simulation was performed with the biomass-constrained parameter set (BMC) and the flux-oriented parameter set (FOPT). In the BMC scheme, only the biomass constraint was applied, and others were left unchanged from the default set. Therefore, this scheme represents steps (I) and (II) in the OPT scheme. In the FOPT scheme, only the carbon flux optimization was applied, which is step (III) in OPT; the allocation proportion parameters used for the biomass constraint in OPT were used for the adjustments of GPP.

To clarify the differences between the three schemes, long-term carbon flux and biomass were additionally simulated by each optimized model. For the long-term simulations,

the meteorological data were prepared by appending the original meteorological forcing data (as prepared in 2.2.2) repeatedly for 300 years. Driven by the extended climate data, projections of cumulative GPP, NPP, NEP, and biomass were simulated to examine how absorbed carbon was partitioned after disturbance events.

2.3. Results

2.3.1. Monthly variations in GPP and RE and annual biomass

Overall, GPP and RE simulated by OPT were reasonably consistent with the observations: seasonal variations of both GPP and RE were consistent overall (Fig. 2.2) and χ^2 was less than 20 gC m^{-2} day^{-1} at all sites (Table 2.2). As consequence, seasonal variations of NEP estimated by OPT was relatively in good agreement with the observations. The simulated biomass (Fig. 2.3a) and below- to above-ground ratio (Fig. 2.3b) coincided with the observations with close proximity, yielding less than 3% difference with respect to the inventories (Table 2.2).

For FOPT, there were no substantial differences in the seasonality and magnitude of GPP, RE, and NEP compared with the result of OPT (Fig. 2.2), as also indicated by the χ^2 values (Table 2.2). However, FOPT yielded a drastic deviation in the estimates of biomass compared with the observations: differences in the total biomass were 260% at TMK, 274% at TKY, 81% at FJY, and 142% at LSH (Fig. 2.3a and Table 2.2). In particular, differences of more than 250% in TMK and TKY were notable.

The total biomass simulated with BMC exhibited a pattern similar to OPT, yielding less than 6% difference with respect to the inventories (Table 2.2); however, GPP and RE resulted in considerable inconsistencies: an underestimation of the growing season GPP and RE (4 – 8 gC m^{-2} day^{-1}) at TMK and LSH, an underestimation of the growing season GPP (2 – 4 gC m^{-2} day^{-1}) at TKY, and an overestimation of the winter season GPP (approximately 2 gC m^{-2} day^{-1})

and growing season RE (4 – 6 gC m^{-2} day^{-1}) at FJY (Fig. 2.2). Despite the inferior performance on GPP and RE, seasonal variations of NEP by BMC showed no significant difference with respect to those by OPT and FOPT. In fact, the χ^2 values indicated that BMC yielded the best statistic for NEP in TMK and TKY sites among the three schemes (Table 2.2).

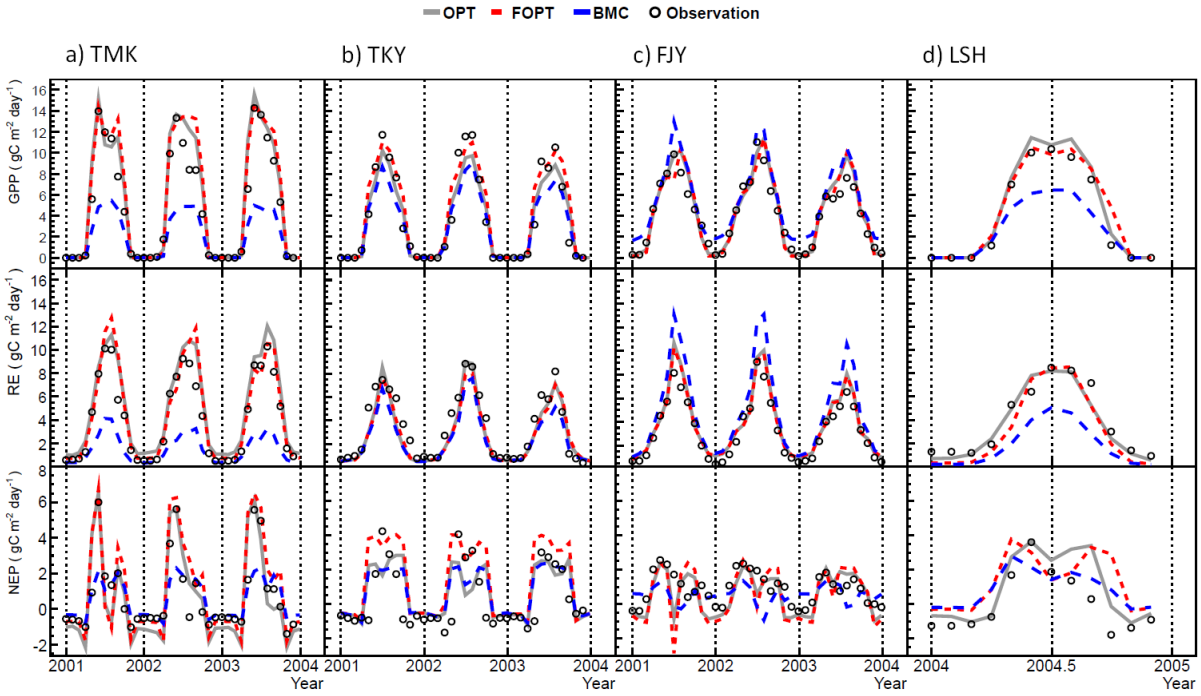

Figure 2.2. Seasonal variations of modeled and observed GPP, RE, and NEP at four eddy flux sites. The results of the three different optimization schemes are shown in different line colors: optimization to both carbon flux and biomass (OPT) (gray) and optimization only to carbon flux (FOPT) (red) and only to biomass (BMC) (blue). The observations are plotted with open circles.

Site		TMK			TKY			FJY			LSH		
Optimization scheme		OPT	FOPT	BMC	OPT	FOPT	BMC	OPT	FOPT	BMC	OPT	FOPT	BMC
GPP (gC m^{-2} day^{-1})	χ^2	12.1	13.8	164.9	16.5	16.9	21.4	11.4	13.4	18.6	1.3	3.4	10.1
RE (gC m^{-2} day^{-1})	χ^2	10.7	7.5	180.1	16.6	15.6	26.4	5.8	5.7	20.7	2.5	15.6	47.6
NEP (gC m^{-2} day^{-1})	χ^2	53.3	51.1	35.3	51.7	99.8	37.9	41.6	68.2	151.9	25.1	27.5	37.0
Biomass (Simulation/Inventory)	Above	0.97	2.42	0.99	0.99	2.78	0.98	0.98	0.82	0.99	0.98	1.43	0.95
	Below	0.98	3.28	0.99	0.99	2.57	0.97	1.02	0.78	0.99	0.99	1.4	0.99
	Total	0.97	2.60	0.99	0.99	2.74	0.97	0.99	0.81	0.99	0.98	1.42	0.96

Table 2.2. χ^2 of simulated fluxes with respect to the observations (GPP, RE, and NEP) and fractions of simulated biomass with respect to the inventories.

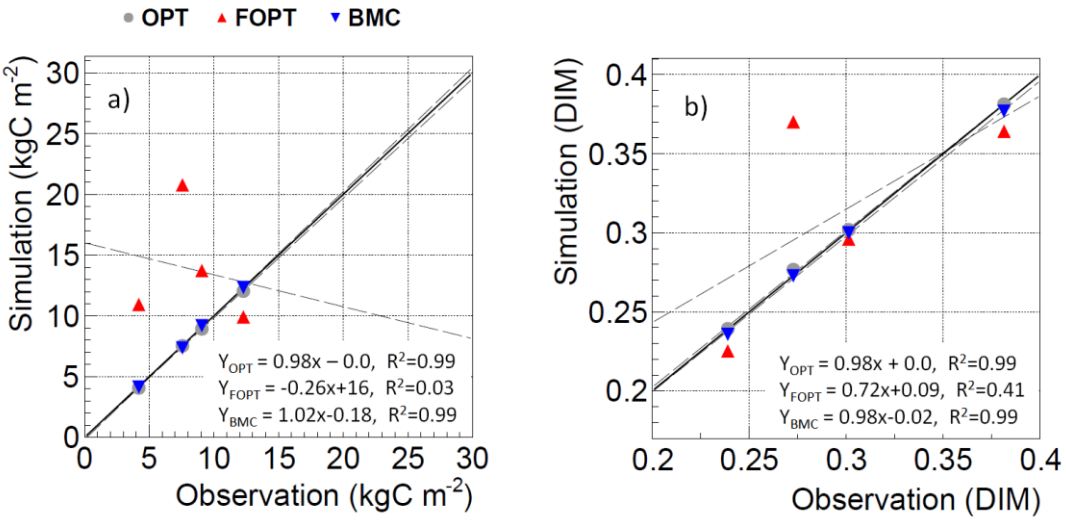

Figure 2.3. Scatter plots of (a) the modeled and observed total biomasses and (b) below- to above-ground biomass ratio. For each site, the inventory data were compared with the model outputs. For simplicity, it was assumed that the ecosystem in each study site possessed the observed biomasses in the first year of flux observation (2001 for TMK, TKY, and FJY and 2004 for LSH). The model results are shown for three different optimization schemes, OPT, FOPT, and BMC.

2.3.2. The long-term projections of carbon partition

Differences among the three schemes became clearer when assessing their long-term projections of carbon partition (cumulative carbon fluxes: ∑GPP, ∑NPP, and ∑NEP and biomass), with the difference most notably exhibited at the TMK site (Fig. 2.4). OPT and FOPT showed a similar pattern of ∑GPP and ∑NPP trajectories, consequently yielding a similar pattern of ∑AR (a difference between ∑GPP and ∑NPP) over 300 years. However, these two schemes remarkably differ in the trajectories of biomass and ∑NEP. Compared to OPT, FOPT yielded four-fold greater biomass over 300 years (Table 2.3), and this difference in biomass directly affected their estimates of heterotrophic respiration ∑HR (a difference between ∑NPP and ∑NEP) through litterfall. As a result, the difference in biomass led to a large offset in ∑NEP between two schemes: 11 kgC m^{-2} for OPT and 39 kgC m^{-2} for FOPT.

OPT and BMC showed a similar pattern of ∑NEP and biomass trajectories, yielding differences in the 300-year cumulative values of less than 2 kgC m^{-2} for both ∑NEP and biomass. However, compared with OPT, ∑GPP was substantially underestimated with BMC by

more than three-fold, and this offset consequently led to a large deviation of ∑HR between the two schemes. This result indicates that the seemingly consistent ∑NEP of the two schemes was actually misleading; a difference between ∑GPP and ∑RE was similar, but their magnitudes were significantly different. In addition to TMK, the other sites exhibited similar patterns of carbon partition among the three schemes (Table 2.3).

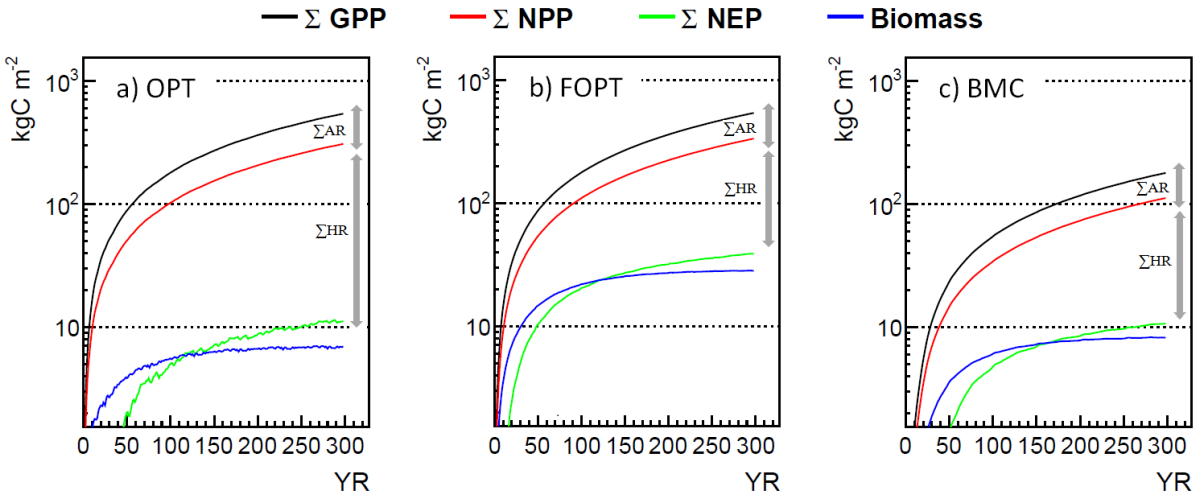

Figure 2.4 Carbon partition plots for simulation with three optimization schemes at the TMK site: (a) OPT, (b) FOPT, and (c) BMC. The cumulative GPP, NPP, NEP, and biomass are shown. The offsets between the cumulative GPP and NPP and cumulative NPP and NEP indicate the cumulative AR and HR, respectively. All the cumulative components were normalized such that the initial points start from zero; thus, the figures represent the carbon partitioning after the occurrence of disturbance events.

Table 2.3. The cumulative fluxes and biomass over 300 years. Results are shown for each optimization scheme and site.

Site	TMK			TKY			FJY			LSH		
Optimization scheme	OPT	FOPT	BMC	OPT	FOPT	BMC	OPT	FOPT	BMC	OPT	FOPT	BMC
∑GPP (kgC m^{-2})	540	539	178	426	417	574	425	451	412	411	401	451
∑NPP (kgC m^{-2})	317	334	112	215	223	307	225	243	142	225	215	237
∑NEP (kgC m^{-2})	11	39	11	18	32	19	22	33	19	28	53	29
BM (kgC m^{-2})	7	28	8	12	24	12	18	27	15	18	33	17

2.4. Discussion

2.4.1. Misleading NEP results

Constraining biomass implies containing net carbon accumulation for woody

components; therefore, it indirectly constrains a proportion of NEP. From this study, we identified that the BMC scheme yielded good performance for NEP with respect to the observations, particularly, it showed the best result with for TMK and TKY among the three schemes (Table 2.2). However this seemingly agreement in NEP is misleading because, even with visual inspection, it is obvious that GPP and RE were most inferiorly simulated with BMC (Figs. 2.2). The apparent consistency in the BMC results is caused because NEP is simply the difference between GPP and RE, and its variation is typically quite smaller than that of GPP and RE. Thus, if both GPP and RE deviated from the observations by the same magnitude and seasonal pattern, the resulting modeled NEP could become similar to the observed NEP. A similar results is indicated in the long-term simulation (Fig. 2.4), OPT and BMC showed good agreement for projections of both biomass and ∑NEP. However, there were substantial differences in the projections of ∑GPP and ∑RE between the two schemes.

This apparent agreement in NEP indicates that an optimization conducted only with biomass is not sufficiently to constrain carbon cycle; rather, it should be applied to GPP or RE as well. The previous model-optimization studies considered only NEP in attempts of carbon flux refinement (Williams et al. 2005; Mitchell et al. 2009; Richardson et al. 2010). The reason for disregarding GPP and RE in their optimizations may be that they were particular about confining the models with the direct observations. NEP (more precisely, net ecosystem exchange: NEE) is directly observed by eddy covariance measurements, and GPP and RE are estimated from the observed NEP (Hirata et al. 2008). However, in the carbon cycle, GPP and RE are true physiological quantities representing photosynthesis and respiration, and NEP is merely a byproduct of these processes. Because a major purpose of the current process-based ecosystem models is to clarify the mechanism of the carbon cycle, it is important to invest more effort to refine GPP and RE. Otherwise, the apparent agreement of NEP, such as in the case of BMC, may cause a misleading interpretation of the model results.

2.4.2. The role of biomass observation in constraining carbon flux

Despite good agreement in monthly variations of carbon fluxes (GPP, RE, and NEP) was identified in the OPT and FOPT schemes during the observed period (Figs. 2.2), the long-term projections of carbon fluxes and biomass were largely different between the two schemes (Fig. 2.4). It is notable that ∑NEPs of OPT and FOPT significantly deviated from each other in the long-term projections. As indicated by the carbon partitioning, these different patterns of ∑NEP projections are the consequence of biomass simulations. Although ∑GPPs of both OPT and FOPT showed similar projections, a substantial offset in their biomass directly affected the projections of ∑RE and ∑HR. Thus, when one attempts to reproduce carbon flux, not only carbon fluxes should invest effort to constrain biomass as well. In fact, biomass constraint should be regarded as a first priority for carbon budget estimation (as it was in this study), otherwise the respiration components would inevitably deviate by a similar amount of deviation in the biomass projection.

Accessibility to biometric observations is the key for the further improvement of carbon flux and biomass simulations. As demonstrated in this study, even a single-year biometric observation can improve simulation of biomass if an approximate stand age is known. Multi-year observations are beneficial, but they are not absolute requirements because annual biomass growth increments are usually small (Ohtsuka et al. 2009). Rather, multi-site single year observations are more useful for the improvement of model simulation. Also, it is desirable to have consistency between biometric and eddy flux measurements. Even within the same research site, not every biometric observation research aims to contribute to carbon cycle research. So it is not always the case that biometric measurements are conducted in the vicinity of an eddy covariance tower. In that case, an ecosystem represented by biometric observation and an eddy flux tower may differ.

2.5. Conclusions

In this analysis, the simultaneous applicability of biomass constraint and carbon flux optimization was tested with the Biome-BGC model using data from four eddy covariance observation sites in East Asia. A comparison of the optimization schemes OPT, FOPT, and BMC revealed that Biome-BGC is capable of reproducing both carbon flux and biomass within a reasonable accuracy.

The biometric observation was the key to predict long-term projections of carbon flux and biomass. Because both the OPT and FOPT schemes explicitly targeted carbon flux, it was expected that GPP and RE would exhibit similar patterns in both schemes; however, their differences in biomass clearly affected carbon flux via respiration. Thus, we emphasize that modelers should avoid partial tuning as much as possible when biometric data are accessible or when they can be reasonably estimated.

The availability of biometric observations is a critical factor in confining and reducing unnecessary freedom in ecosystem model simulations. Estimates from ecosystem models often deviate from the observations with the default parameter set. This undesirable model behavior can be refined by constraints with biometric data. Thus, we encourage active collaboration between modelers and field ecologists toward a better understanding of terrestrial ecosystems.

Chapter 3

Impact of anomalous climates on carbon allocation to biomass production of leaves, woody components, and fine roots in a cool-temperate deciduous forest

Abstract

We investigated carbon allocation in a cool-temperate forest in central Japan in years of contrasting climate anomalies: an early spring warming induced by the El Niño Southern Oscillation (ENSO) in 2002 and a low summer photosynthetic photon flux density (PPFD) induced by a stationary rain front in 2003. Observations of eddy flux, biometric variables, and chamber measurements from 1999 to 2006 and interannual variations in fine root net primary production (frNPP) were analyzed in conjunction with a terrestrial biosphere model simulation with multiple biometric constraints. Compared to the annual means (excluding 2002 and 2003), the low summer PPFD in 2003 reduced the annual gross primary productivity (GPP: -6%), soil respiration (SR: -11%), and ecosystem respiration (RE: -5%). Under the low summer PPFD, CO_2 fluxes commonly decreased but components of the NPP were not affected. The low variation in NPP is explained by previous findings that NPP is more sensitive to climate conditions before or during the early stage of the growing season. The early spring warming in 2002 increased the GPP (8%) and woody tissue NPP (wNPP: 55%) and decreased the frNPP (-33%) and SR (-6%). Although early spring warming prolonged the growing season, the foliage NPP (fNPP) and litterfall were invariant. The increase in wNPP and the decrease in frNPP imply that the forest decreased frNPP in favor of wNPP under the high spring temperature. Although the frNPP was estimated by model-data integration, we argue that the decrease in frNPP is plausible because the decrease in SR cannot be explained without the

contribution from fine root respiration. These results suggest that increasing or decreasing patterns of component fluxes cannot necessarily be inferred from the GPP. Factors such as the nature and duration of climate anomalies and allocation shift between components of the NPP may need to be considered when characterizing carbon allocation under anomalous climate events.

(Based on: Kondo M., Ichii K., Ueyama M. (2014) Impact of anomalous climates on carbon allocation to biomass production of leaves, woody components, and fine roots in a cool-temperate deciduous forest, Agricultural and Forest Meteorology, 201, 38-50, doi:10.1016/j.agrformet.2014.11.005)

3.1. Introduction

Carbon allocation plays a key role in the dynamics of the terrestrial carbon cycle. It influences carbon flux, standing biomass production, and soil carbon accumulation by controlling the investments of photosynthate into leaves, woody organs, and fine roots (Friedlingstein et al., 1999). In general, forests allocate photosynthates to maximize plant growth and minimize limitations by adjusting the balance between aboveground and belowground resource supplies (Enquist and Niklas, 2001). For example, nitrogen fertilization experiments have shown that an alleviation of nutrient limitations induced an allocation shift from the belowground to aboveground components (Gower et al., 1992; Haynes and Gower, 1995; Maier and Kress, 2000; Giardina et al., 2003; Janssens et al., 2010). Several studies have reported that carbon allocation changes with stand age (e.g., competition for light resources promotes aboveground production in young stands; Davidson et al., 2002; Ryan et al., 2004), whereas belowground resource limitation overwhelms the light limitation in older stands (Chapin et al., 2002). These studies have confirmed that changes in environmental conditions are a key factor for understanding the mechanisms underlying carbon allocation.

Anomalous climate events may be useful for investigating the mechanism of carbon allocation because they abruptly change the environmental conditions in forest ecosystems. The frequency of anomalous climate events has been increasing in recent decades (e.g., Alexander et al., 2006; Huntington, 2006; Min et al., 2010). In particular, the intense and persistent El Niño events that occurred during the 1980s and 1990s (e.g., 1982–1983, 1987–1988, and 1997–1998) influenced the carbon cycle of forest ecosystems. For example, the El Niño event in 1998 induced above-average temperatures in the spring across the Canadian inland and western coast. In response to this high temperature anomaly, a high anomalous carbon sequestration (net ecosystem production; NEP) was observed in a boreal deciduous forest in Saskatchewan (Black et al., 2000) and in secondary Douglas fir stands on Vancouver Island (Morgenstern et al., 2004). Although in numerous studies the forest response to anomalous climates has been investigated as a factor of changes in vegetation indexes, photosynthesis (gross primary productivity; GPP), and carbon sequestration (e.g., Asner et al., 2000; Black et al., 2000; Foley et al., 2002; Nemani et al., 2003; Morgenstern et al., 2004; Saigusa et al., 2010), our understanding of the climate control of carbon allocation remains limited. Potential changes in the carbon allocation associated with climate anomalies may alter woody biomass and forest soil carbon accumulation, and in turn influence the subsequent overall carbon emission and feedback to climate change.

This study investigated the impact of anomalous climates on the carbon allocation of a cool-temperate forest in the Takayama Forest Research Site, Japan. Multi-year biometric observations are available for the majority of the Takayama site's carbon cycle components, such as woody tissue net primary productivity (wNPP), foliage NPP (fNPP), aboveground and belowground woody biomass, litterfall, recruitment, and mortality, with the exception of fine root NPP (frNPP). One year data of frNPP were compensated by estimates from a model-data integration technique, in which a process-based biosphere model is combined with multi-year

biometric observations to inversely estimate the plausible carbon allocation to fine roots. The availability of observed carbon cycle components (GPP, fNPP, wNPP, and litterfall) constrains unnecessary freedom in the simulation of frNPP; thus, a reliable estimate of frNPP is expected.

The goal of the current study was to evaluate the sensitivity of allocation patterns to interannual climate variability using observations-constrained modelling. Specifically, we evaluated the allocation pattern in years of contrasting climate anomalies: the early spring warming induced by El Niño in 2002 and the mid-summer low photosynthetic photon flux density (PPFD) in 2003. By analyzing the carbon allocations in 2002 and 2003, we characterized how carbon allocation is affected by contrasting anomalous climates.

3.2. Materials and Methods

3.2.1. Study site

This study was conducted in the Takayama Forest Research Site, which is located in a mountainous region in the central part of the main island of Japan (36° 08′ N, 137° 25′ E, 1,420 m above sea level). The site is characterized by a cool-temperate climate, with a mean annual temperature and annual precipitation of 7.2°C and 2275 mm, respectively.

Deciduous broadleaf trees dominate the forest (*Quercus crispula*, *Betula ermanii*, and *Betula platyphylla* var. japonica), occupying 66.1% of the basal area; the forest floor is covered by evergreen dwarf bamboo (*Sasa senanensis*). The forest is a secondary forest and is approximately 50 years old (Saigusa et al., 2002). The growing season leaf area index (LAI) is approximately 5 m^2 m^{-2} for canopy trees and 2 m^2 m^{-2} for understory species (Nasahara et al., 2008). The typical tree height is approximately 20 m (Ohtsuka et al., 2005). The soil type is a dystric cambisol with a thick organic layer containing considerable organic carbon (318 MgC ha^{-1}; Jia and Akiyama, 2005).

Eddy fluxes have been measured since the summer of 1997. Beneath the eddy

covariance tower, a permanent 100 m × 100 m study plot was established to monitor tree growth by measuring biometric variables, including NPP (foliage, wood, and the understory Sasa), woody biomass (aboveground and belowground), stem mortality, and recruitment (Ohtsuka et al., 2007, 2009). frNPP was measured for one year from June 2000 to June 2001 using the minirhizotron method, in which fine roots in the soil-minirhizotron tube boundary layer are observed with a charge-coupled device camera (Satomura et al., 2006). Diurnal and seasonal changes in SR were measured continuously for 24–48 hours once or twice a month by the open-flow infrared gas analyzer method using four chambers near the flux tower (Mo et al., 2005).

The years 2002 and 2003 were characterized by contrasting climate anomalies. In 2002, the Takayama site was under the influence of an El Niño event that induced an early spring warming, early foliation, and an anomalously long growing season (Saigusa et al., 2005). Because of the high temperature anomaly in the spring (Fig. 3.1a), NEP in 2002 began to increase earlier (DOY 130–140) than in other years (approximately DOY 150) (Saigusa et al., 2005). In the summer of 2003, the Takayama site experienced an unusually long rainy season (accompanied by high precipitation; Fig. 3.1b) induced by a stationary rain front (Saigusa et al., 2010). As a consequence, PPFD was substantially lower during the summer in 2003 than in other years (Fig. 3.1c). The monthly PPFD in July was 32% lower in 2003 than in previous years, which caused a 26% lower GPP in July 2003 compared to previous years (Saigusa et al., 2010). In the period 1999–2006, the mean annual NEP was the highest in 2002 (0.75 MgC ha^{-1} yr^{-1}) and the lowest in 2003 (-0.37 MgC ha^{-1} yr^{-1}).

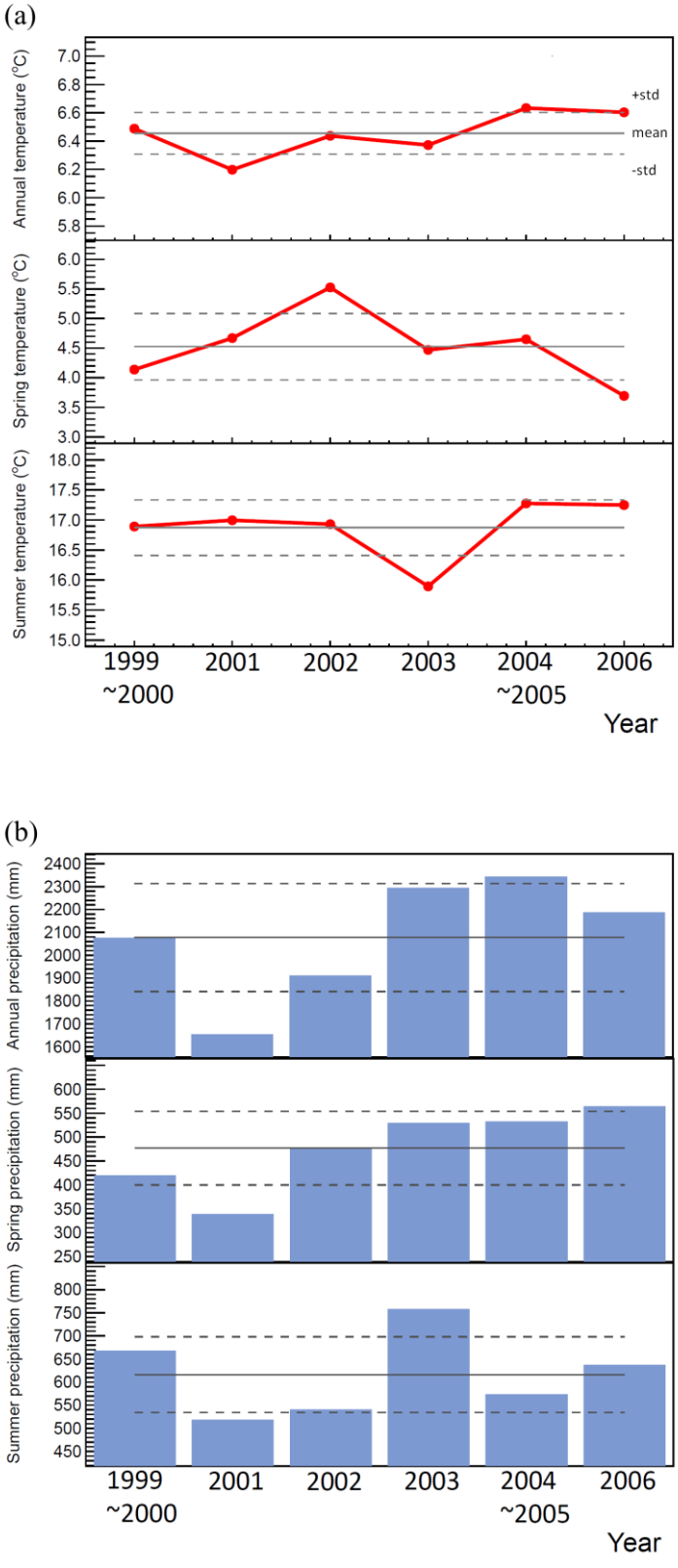

Figure 3.1. Interannual variations in the annual, spring (March–May), and summer (June–August) (a) temperature (°C), (b) precipitation amount (mm), and (c) PPFD (W m^{-2}) observed from 1999 to 2006 at the Takayama site. Temporal coverage was set to the same as that of inventory measurements from Ohtsuka et al., (2009).

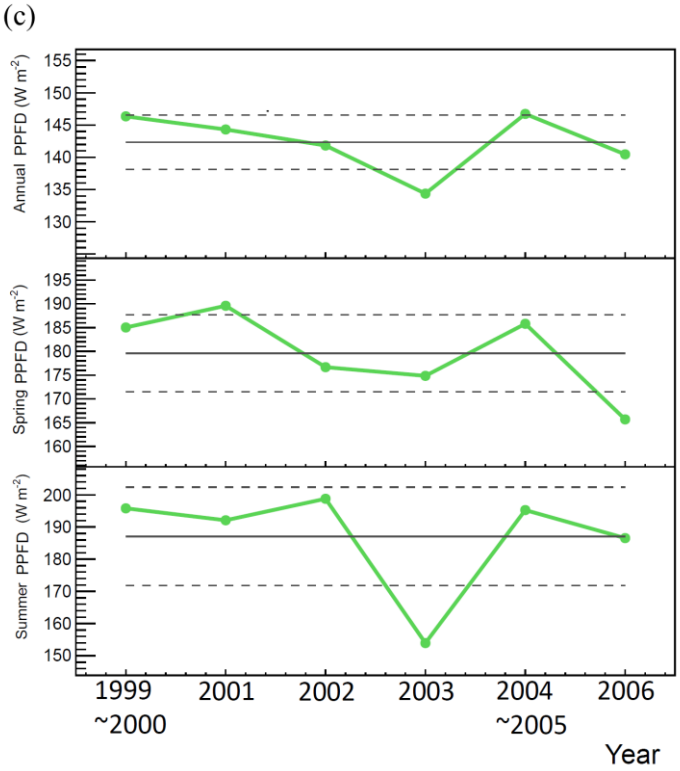

Figure 3.1. continued

3.2.2. Terrestrial Biosphere Model: Biome-BGC

The present study employed a prognostic terrestrial biosphere mode, the Biome-BGC model (Thornton et al., 2002). In this model, biomass, litter, and soil carbon were treated as cumulative compartments from the daily carbon transfer allocated by the following predefined allocation parameters: allocation proportion of stem carbon to leaf carbon (StemC:LeafC), fine root carbon to leaf carbon (FrootC:LeafC), coarse root carbon to stem carbon (CrootC:StemC), and live-wood carbon to total wood carbon (LivewoodC:TotalwoodC). StemC:LeafC, FrootC:LeafC, and CrootC:StemC determine the partitioning of NPP into the leaf, stem, coarse root, and fine root. StemC:LeafC is the primary controlling parameter for the amount of carbon sequestration into the stem carbon. Similarly, FrootC:LeafC controls the amount of carbon sequestration into fine roots. CrootC:StemC determines a proportion of stem carbon allocated to

the coarse roots. LivewoodC:TotalwoodC controls a fraction of the live-wood production with respect to the total wood carbon (sum of the live-wood and dead-wood carbon); thus, LivewoodC:TotalwoodC indirectly controls the annual rate at which live-wood mass converts to necromass. Sequestered carbon in the leaf, fine root, and woody components is removed by the annual leaf-fine root turnover rate (fixed to 1 yr^{-1} for deciduous forests) and live-wood turnover rate. In addition to turnover rates, the litterfall rate of woody components is controlled by the whole-plant mortality rate. The description of the photosynthetic and respiration mechanisms is provided in section 2.2.1.

3.2.3. Model setup

The Biome-BGC model requires the following set of predefined parameters: (1) site information, including latitude, elevation, soil texture, and effective soil depth, and (2) static eco-physiological parameters. A combination of eco-physiological parameters defines the vegetation type in a subject area. In this study, the literature-based parameter set for deciduous broadleaf forests (White et al., 2000) was used as default eco-physiological parameters.

The forest is approximately 50 years old. Therefore, the simulation was conducted for the 1960–2010 period after a maximum of 3000 spinup years, during which the model was run repeatedly until the soil carbon reached equilibrium. At the beginning of the simulation, a disturbance scheme introduced by Thornton et al. (2002) was applied to construct a time series of forest regrowth. In this process, a prescribed harvested fraction from the aboveground live and dead carbon and nitrogen pools was removed from the site. The same fraction from the leaf and fine root carbon and nitrogen pools and belowground live and dead carbon and nitrogen pools was transferred to the fine litter and coarse woody debris pools, respectively. The removed fraction and replanted biomass were set to 95% and 10 gC m^{-2}, respectively.

The meteorological data for the model input were based on Ichii et al. (2013), i.e., the data from the NCEP/NCAR Reanalysis (Kalnay et al., 1996), CRU TS 3.1 (Harris et al., 2014), and tower meteorological observations were merged. The air temperature and vapor pressure deficit (VPD) at were calculated for the period from 1901 to 2010 by merging the NCEP/NCAR reanalysis and CRU TS 3.1 data and calibrating the results with the tower meteorological observations. Precipitation and solar radiation data were similarly generated from CRU TS 3.1 precipitation data and ISCCP-FD solar radiation data (Zhang et al., 2004), respectively.

3.2.4. Model-data integration

The purpose of the current study was to fully evaluate allocation responses to contrasting anomalous climates. For this purpose, a plausible simulation result for fine root allocation is required because frNPP is a major fraction of the total NPP (Jackson et al., 1997). The default model simulation reflects climatic and site information. However, it is not sufficient to yield plausible results for fine roots because there are several degrees of freedom in the model simulation (i.e., parameters and carbon pools). To refine the simulation, we applied a model-data integration technique in which unnecessary freedom in the model simulation was constrained using observed quantities.

We calculated the frNPP using the Biome-BGC model with multiple constraints from biometric observations based on Kondo et al. (2013). Considering partitioning of assimilated carbon (GPP) to different fractions (Fig. 3.2), carbon components and routes were constrained with observations at the Takayama site, except for FrootC:LeafC. Specifically, the input (GPP), production of woody tissues (aboveground and belowground wNPP), intermediate routes (allocation proportions), and outputs (fine root and live-wood turnovers and mortality) were subjected to constraints.

Model-data integration was conducted on an annual basis and individually for each

period of biometric measurements (1999–2000, 2001, 2002, 2003, 2004–2005, and 2006), which were set to be equal to the biometric measurement periods from Ohtsuka et al., (2009). Each set of biometric observations was conducted for a designated period (Table 3.1). For each period of biometric measurements, frNPP was estimated according to the steps described below.

Table 3.1. Carbon dynamics at the Takayama site for eight consecutive years from 1999 to 2006 based on observation data from Ohtsuka et al. (2007; 2009). *Since litterfall measurements are available only for the 1999–2003 period (Ohtsuka et al., 2007), an average for the 1999–2003 period is used for values of 2004–2006.

	1999-2000	2001	2002	2003	2004-2005	2006
NPP (MgC ha^{-1} yr^{-1})						
Foliage NPP	1.66	1.94	1.92	1.92	2.03	1.69
Woody tissue NPP	0.88	1.38	1.96	1.22	1.32	1.47
Aboveground	0.73	1.15	1.64	1.02	1.10	1.23
Belowground	0.15	0.23	0.33	0.2	0.22	0.25
Biomass (MgC ha^{-1})						
Aboveground	61.0	61.1	60.8	62.0	62.0	63.0
Belowground	14.7	14.6	14.4	14.7	14.6	14.7
Litterfall (MgC ha^{-1} yr^{-1})						
Foliage	1.65	1.92	1.90	1.91	1.85*	1.85*
Coarse root	0.21	0.67	0.58	0.70	0.54*	0.54*
Soil respiration (MgC ha^{-1} yr^{-1})	7.34	7.40	6.94	6.56	--	--
Mortality (yr^{-1})	0.023	0.045	0.012	0.039	0.016	0.021
Recruitment (yr^{-1})	0.004	0.003	0.003	0.004	0.002	0.001

Step 1: Setting of the model parameters using biometric observations

StemC:LeafC, CrootC:StemC, LivewoodC:TotalwoodC, and the whole-plant mortality were set by ratios of observed aboveground wNPP and fNPP, observed belowground and aboveground wNPP, observed recruitment and mortality, and observed litterfall and aboveground biomass, respectively (Table 3.1).

We set the value for the live-wood turnover rate to 0.7 yr^{-1}. The conventional definition of the live-wood turnover rate (the average of tree mortality and recruitment rates) does not

apply to Biome-BGC because the live-wood pool in Biome-BGC is conceptually based on cambium. Because cambium is replaced on an annual basis, the turnover rate should be set to 1.0 yr^{-1}. White et al. (2000) proposed a value for the live-wood turnover rate of 0.7 yr^{-1} because the living and respiring portion of the sapwood originates from cambium. Therefore, some of the live-wood must be retained; hence, 0.7 yr^{-1} was used for the live-wood turnover rate instead of 1.0 yr^{-1}.

The resulting values of StemC:LeafC, CrootC:StemC, LivewoodC:TotalwoodC, whole-plant mortality, and live-wood turnover rate for each period of biometric measurements are listed in Table 3.2.

Table 3.2. Model parameters and their values estimated by biometric observations from Ohtsuka et al. (2007; 2009) and by optimization.

Eco-physiological parameter	Unit	1999-2000	2001	2002	2003	2004-2005	2006
Observation based							
Whole plant mortality rate	yr^{-1}	0.003	0.01	0.011	0.011	0.011	0.011
Live-wood turnover rate	yr^{-1}	0.70	0.70	0.70	0.70	0.70	0.70
StemC:LeafC	gC gC^{-1}	0.43	0.59	0.85	0.53	0.54	0.72
CrootC:StemC	gC gC^{-1}	0.21	0.22	0.20	0.20	0.20	0.20
LivewoodC:TotalwoodC	gC gC^{-1}	0.17	0.07	0.29	0.11	0.11	0.05
Optimization based							
FrootC:LeafC	gC gC^{-1}	1.24	1.16	0.78	1.24	1.2	1.15

Step 2: Determination of FrootC:LeafC

Having set the parameters from step 1, we determined the FrootC:LeafC value that produces the smallest difference between the observed and simulated GPP and wNPP (a sum of aboveground and belowground wNPP). To identify the optimal value, FrootC:LeafC was set to vary in the range of 1% to 200% with 1% increments from the default values (1.0 gC gC^{-1}).

Among simulation results with varying FrootC:LeafC, the FrootC:LeafC value that yielded the smallest differences with respect to both the observed GPP and wNPP ($\Delta_{minimum}$ = {Δ_{GPP}, Δ_{wNPP}}$_{minimum}$) was identified (Table 3.2). Δ is expressed as

$$\Delta = \frac{(obs - sim)^2}{obs} \qquad (1)$$

Eighty percent of the GPP was considered absorbed by trees and used for the constraint because the field study identified that approximately 20% of the GPP was attributable to the understory vegetation (Ohtsuka et al., 2007).

Step3: Simulation of frNPP

The model simulation was conducted to estimate the frNPP and other carbon cycle components (GPP, wNPP, fNPP, litterfall, and SR) using all six parameters estimated from the above-described method. Uncertainties of these fluxes were estimated by considering variations of six constrained parameter values. The parameters were set to vary individually ±30% with 1% increments from the values constrained by the prescribed procedure. From ensembles of these simulations, a mean deviation from the constrained flux was considered as uncertainty. While varying the six parameters, we also assessed sensitivity of each parameter to annual GPP, wNPP, fNPP, litterfall, SR, and frNPP in terms of deviations from the constrained simulation (deviation (%) = |(constrained flux - x)/constrained flux|, for x being simulation with varied parameter values).

To validate the performance of the model-data integration, interannual variations in the modeled GPP, wNPP, fNPP, litterfall, and SR were compared with those from observation

and default simulation. The GPP and wNPP were directly constrained components in the carbon flow (Fig. 3.2), whereas the fNPP, litterfall, and SR were indirectly constrained (do not explicitly appear in the carbon flow in Figure 3.2) via the allocation proportions, litterfall rates, and mortality rate, and they were also heavily dependent on the constrained GPP and wNPP. We consider that the reliability of the estimated frNPP is indirectly indicated by how accurately these carbon fluxes are reproduced.

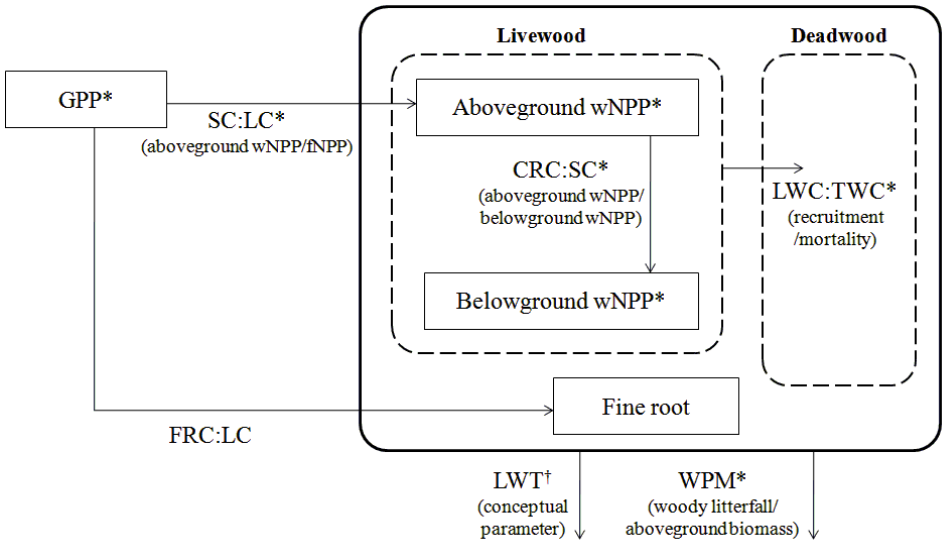

Figure 3.2. A simple schematic of carbon flow in the Biome-BGC model, illustrating carbon fluxes and parameters constrained in the present study. Abbreviations of model parameters: StemC:LeafC (SC:LC), FrootC:LeafC (FRC:LC), CrootC:StemC (CRC:SC), LivewoodC:TotalwoodC (LWT:TWC), live-wood turnover rate (LWT), and whole-plant mortality (WPM). *Observed values are available to constrain components. †Values for components can be conceptually fixed.

3.3. Results

3.3.1. Validation of the model-data integration

The model-data integration successfully constrained the components of the carbon flow shown in Figure 3.2. From 1999 to 2006, the constrained mean annual GPP simulation was 8.3 ± 0.9 MgC ha^{-1} yr^{-1} (Fig. 3.3a). For the same period, the mean annual GPP estimated from the eddy flux observation (Saigusa et al., 2005) was 10.2 ± 0.5 MgC ha^{-1} yr^{-1} and the potential amount absorbed by trees was 8.1 MgC ha^{-1} yr^{-1} (80% of the total GPP used as a

constraint). The constrained and observed (80%) GPP were strongly correlated (R^2 = 0.91; Fig. 3.3a), whereas the default model simulation estimated overall higher GPP (10.2 ± 0.4 MgC ha^{-1} yr^{-1}) than the constrained simulation and the observation, consequently yielding a low correlation with the observed GPP (R^2 = 0.1).

The constrained mean annual wNPP and fNPP were 1.4 ± 0.2 and 1.9 ± 0.3 MgC ha^{-1} yr^{-1}, respectively, from 1999 to 2006 (Fig. 3.3b and 3.3c), and the constrained mean annual litterfall was 2.4 ± 0.4 MgC ha^{-1} yr^{-1} from 1999 to 2003 (Fig. 3.3d; simulation was conducted from 1999 to 2006). Multi-year biometric measurements (Ohtsuka et al., 2007, 2009) yielded a mean annual wNPP and fNPP of 1.4 ± 0.4 and 1.9 ± 0.2 MgC ha^{-1} yr^{-1}, respectively, from 1999 to 2006, and a mean annual litterfall of 2.4 ± 0.4 MgC ha^{-1} yr^{-1} from 1999 to 2003. A strong correlation was identified between the constrained simulation and observation for wNPP (R^2 = 0.99; Fig. 3.3b) and litterfall (R^2 = 0.97; Fig. 3.3c), and a moderate correlation was found for fNPP (R^2 = 0.79; Fig. 3.3d). In contrast, the default simulations of wNPP, fNPP, and litterfall substantially differed both in magnitude and interannual variation with respect to the observations, resulting in low correlations (R^2 = 0.47, 0.0, and 0.37 for wNPP, fNPP, and litterfall, respectively).

Interannual variations in frNPP substantially differed between the constrained and default simulations (Fig. 3.3e). From 1999 to 2006, the mean annual frNPPs were 2.1 ± 0.3 MgC ha^{-1} yr^{-1} and 2.7 ± 0.1 MgC ha^{-1} yr^{-1} for constrained and default simulations, respectively. Between the two, the constrained mean annual frNPP was close to the observed 1-year value for June 2000 to June 2001 (i.e., 1.8 ± 0.3 MgC ha^{-1} yr^{-1}; standard deviation of the values for different soil depths (n = 8); Satomura et al., 2006). Interannual variations in the two frNPP simulations were characterized by contrasting trends, in which a moderate increase in 2002 that was found in the default simulation turned into a substantial decrease in the constrained simulation.

The performance of SR simulation was inferior compared to GPP, wNPP, fNPP, and litterfall simulations (R^2 = 0.71; Fig. 3.3f). The mean annual value of 5.5 ± 0.6 MgC ha^{-1} yr^{-1} was lower than the observed value of 7.1 ± 0.4 MgC ha^{-1} yr^{-1}, whereas an estimate from the default simulation, 7.1 ± 0.4 MgC ha^{-1} yr^{-1}, was rather close to the observation. However, interannual variations in the constrained and observed SR showed a consistent pattern for the period 1999–2003 with a decreasing trend following after a peak value in 2001. On the other hand, a contrasting pattern of interannual variation was identified in the default simulation: an increasing trend following the lowest value in 2001.

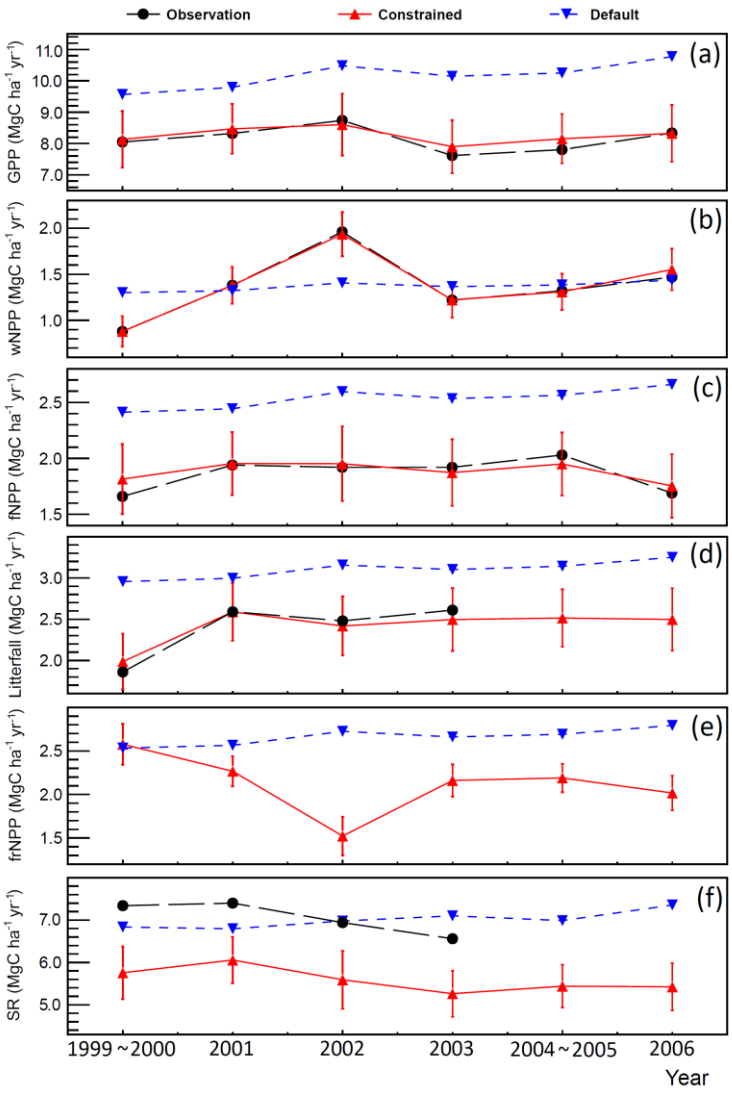

Figure 3.3. Interannual variations in observed and modeled (the constrained and default simulations) carbon fluxes (MgC ha^{-1} yr^{-1}). (a) GPP (80% of the actual value), (b) wNPP, (c) fNPP, (d) litterfall (sum

of foliage and coarse root liters), (e) SR, and (f) frNPP. Correlations between constrained and observed fluxes (R^2, $p < 0.05$) were 0.91 for GPP, 0.99 for wNPP, 0.79 for fNPP, 0.97 for litterfall, and 0.71 for SR. Uncertainties in modeled carbon fluxes are model deviations due to iteratively varied parameter values (described in section 3.2.4).

3.3.2. Allocation patterns in contrasting climate anomalies

Annual variation in component fluxes in 2002 and 2003 were investigated with observations, except for the annual frNPP from the constrained simulation that was used to supplement the limited frNPP observation data. In this analysis, climate anomalies were assumed to affect the carbon cycle components if the anomalies were twice as large as the standard deviations of the interannual variations in the normal meteorological years (1999–2006, except 2002 and 2003) (Table 3.3).

Climate anomalies in 2002 and 2003 affected the annual GPP of the corresponding years. The interannual variation in GPP displayed an anomalous increase in 2002, followed by an anomalous decrease in 2003 (Fig. 3.3a). Corresponding to the high annual GPP (8%), a substantially high annual wNPP was identified in 2002 (56% aboveground and 55% belowground). In 2003, the year with low annual GPP (-6%), the annual wNPP did not differ compared to the normal meteorological years (-3% aboveground and -6% belowground). Despite the contrasting GPP anomalies in 2002 and 2003, the annual fNPP and litterfall did not display notable variations in either 2002 or 2003. Furthermore, variations in the annual frNPP and SR were not consistent in 2002 and 2003; the annual frNPP notably decreased in 2002 (-33%) and varied slightly in 2003 (-5%), and the annual SR anomalously decreased in both 2002 (-6%) and 2003 (-11%). In contrast to the variation in the SR, the decrease in the annual RE was larger in 2003 (-5%) than in 2002 (-2%).

Collectively, the GPP and wNPP in 2002 exhibited contrasting anomalies with respect to the annual frNPP and SR. The positive GPP anomaly (8%) and the less-varied RE led to a positive NEP anomaly (34%). In 2003, the GPP, RE, and SR displayed negative anomalies, but

the NEP did not vary notably in 2003 (-10%) compared to the normal meteorological years because of the common decrease in GPP (-6%) and RE (-5%).

Table 3.3. Anomalies in the observed aboveground and belowground carbon fluxes and productions, and the modeled fine root production in 2002 and 2003. *Anomalies with a magnitude twice as large as the standard deviation (SD) of the interannual variations of the normal meteorological years (from 1999 to 2006, excluding 2002 and 2003). Statistics for the observed carbon fluxes are calculated using the values in Table 3.1.

		Average ± SD from 1999-2006 except 2002 and 2003 MgC ha^{-1} yr^{-1}	Anomaly of 2002 MgC ha^{-1} yr^{-1} (%)	Anomaly of 2003 MgC ha^{-1} yr^{-1} (%)
GPP	Observed (1999-2006)	10.2±0.3	0.8 (8)*	-0.6 (-6)*
RE	Observed (1999-2006)	7.6±0.1	-0.1 (-2)	-0.3 (-5)*
NEP	Observed (1999-2006)	2.6±0.4	0.9 (34)*	-0.4 (-10)
Aboveground				
fNPP	Observed (1999-2006)	1.8±0.2	0.1 (5)	0.1 (5)
Aboveground wNPP	Observed (1999-2006)	1.1±0.2	0.6 (56)*	-0.03 (-3)
Litterfall	Observed (1999-2003)	2.2±0.5	0.3 (12)	0.4 (17)
Belowground				
Belowground wNPP	Observed (1999-2006)	0.2±0.04	0.1 (55)*	-0.01 (-6)
SR	Observed (1999-2003)	7.4±0.04	-0.4 (-6)*	-0.8 (-11)*
frNPP	Constrained simulation (1999-2006)	2.3±0.2	-0.7 (-33)*	-0.1 (-5)

3.4. Discussion

3.4.1. Performance of model-data integration

Both the directly constrained fluxes (GPP and wNPP) and the indirectly constrained fluxes (fNPP, litterfall, and SR) were reproduced well by the model-data integration (Fig. 3.3). Good correlations between the constrained simulation and observation were commonly found for the five fluxes (R^2 = 0.7–0.9; Fig. 3.3). Moreover, the default simulation failed to capture the observed patterns of interannual variation (Fig. 3.3). A pairwise correlation analysis showed that correlation patterns between component fluxes were similar between the observation (Table 3.4a) and constrained simulation (Table 3.4b). In both cases, wNPP was significantly correlated with GPP, and litterfall was moderately correlated with wNPP. A slight disagreement

between the two was found in the fNPP and litterfall, in which the observation indicated a strong correlation between them (R = 0.9; Table 3.4a), while the constrained simulation showed a weak correlation (R = 0.4; Table 3.4b). This is because a constraint on fNPP was less effective compared to GPP, wNPP, and litterfall. In the default simulation, interannual variations in component fluxes were similar to that of GPP without exception (Fig. 3.3). As a consequence, all component fluxes were strongly and positively correlated with each other (R = 0.8–1.0; Table 3.4c).

This result implies that the biometric constraint is a necessary process for accurately assessing the impact of climate anomalies on carbon cycle components. In previous studies, the modeled GPP, NPP, or NEP of forest ecosystems showed common responses to anomalous climate events (Black et al., 2000; Foley et al., 2002; Li et al., 2010). For example, Li et al. (2010) demonstrated a direct association between precipitation anomalies and modeled NPP and NEP in an Amazon ecosystem using the Biome-BGC model. However, these modeled behaviors may not necessarily reflect observed patterns. As opposed to the constrained simulation and observation (Table 3.4a and 3.4b), the linkage between GPP and component fluxes was too strong in the default simulation (Table 3.4c). Without constraints from observation, therefore, annual variations in NPP (and its components), litterfall, and SR in response to a climate anomaly would be misleadingly determined by GPP.

Table 3.4. Correlation matrix (R) of carbon cycle components for (a) the observation, (b) constrained simulation, and (c) default simulation. Statistically significant trends are indicated as * ($p < 0.01$).
(a) Observation

	GPP	SR	wNPP	fNPP	Litterfall
GPP	1.00				
SR	0.41	1.00			
wNPP	0.72*	-0.25	1.00		
fNPP	-0.18	-0.42	0.38	1.00	
Litterfall	0.05	-0.48	0.59	0.99*	1.00

(b) Constrained simulation

	GPP	SR	wNPP	fNPP	Litterfall	frNPP
GPP	1.00					
SR	0.11	1.00				
wNPP	0.74*	-0.50	1.00			
fNPP	0.33	0.04	0.32	1.00		
Litterfall	0.21	-0.12	0.55	0.40	1.00	
frNPP	-0.73*	0.52	-0.83*	-0.11	-0.01	1.00

(c) Default simulation

	GPP	SR	wNPP	fNPP	Litterfall	frNPP
GPP	1.00					
SR	0.85*	1.00				
wNPP	1.00*	0.84*	1.00			
fNPP	1.00*	0.86*	1.00*	1.00		
Litterfall	0.99*	0.88*	0.99*	1.00*	1.00	
frNPP	1.00*	0.86*	1.00*	1.00*	1.00*	1.00

Among the constrained parameters, FrootC:LeafC and StemC:LeafC were the major attributions to the consistency between the constrained simulation and observation. Sensitivity analysis showed that variations in FrootC:LeafC and StemC:LeafC from the constrained values induced 15–40% and 12–19% offsets from the constrained fluxes, respectively (Fig. 3.4). In 2002, values of these parameters diverged greatly from the multiyear mean: an increase in StemC:LeafC and a decrease in FrootC:LeafC (Table 3.2). Similar variation patterns found in the corresponding wNPP and frNPP simulations implies a tradeoff between these pools, and that FrootC:LeafC and StemC:LeafC are largely responsible for the variation in NPPs in 2002 (Fig. 3.3b and 3.3e). Prior to the present study, the importance of FrootC:LeafC and StemC:LeafC was stressed in the optimization study of GPP, RE, NEP, and biomass simulations in Biome-BGC (Kondo et al., 2013). The strong sensitivity of these two allocation parameters suggests that preservation of an appropriate allocation proportions between major vegetation components (leaf, wood, and fine roots) is a key for accurately simulating carbon

cycle. Variations in other parameter values (CrootC:StemC, LivewoodC:TotalwoodC, whole-plant mortality, and live-wood turnover rate) induced a few offsets, but that does not necessarily mean that these parameters are not important: a sum of these offsets amounts to approximately 10%.

We consider that the constrained simulation provides a reliable interannual variation in frNPP compared with that of the default simulation because unnecessary freedom in frNPP simulation was successfully constrained. The interannual variations in the constrained component fluxes (GPP, wNPP, fNPP, litterfall, and SR) displayed patterns consistent with the observations whereas those in the default simulation substantially differed (Fig. 3.3). This result suggests that the interannual variations in the constrained frNPP reflected observed variations as they were largely attributable to interannual variations of biometric observations used as constraints, whereas the interannual variations in the default frNPP were influenced by underrepresented component fluxes.

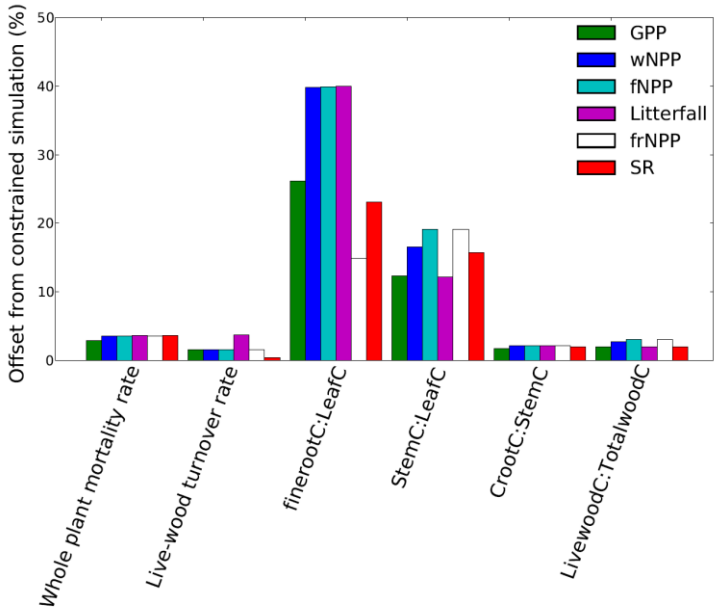

Figure 3.4. Model parameter sensitivity to annual GPP, wNPP, fNPP, litterfall, frNPP, and SR. For ±30% range from the constrained parameter value, deviations from the constrained simulation (deviation (%) = |(*constrained flux*-*x*)/*constrained flux*|, for *x* being simulation with varied parameter values) were calculated for each parameter. The averages of the maximum deviation from 1999 to 2006 are shown here.

Interannual variation in the SR was the least well reproduced flux in the constrained simulation because of two potential reasons. (1) The SR simulation in the present study does not include a contribution from an understory vegetation. In the present study, the Biome-BGC simulation was constrained only by biometric observations of trees (Table 3.1) due to limited observation of an understory vegetation. Overall underestimation found in the constrained SR (Fig. 3.3f) may be attributable to our treatment for GPP that 80% of the observed GPP was considered as a potential amount absorbed by trees based on a previous study (Ohtsuka et al., 2007). (2) Only input fluxes to the belowground carbon cycle (i.e., belowground wNPP, litterfall, and frNPP) were constrained in the current scheme. Parameters related to the annual soil organic carbon change, annual litter carbon change, and root respiration and decomposition rates were not constrained due to limited observation. Despite of these issues, an interannual variation pattern from 1999 to 2003 was reproduced reasonably well with respect to the observed SR showing a decreasing trend from 2001 to 2003 (Fig. 3.3e). This result possibly reflects effectiveness of constraining the input fluxes to belowground.

3.4.2. Allocation pattern under the low summer PPFD in 2003

The results from the present study indicated that the SR notably decreased with the decreasing GPP in 2003 (Table 3.3). Although the aboveground and belowground wNPP and the frNPP appeared to decrease, their variations were not significant compared with those of the normal meteorological years. Similarly, influence from the low summer PPFD was not identified in the fNPP and litterfall.

The decreases in the GPP and SR were attributable to the low summer PPFD and the accompanying low summer temperatures (Fig. 3.1c and 3.1a). The monthly scale attribution of these anomalies to GPP was previously investigated and a 26% lower GPP was found in July

2003 compared to previous years (Saigusa et al., 2010). We found that the impact of these anomalies was also apparent at the annual scale (6% reduction of annual GPP), and a similar order of reduction was identified in the annual SR (11% reduction). Both the annual GPP and SR were lowest in 2003 for the period 1999–2006, and the attribution of the reduced temperature was clearly illustrated from their relationships to the summer temperature (Fig. 3.5a and 3.5f). Furthermore, for variations in other component fluxes in 2003, we did not identify an indication of attribution of the reduced temperature (Fig. 3.5b–3.5e). It is rather difficult to explain the decrease in SR with variations in belowground fluxes (litterfall, frNPP, and belowground wNPP). Both the annual frNPP and belowground wNPP decreased only slightly in 2003, and these anomalies were less than half of the standard deviations of the interannual variability for normal meteorological years (Table 3.3).

The weak influence of the low summer PPFD and temperature on components of the NPP suggests that climate anomalies in the growing season may not affect forest production. Low variations in the fNPP and litterfall can be explained by the observed result that the foliation of the study forest had reached maximum expansion in the spring prior to the low PPFD in the summer (Muraoka and Koizumi, 2005). The previous study similarly explained the low variation of the annual fNPP of a European Beech forest under a summer drought event (Campioli et al., 2011). The woody and fine root productivity of the study forest are characterized by a high growth rate during the growing season with a peak at the end of summer (Kawamura et al., 2001; Muraoka and Koizumi 2005; Satomura et al., 2006). Although the occurrence of the low PPFD and temperature overlapped with the high-productivity period of wNPP and frNPP, a notable influence was not identified for either component. As previous studies suggested, climate conditions before the peak growing season, such as the temperature in the early growing season (Vaganov et al., 1999; Noormets et al.,

2008), or the annual radiation and temperature in previous years (Gough et al., 2008; Campioli et al., 2011), may have a greater effect on forest NPP.

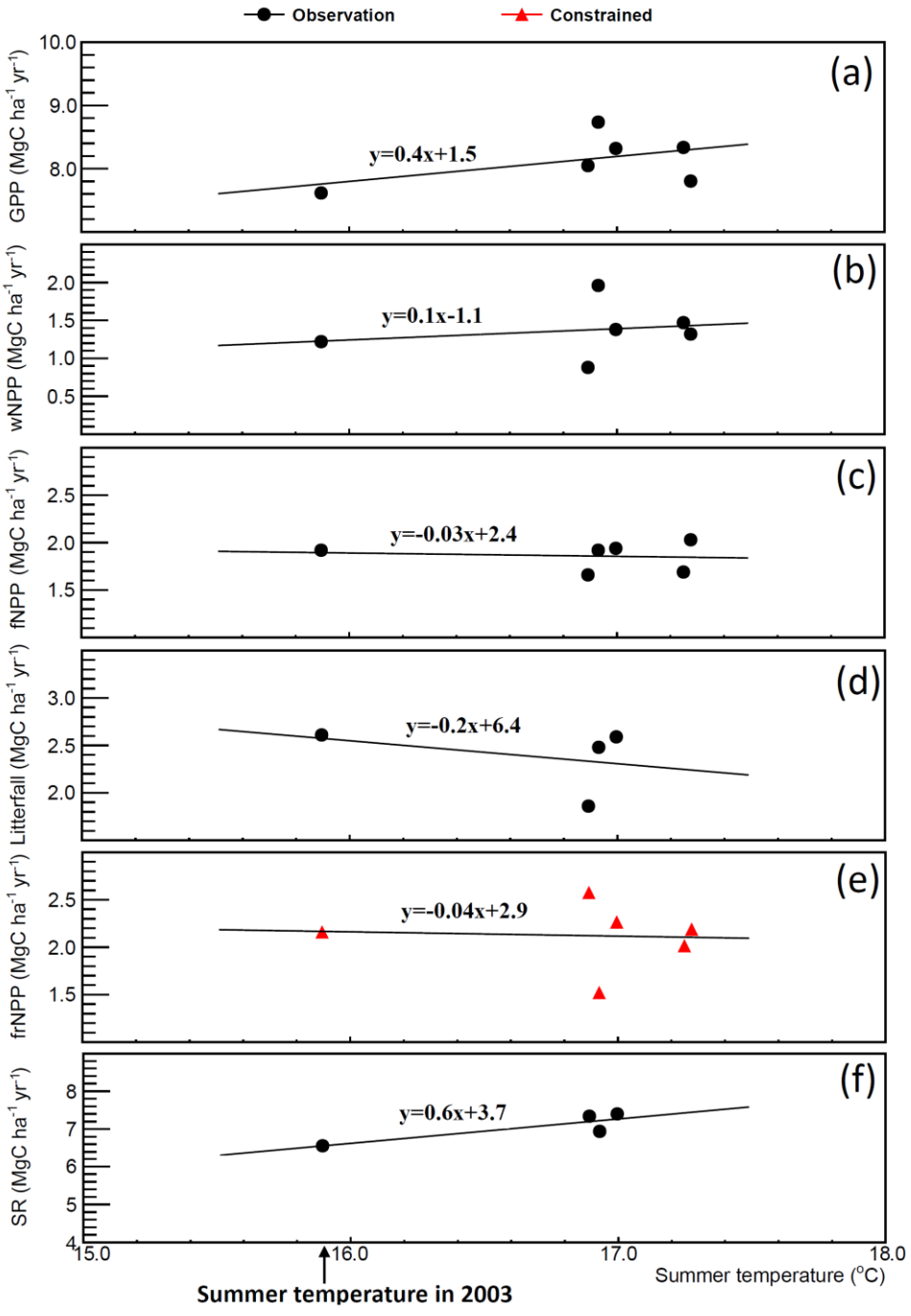

Figure 3.5. Relationships between the summer temperatures (June–August) and annual carbon fluxes: (a) GPP, (b) wNPP, (c) fNPP, (d) litterfall, (e) frNPP (constrained simulation), and (f) SR.

3.4.3. Allocation pattern under the early spring warming in 2002

In contrast to the negative summer climate anomaly in 2003, the spring warming in 2002 substantially increased the annual GPP and wNPP (Table 3.3). The previous studies found that foliation of the study forest began 10-20 days earlier in 2002 than in previous years because of the early spring warming, and the elongation of the growing season was largely attributable to the increase in the annual GPP (Saigusa et al., 2005, 2010). Ohtsuka et al. (2009) explained that the high early spring temperatures could have caused the notable increase in the wNPP based on the hypothesis of Vaganov et al. (1999) that early spring temperatures are a primary determinant of the magnitude of annual stem increments in temperate climatic regions. As consistent with these studies, we found that the largest annual GPP and wNPP in 2002 corresponded to the high spring temperature (Figs. 3.6a and 3.6b). Similar to the case of the low summer PPFD in 2003, the spring warming in 2002 did not significantly affect the fNPP and litterfall (Table 3.3, Fig. 3.6c, and 3.6d). These low variations under two contrasting climate anomalies indicate that the seasonal climate conditions may not be effective indicators for the annual fNPP and litterfall of the study forest.

Our result indicates that the carbon allocation in 2002 is characterized by contrasting variation patterns of belowground and aboveground NPPs. For the 1999-2006 period, the aboveground NPP (fNPP and aboveground wNPP) and the belowground NPP (belowground wNPP and frNPP) exhibited contrasting variation patterns; the former tends positively and the latter negatively varied with the spring temperature (Fig. 3.7). Correspondingly, a clear allocation shift toward the aboveground NPP was identified in response to the high early spring temperature in 2002. In previous studies, a similar allocation shift (a decrease in the belowground NPP and an increase in the aboveground NPP) has been identified by alleviating water or nitrogen limitation (e.g., Haynes and Gower, 1995; Maier and Kress, 2000; Giardina et al., 2003). In the current case, a limiting factor of the study forest is possibly alleviated by the spring warming as indicated by the relationship in Figure 3.7. Because the region around

the study forest is characterized by a humid and cool-temperate climate, cool temperatures rather than water availability are a limiting factor.

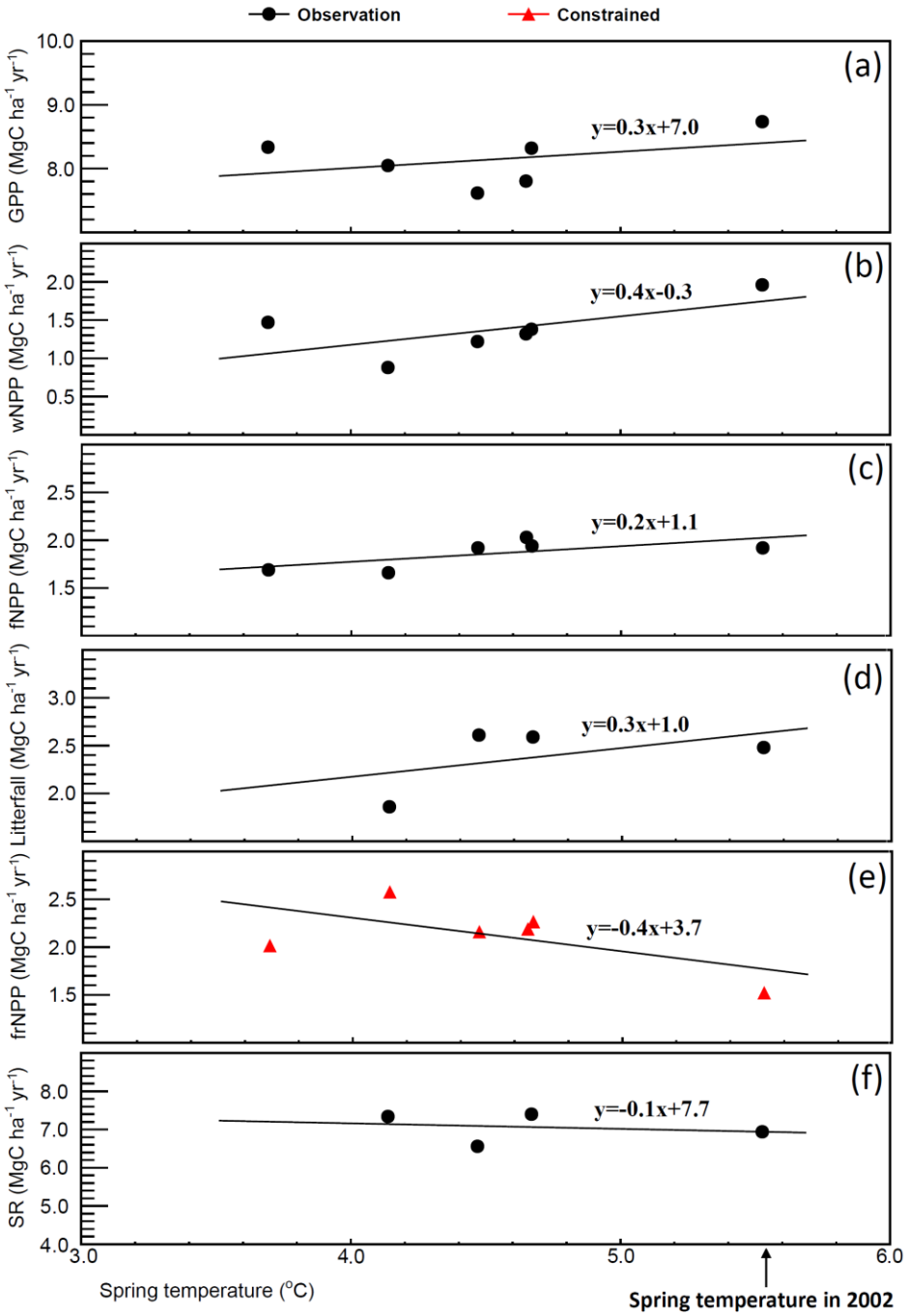

Figure 3.6. Relationships between the spring temperatures (March–May) and annual carbon fluxes: (a) GPP, (b) wNPP, (c) fNPP, (d) litterfall, (e) frNPP (constrained simulation), and (f) SR.

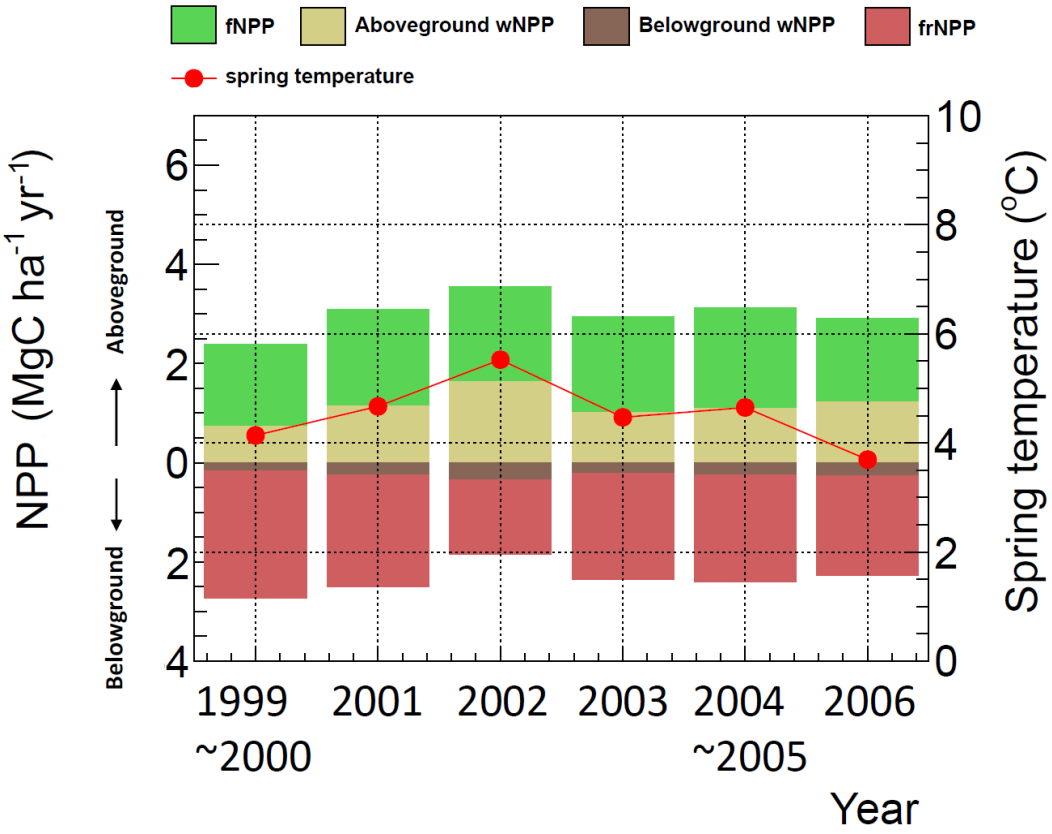

Figure 3.7. Interannual variations in the aboveground NPP (fNPP and aboveground wNPP), belowground NPP (belowground wNPP and frNPP), and spring temperatures (March–May).

Among the components of NPP, the aboveground wNPP and frNPP were major attributions to this allocation shift as they exhibited the opposite trends of interannual variability (Fig. 3.3b and 3.3f). Especially in 2002, they exhibited substantial and opposite variations: 56% increase in the aboveground wNPP and 33% decrease in the frNPP (Table 3.3). Despite the increase in 2002, the contribution from the belowground wNPP to the allocation shift was rather small because the magnitude of the belowground wNPP was substantially smaller than those of the aboveground wNPP and frNPP (Table 3.3). The contribution from the fNPP is negligible because it was invariant in 2002 compared with the multiyear mean. This temperature driven allocation shift between the aboveground wNPP and frNPP was demonstrated in previous studies that analyzed flux and biometric measurements taken along the transect in the Ecuadorian Andes (Roderstein et al., 2005; Leuschner et al. 2007; Zach et al.,

2010; Unger et al., 2012). A threefold increase in frNPP (Roderstein et al., 2005) and a decrease in canopy height and stem productivity (Unger et al., 2012) were identified with decreasing temperature with altitude. Potential mechanisms behind the allocation shift found in the Ecuadorian Andes was implied by Leuschner et al. 2007, in which they argued that lower temperatures caused low nutrient supply via reducing (i) microbial nutrient mineralisation rates, (ii) activity of mycorrhizal fungi (reducing nutrient supply function), and (iii) nutrient uptake rates of roots (because activity in the plasma membranes is temperature sensitive). Conversely, in the case of the study forest, the early spring warming conceivably induced a high nutrient supply by stimulating these temperature-sensitive processes; consequently, enhancing the aboveground wNPP and reducing the frNPP by the law of the limiting resource (Enquist and Niklas, 2001). This explanation suggests that the strong relationship between the early spring temperature and the annual stem increment (implied by Vaganov et al., 1999) may be related to nutrient availability. A clear mutual trend of the frNPP (decreasing) and the wNPP (increasing) with the spring temperature (Fig. 3.6a and 3.6e) are consistent with such potential potential mechanism.

The decrease in SR possibly resulted from the decrease in frNPP rather than a meteorological effect. Seasonal variations in air temperature, precipitation, and soil temperature in 2002 did not indicate a meteorological event causing the negative effects on SR (Mo et al., 2005). In the present study, we did not identify a particular effect from the high spring temperature on the SR in 2002 (Fig. 3.6f). However, the decrease of fine root respiration is inferred by the decreased frNPP. By exploring the result of the constrained simulation further, we found that both MR and GR of fine roots decreased in 2002, but with a greater decrease in GR than MR (Fig. 3.8a). In Biome-BGC, GR of fine roots is solely a function of allocated carbon to fine roots; thus, the decrease of the frNPP directly affects the GR. While MR of fine roots is modeled as a function of a nitrogen content and soil temperature. Similar to the GR, the

decrease of the MR is attributable to the decreased frNPP because the nitrogen content of fine roots varies with a production rate in the model; however, the reduction was less profound in the MR because of the positive temperature dependence. Compared with fine root respirations, coarse root respirations were substantially small (Fig. 3.8a), which is reasonable because the respiration of fine roots has been identified as a major contributor to SR (Lee and Jose, 2003). Heterotrophic respiration (HR) comprised a major proportion of SR, but it did not indicate a decreasing trend in 2002 (Fig. 3.8b). These results suggest that the AR of fine roots is responsible for the decrease of the SR in 2002.

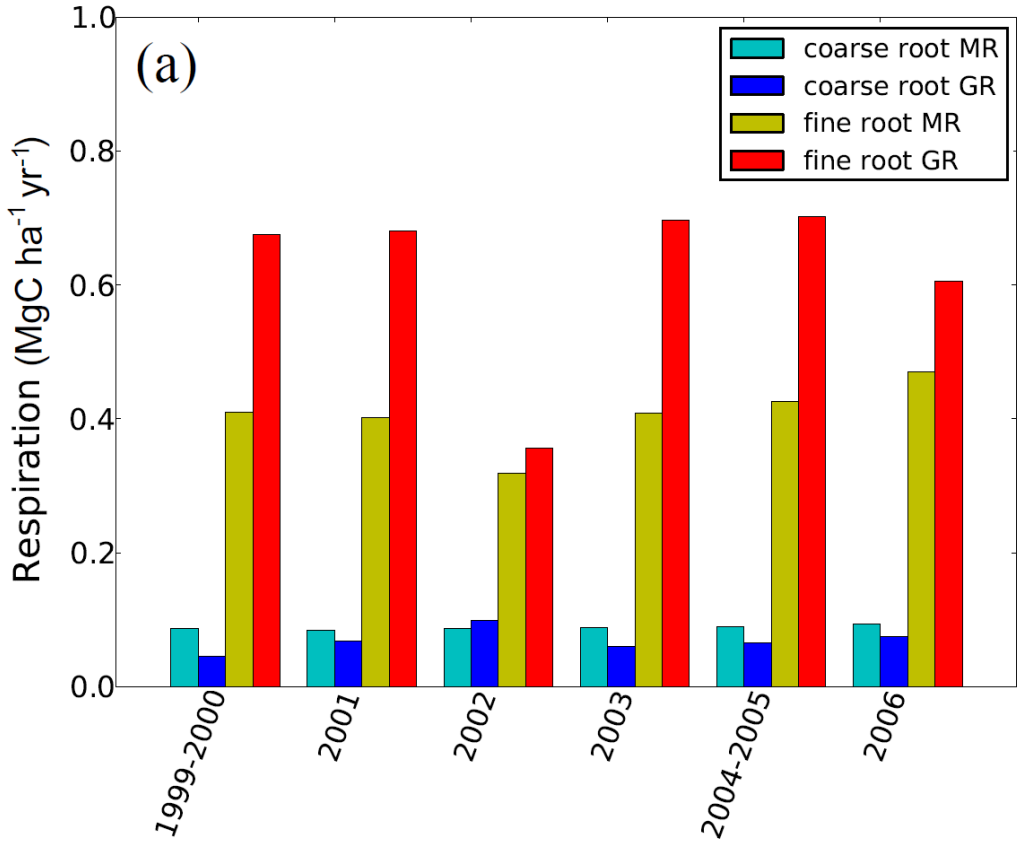

Figure 3.8. Constrained simulation results for (a) fine root and coarse root maintenance respiration (MR) and growth respiration (GR), and (b) fine root and coarse root autotrophic respiration (AR), heterotrophic respiration (HR), and SR.

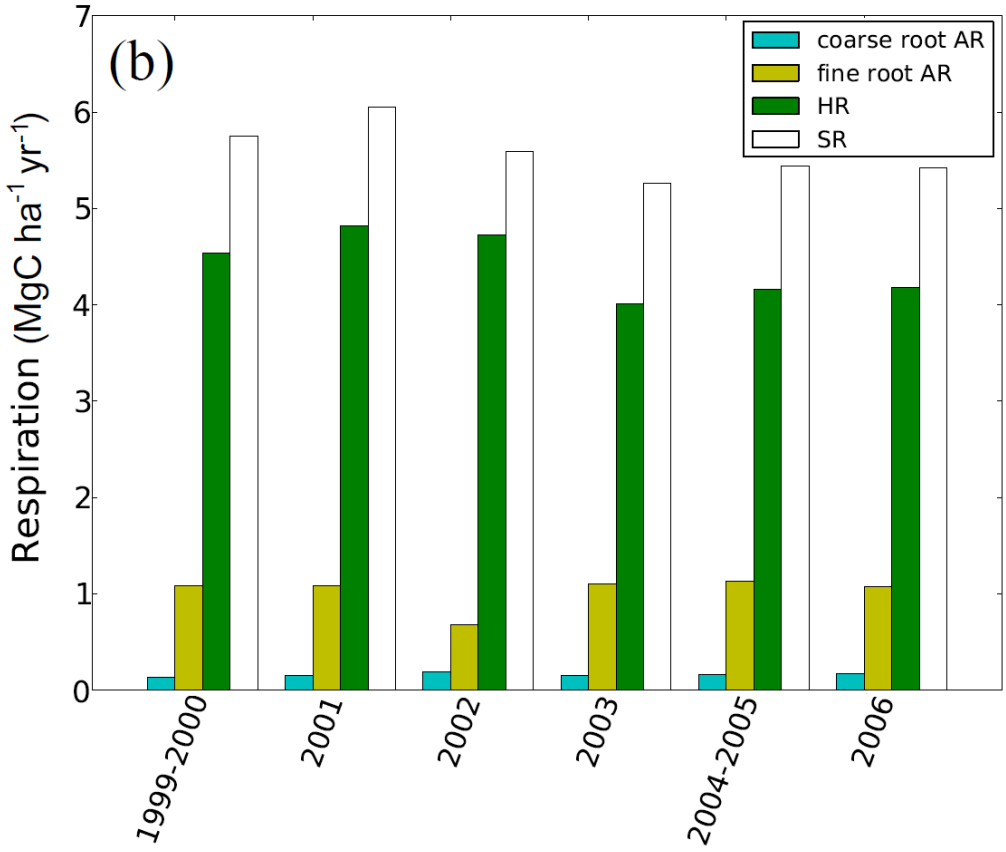

Figure 3.8. continued

5. Conclusion

We characterized the carbon allocation patterns under contrasting climate anomalies using multi-year biometric and flux observations (GPP, fNPP, litterfall, wNPP, and SR) and frNPP values estimated by the model-data integration (refer to the summary in Table 3.5). (1) The low summer PPFD in 2003 decreased the CO_2 fluxes (GPP, SR, and RE) but did not affect the components of NPP. (2) The early spring warming in 2002 increased the GPP and wNPP and decreased the frNPP and SR. Similar to the case in 2003, the fNPP and litterfall were unaffected. The wNPP and frNPP displayed opposite responses, which suggests that the early spring induced the allocation shift between the frNPP and wNPP, and that this may have been mediated by temperature-driven difference in microbial nitrogen mineralization and its

availability to trees. Although the frNPP was estimated by the model-data integration, the decrease in frNPP is plausible because the decrease in SR cannot be explained without the contribution of fine roots.

Allocation patterns identified in synthesis studies have advanced our understanding of the carbon cycle dynamics (e.g., Litton et al., 2007; Malhi et al., 2011). The present study demonstrated that climate anomalies can induce allocation patterns that are not necessarily consistent with this result and that increasing and decreasing patterns of component fluxes cannot always be inferred from the GPP. Factors such as the timing and duration of the climate anomaly and allocation shift between components of the NPP need to be considered when characterizing the impact of anomalous climate events on allocation patterns.

Table 3.5. Summary of variations in carbon fluxes and potential causes under climate anomalies in 2002 and 2003.

	2002: early spring warming	2003: low summer PPFD
GPP	Increased due to the prolonged growing season	Decreased due to the low summer PPFD and temperature
RE	Did not notably change	Decreased due to the decreased SR
NEP	Increased due to the increased GPP	Did not notably change
wNPP	Substantially increased due to the high nutrient availability induced by spring warming.	Did not notably change
fNPP	Did not notably change	Did not notably change
Litterfall	Did not notably change	Did not notably change
frNPP	Decreased due to the high nutrient availability induced by spring warming.	Did not notably change
SR	Decreased due to the low fine root respiration, which is implied by the decreased frNPP	Decreased due to the low summer temperature

Chapter 4

Comparison of the data-driven top-down and bottom-up global terrestrial CO_2 exchanges: GOSAT CO_2 inversion and empirical eddy flux upscaling

Abstract

We examined the consistency between terrestrial biosphere fluxes (terrestrial CO_2 exchanges) from data-driven top-down (GOSAT CO_2 inversion) and bottom-up (empirical eddy flux upscaling based on a support vector regression (SVR) model) approaches over 42 global terrestrial regions from June 2009 to October 2011. Seasonal variations of the biosphere fluxes by the two approaches agreed well in boreal and temperate regions across the Northern Hemisphere. Both fluxes also exhibited strong anomalous signals in response to contrasting anomalous spring temperatures observed in North America and boreal Eurasia. This indicates that the CO_2 concentration data integrated in the GOSAT inversion and the meteorological and vegetation data in the SVR models are equally effective in producing spatiotemporal variations of biosphere flux. Meanwhile, large differences in seasonality were found in sub-tropical and tropical South America, South Asia, and Africa. The GOSAT inversion showed seasonal variations pivoted around CO_2 neutral, while the SVR model showed seasonal variations that tended towards CO_2 sink. Thus, a large difference in CO_2 budget was identified between the two approaches in sub-tropical and tropical regions across the Southern Hemisphere. Examination of the integrated data revealed that the large tropical sink of CO_2 by the SVR model was an artifact due to the underrepresented biosphere fluxes predicted by limited eddy flux data for tropical biomes. Because of the global coverage of CO_2 concentration data, the GOSAT inversion provides better estimates of continental CO_2 flux than the SVR model in the Southern Hemisphere.

(Based on: Kondo M., Ichii K., Takagi H., Sasakawa, M., Comparison of the data-driven top-down and bottom-up global terrestrial exchanges: empirical eddy flux upscaling and GOSAT CO_2 inversion, Journal of Geophysical Research – Biogeosciences, 120, doi:10.1002/2014JG002866)

4.1. Introduction

Estimation of the exchange of CO_2 between the land biosphere and the atmosphere is challenging because of the complex relations among the physical, chemical, and biological processes involved (Friedlingstein et al., 2006). In addition to the complexity of the system, the validation of the estimates can only be conducted at the point scale because reliable data are only available from ground observations (e.g., eddy flux observations). For these reasons, the reliable estimation of regional or global terrestrial CO_2 exchange has remained a challenge for decades (e.g., Tans et al. 1989; Ciais et al., 1995; Law et al., 1996; Gurney et al., 2004; Sitch et al., 2008; Piao et al., 2012; Patra et al., 2013).

Currently, two principal approaches are used to estimate terrestrial CO_2 exchange: top-down and bottom-up. The top-down approach estimates the terrestrial CO_2 exchange that is optimally consistent with atmospheric CO_2 concentration measurements. Previous works have used an atmospheric inversion model in the top-down approach (e.g., Taguchi, 1996; Chevallier et al., 2005; Peters et al., 2007; Maksyutov et al., 2008). This method uses a forward-running atmospheric transport model and a priori initial estimates of the surface fluxes—CO_2 exchanges for land, ocean, and other CO_2 emission attributions (e.g., biomass burning and fossil fuel emissions)—to predict observed concentrations and to estimate the terrestrial CO_2 exchange, while seeking consistency between simulated and observed CO_2 concentrations. The bottom-up approach can be classified into two broad categories: process-based model simulation and empirical-model-based upscaling. Process-based models

simulate the ecosystem-scale carbon cycle by considering the internal biochemical mechanisms of carbon flows (e.g., photosynthesis, respiration, and decomposition) for each prescribed vegetation type (e.g., Cox et al., 2001; Thornton et al., 2002; Sitch et al., 2003; Sato et al., 2007; Ito, 2008). Empirical-model-based upscaling is driven by empirically obtained relations between CO_2 flux and environmental factors such as air temperature, precipitation, radiation, and vegetation parameters as the appropriate input data (e.g., Detling et al., 1997; Saito et al., 2009; Beer et al., 2010).

Since the early 2000s, the research community has invested substantial effort in the development of bottom-up and top-down CO_2 exchange estimations; however, current estimates of terrestrial CO_2 exchange by the two approaches remain inconsistent (Ciais et al., 2013). Regional CO_2 exchanges, estimated by 10 ecosystem models and 11 inversion models that were submitted to model intercomparison projects (i.e., the TRENDY dynamic vegetation model intercomparison project (Sitch et al., 2008; Le Quéré et al., 2009) and the TransCom inversion intercomparison project (Peylin et al., 2013)), showed that the inversion models tend to indicate stronger CO_2 sinks in temperate and boreal regions than the ecosystem models do. Furthermore, the two approaches exhibited contrasting CO_2 sink–source trends in the tropics; the ecosystem models indicated CO_2 sinks and the inversion models CO_2 sources (Ciais et al., 2013). As illustrated by these inconsistencies, a consensus on the geographic distribution of the terrestrial CO_2 budget has yet to be established among the research community.

Progress in data integration is expected to facilitate improved performance of the top-down and bottom-up CO_2 exchange estimations, and major advances in atmospheric CO_2 concentration measurements have progressed estimations of CO_2 exchange by the top-down approach. The Greenhouse gases Observing SATellite (GOSAT) launched by the Japan Aerospace Exploration Agency (JAXA) in January 2009 is the first operational satellite that delivers global atmospheric CO_2 concentration measurements (Kuze et al., 2012). Unlike

previous inversion models that were constrained by statistically limited atmospheric CO_2 concentration measurements, the GOSAT inversion model (GOSAT Level 4A data product: hereafter, GOSAT L4A) takes full advantage of the global coverage of atmospheric CO_2 concentration measurements (Takagi et al., 2011, 2014; Maksyutov et al., 2013). Similarly, a global network of eddy flux observations (FLUXNET) (Baldocchi, 2008) and a data integration technique with machine-learning-based empirical upscaling have progressed bottom-up CO_2 flux and exchange estimations (Papale and Valentini, 2003; Yang et al., 2006, 2007; Xiao et al., 2008; Jung et al., 2009, 2011). This machine-learning model develops an empirical regression via a learning processes in which the model searches for certain patterns and relations between CO_2 fluxes and relevant predictors from meteorological observations and/or satellite remote sensing, such as air temperature, radiation, vegetation parameters, e.g., the enhanced vegetation index (EVI), normalized difference vegetation index (NDVI), and leaf area index (LAI). These advances in data integration are expected to improve both bottom-up and top-down CO_2 exchange estimations.

To validate the consistency between the data-integrated approaches, the present study conducted a global-scale comparison of data-driven top-down and bottom-up terrestrial CO_2 exchanges. Specifically, we compared the bottom-up estimate from the machine-learning-based empirical upscaling of eddy flux observations and the top-down estimate from GOSAT L4A for the period June 2009 to October 2011 (the temporal coverage of GOSAT L4A version 02.02). We investigated the level of agreement between the two estimates in relation to seasonal variability and budget on both regional and global scales. We identified potential causes for agreement or/and inconsistencies between the two approaches, and discussed the advantages and limitations of data integration and prospects for the refinement of global CO_2 budget estimations.

4.2. Materials and Methods

4.2.1. Satellite remote sensing data

The majority of satellite observation data used in this study were measured by the Moderate-resolution Imaging Spectroradiometer (MODIS) onboard the Terra satellite: NDVI and EVI (MOD13A2) (Huete et al., 2002), fraction of photosynthetically active radiation (FPAR) and LAI (MOD15A2) (Myneni et al., 2002), daytime and nighttime land surface temperatures (LSTs:MOD11A2) (Wan et al., 2002), and nadir bidirectional reflectance distribution function (BRDF)-adjusted surface reflectance product (MOD43B4) (Schaaf et al., 2002). The original temporal resolutions of LAI, LST, and surface reflectance are 8 days and those of NDVI and EVI are 16 days. For each time step, we averaged the MODIS observations using only the high-quality pixels (with a mandatory quality assurance or QA flag of zero in the QA data) based on the methods of Yang et al. (2007) and Ueyama et al. (2013). Missing data were replaced by a 2001–2010 average that was calculated using the high-quality pixels. All gaps in the data were filled using the averaged 8-day data (some 16-day data were used to fill two consecutive 8-day periods) calculated from 2001–2010 at each grid point, if the QA flags were unacceptable. The surface reflectance product (MOD43B4) was used to calculate the 8-day composite of the green ratio (GR) (Harazono et al., 2009), NDVI, and EVI (hereafter GR43, NDVI43, and EVI43, respectively).

Shortwave radiation (SRAD) data used in this study were estimated using the 400–700-nm channels of MODIS sensors carried by the Terra satellite and the Sea-viewing Wide Field-of-view Sensor (SeaWiFS) carried by the SeaStar satellite (Frouin and Murakami, 2007). The data for 2001–2010 were processed by the SeaWiFS algorithm (Frouin et al., 2003) and were reproduced as daily means with 5-km resolution. The SRAD data were converted to daily values using the diurnal cycle of the solar zenith angle and the satellite-observed instantaneous atmospheric conditions. Descriptions of the satellite-based data prepared for the

present study are provided in Table 1.

Table 4.1. Satellite-based products used in this study, their descriptions, and reflectance band compositions. MODIS bands: red (Band1: 620−670 nm), near-infrared (Band 2: 841−876 nm), blue (Band 3: 459−479 nm), green (Band 4: 545−565 nm), and shortwave infrared (Band 6: 1628−1652 nm).

Product	Resolution		Description	Reference
	Spatial	Temporal		
MOD13A2 NDVI	1000 m	16 day	Normalized difference vegetation index (NDVI) computed from MOD09 reflectance product: NDVI = (Band2 - Band1)/(Band2 + Band1)	Huete et al. (2002)
MOD13A2 EVI	1000 m	16 day	Enhanced vegetation index (EVI) computed from MOD09 reflectance product: EVI = 2.5(Band2 - Band1)/(Band2 + 6Band1 - 7.5Band3 + 1)	Huete et al. (2002)
MOD15A2 FPAR, LAI	1000 m	8 day	Fraction of photosynthetically active radiation (FPAR) and leaf area index (LAI, one sided) computed from 1km surface reflectance and land cover definition using radiative transfer or empirical (backup) methods	Myneni et al. (2002)
MOD11A2 LST	1000 m	8 day	Land surface temperature (LST) retrieved by the generalized split-window algorithm. The daytime and nighttime LSTs were retrieved from pairs of day and night MODIS observations in seven thermal infrared bands	Wan et al. (2002)
MOD43B4	1000 m	8 day	Nadir bidirectional reflectance distribution function (BRDF)-adjusted reflectance from MODIS bands	Schaaf et al. (2002)
GR43	1000 m	8 day	Green ratio (GR) computed as a simple ratio of green to total visible bands: GR = Band4/(Band1 + Band4 + Band3) using reflectance products of MOD43B4	Harazono et al. (2009)
NDVI43	1000 m	8 day	Same algorithm used in MOD13A2, but reflectance products were based on MOD43B4	Ahl et al. (2006)
EVI43	1000 m	8 day	Same algorithm used in MOD13A2, but reflectance products were based on MOD43B4	Ahl et al. (2006)
SRAD	5000 m	Daily	Shortwave radiation (SRAD) computed by composition of broadband visible (400–700 nm) from MODIS (on Terra satellite) and SeaWiFS (on SeaStar satellite)	Frouin et al. (2003); Frouin and Murakami (2007)

4.2.2. Top-down approach: GOSAT L4A

GOSAT L4A is a data product that stores monthly flux estimates for 64 regions on sub-continental and ocean-basin scales, as defined by Patra et al. (2005) (42 tiles for land and 22 tiles for ocean; see the land tile distribution of Fig. 4.1a). They are estimated by Bayesian inverse modeling in which the observations are incorporated with the corresponding predictions from an atmospheric transport model (Maksyutov et al., 2013). Compared with the common atmospheric inversion models, GOSAT L4A has the advantage of integrating into the

inversion process satellite-based atmospheric CO_2 concentration measurements obtained from high-resolution shortwave infrared (SWIR) spectra. The column-averaged dry air molar fraction of CO_2 (referred to as XCO_2) was estimated from high-resolution spectra of reflected sunlight in four spectral wavebands collected by the Thermal And Near infrared Sensor for carbon Observation-Fourier Transform Spectrometer (TANSO-FTS) onboard the GOSAT satellite. Another sensor, the Cloud and Aerosol Imager (CAI), uses high-spatial-resolution images to detect cloud and aerosols within the instantaneous field of view (IFOV) of TANSO-FTS. The SWIR spectra from TANSO-FTS provide information on the CO_2 concentrations in the mid- to lower troposphere and on the entire CO_2 column with a footprint area of approximately 90 km^2. Using the information collected by TANSO-FTS, the XCO_2 was retrieved by optimal estimation (Yokota et al., 2008). In conjunction with CO_2 concentration data from the global network of surface in situ CO_2 measurement sites (GLOBALVIEW-CO_2: GV hereafter), the XCO_2 retrievals were fed into the inversion for the estimation of surface CO_2 flux.

The a priori flux dataset used for the GOSAT L4A inversion comprises four components: daily net ecosystem exchange (NEE) predicted by the Vegetation Integrative SImulator for Trace gases (VISIT) (Ito, 2008, 2010); monthly ocean–atmosphere CO_2 fluxes generated from observations of surface ocean CO_2 partial pressure (pCO_2) (Valsala and Maksyutov, 2010); monthly CO_2 emissions due to biomass burning from the Global Fire Emissions Database (GFED) version 3.1 (van der Werf et al., 2010); and monthly fossil fuel CO_2 emissions obtained by merging the Open source Data Inventory of Anthropogenic CO_2 emissions (ODIAC) dataset (Oda and Maksyutov, 2011) and the Carbon Dioxide Information Analysis Center dataset (Andres et al., 2011). The land–atmosphere and ocean–atmosphere a priori fluxes were optimized against observations. Daily NEE simulation of the VISIT model was optimized to fit the GV CO_2 seasonal variability using a Bayesian inversion approach from

Nakatsuka and Maksyutov (2009), and net primary production (NPP) and aboveground biomass estimates were kept consistent with observations obtained from the Global Primary Production Data Initiative (GPPDI) (Scurlock et al., 1999; Olson et al., 2001) and International Institute for Applied Systems Analysis (IIASA) global biomass map (Kindermann et al., 2008), respectively. The ocean–atmosphere CO_2 flux was optimized by constraining the surface ocean dissolved inorganic carbon with respect to observational values derived from the observed pCO2, as summarized in Takahashi et al. (2011).

The National Institute for Environmental Studies global atmospheric tracer Transport Model (NIES-TM) was used for performing forward simulations of atmospheric CO_2. Atmospheric transport was driven by merged reanalysis data, i.e., the Japanese 25-year Reanalysis (JRA-25) for 1979–2004 and a real-time operational analysis by the Japan Meteorological Agency (JMA) Climate Data Assimilation System (JCDAS) for 2005–present (Onogi et al., 2007). The monthly surface CO_2 fluxes were calculated using Bayesian inverse modeling schemes based on the fixed-lag Kalman Smoother (Bruhwiler et al. 2005) for the 64 global tiles, while CO_2 concentrations were constrained by the GV dataset and GOSAT XCO_2 data. Further detailed description of GOSAT L4A is provided by Maksyutov et al. (2013).

In the present study, we used the monthly surface CO_2 flux of GOSAT L4A version 02.02, which covers June 2009–October 2011. The bottom-up surface CO_2 flux used in this study only considers biosphere flux (see section 2.3). Therefore, to be directly comparable with the bottom-up biosphere flux, emissions from fossil fuel and biomass burning were subtracted from the total flux of GOSAT L4A. Hereafter, we refer to this remaining flux as the GOSAT biosphere flux (Fig. 4.1b).

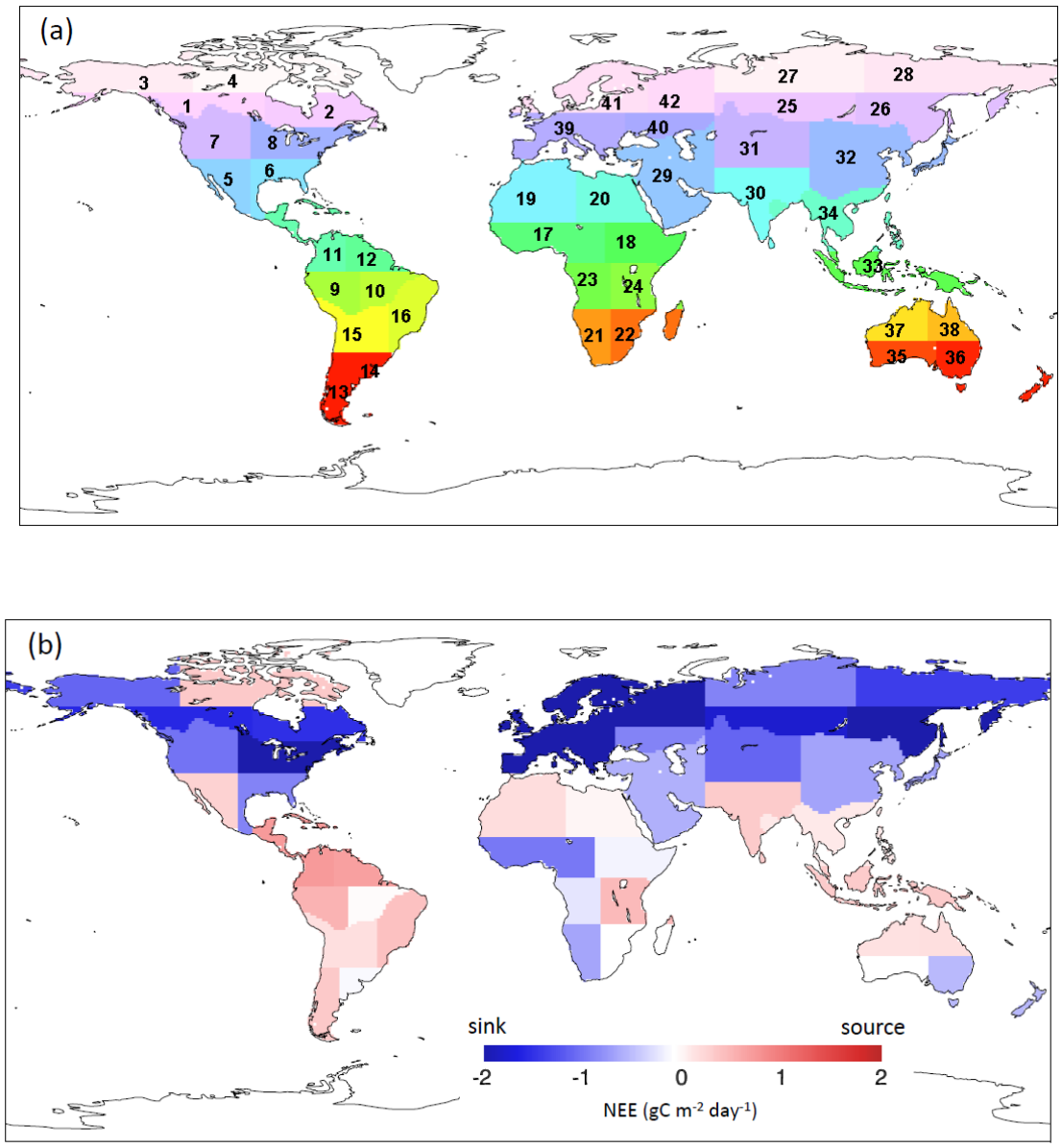

Figure 4.1. (a) Terrestrial region ID of GOSAT L4A and (b) global GOSAT biosphere flux on June 2009.

4.2.3. Bottom-up approach: support vector regression

Machine-learning-based regression was used to obtain spatiotemporal variations of surface CO_2 fluxes from ground observation data. The method was based on support vector regression (SVR), which is an empirical model based on a regression-type support vector machine that transforms nonlinear regressions into linear regressions by mapping the original low-dimensional input space into a higher-dimensional feature space using kernel functions

(e.g., Cristianini and Shawe-Taylor, 2000). As with other machine-learning models such as artificial neural networks or decision-tree learning algorithms, SVR requires a training process that determines a set of model parameters by minimizing the generalization error. SVR has advantages over other machine-learning models because the training always converges to a global optimal solution and the architecture of the SVR model does not need to be determined by experimentation, unlike artificial neural networks. SVR-based surface CO_2 flux estimation requires eddy flux observation data for the training and validation of the SVR model, and satellite remote sensing data for the construction of the SVR model and prediction of the spatiotemporal variations of surface CO_2 flux. The method was pioneered by Yang et al. (2006, 2007) for the estimation of regional gross primary productivity (GPP) and evapotranspiration across the conterminous U.S. To date, the SVR model has been applied and found effective in the prediction of surface CO_2 fluxes in Japan, East Asia, and Alaska (Ichii et al., 2010; Saigusa et al., 2010; Ueyama et al., 2013).

In the present study, the SVR models were constructed using a set of satellite remote sensing data in conjunction with CO_2 flux data (GPP and NEE) from 144 eddy covariance observation sites registered as Free Access FLUXNET data (available from http://www.fluxdata.org/DataInfo/default.aspx). CO_2 fluxes observed from 2001–2004 were used to train the SVR model and the remaining data after 2005 were used for validation of the model results. In the training phase of the SVR model, a threefold cross-validation process was used to determine three model parameters: a constant determining the trade-off between model complexity and training error, the width of an insensitive error band, and a kernel parameter. In this process, training data (CO_2 fluxes before 2005) were divided randomly into three non-overlapping subsets. Training was performed three times on two of the subsets and the remaining subset reserved for testing. Parameters yielding the lowest cross-validation errors (minimum RMS errors between prediction and observation) were identified by optimization

using the Levenberg–Marquhart method, also known as the dumped least squares method (Levenberg, 1944).

Following the above training method, 24 SVR models were generated based on combinations of the 10 sets of satellite remote sensing data shown in Table 4.1 (spatial resolution converted to 0.25º × 0.25º equirectangular projection). Including the combination used in the GPP estimation across North America (SRAD, daytime LST, and EVI) (Yang et al., 2007), 24 variations were created based on the following considerations: (1) two types of LST (daytime or daily average), (2) three types of vegetation parameters (EVI, NDVI, or LAI), (3) FPAR in place of vegetation parameters, (4) temporal coverages of vegetation parameters (16 days or 8 days: MOD13A2 or MOD43B4-based products), and (5) mixed uses of vegetation parameters (from two to four parameters). These combinations of remote sensing data (see Table 4.2) were used to create the SVR models for both the GPP and NEE estimations.

Among the 24 SVR models for GPP and NEE, we obtained a slight variation in performance against observations (R = 0.72−0.77 for GPP and R = 0.62−0.66 for NEE: Fig. 4.2a and 4.2b). Results from the multiple combinations did not vary significantly from those of the combination used in the original work of Yang et al. (2007) (model 1 in Table 4.2). This suggests that the inclusion of key variables (i.e., SRAD, LST, and a vegetation parameter) is rather more important for predicting CO_2 fluxes than for considering their variations. Based on the results of the 24 SVR models, the ensemble mean and uncertainty of global monthly GPP and NEE were calculated for 2001−2011 at a resolution of 0.25º × 0.25º (Fig. 4.3a). Although the uncertainties in the SVR flux and the GOSAT biosphere flux are addressed in the analysis, it should be noted that they are not directly comparable because the former represent a spread around the best estimate and the latter represents a spread of the Gaussian distribution. Subsequently, to be compatible with the GOSAT biosphere flux, the estimated NEE was converted to the 42-tile average configuration (Fig. 4.3b). Hereafter, we refer to the SVR-based

NEE, prepared using the aforementioned process, as the SVR biosphere flux.

Table 4.2. Combinations of satellite-based data used to construct the 24 SVR models. The 10 input parameters used for the construction of the models were SRAD, daytime LST, daily LST, EVI, NDVI, LAI, FPAR, GR43, NDVI43, and EVI43.

Model	SRAD	Daytime LST	Daily LST	EVI	NDVI	LAI	FPAR	GR43	NDVI43	EVI43
1	O	O	-	O	-	-	-	-	-	-
2	O	O	-	-	O	-	-	-	-	-
3	O	O	-	-	-	O	-	-	-	-
4	O	O	-	-	-	-	O	-	-	-
5	O	O	-	-	-	-	-	O	-	-
6	O	O	-	-	-	-	-	-	O	-
7	O	O	-	-	-	-	-	-	-	O
8	O	-	O	O	-	-	-	-	-	-
9	O	-	O	-	O	-	-	-	-	-
10	O	-	O	-	-	O	-	-	-	-
11	O	-	O	-	-	-	O	-	-	-
12	O	-	O	-	-	-	-	O	-	-
13	O	-	O	-	-	-	-	-	O	-
14	O	-	O	-	-	-	-	-	-	O
15	O	-	O	O	O	O	-	-	-	-
16	O	-	O	O	O	O	-	O	-	-
17	O	-	O	-	-	O	-	O	O	O
18	O	-	O	-	-	O	-	-	O	O
19	O	-	O	-	-	O	-	O	-	-
20	O	-	O	-	-	O	-		O	-
21	O	-	O	-	-	O	-	-	-	O
22	O	-	O	-	-	-	-	O	O	-
23	O	-	O	-	-	-	-	O	-	O
24	O	-	O	-	-	-	-	-	O	O

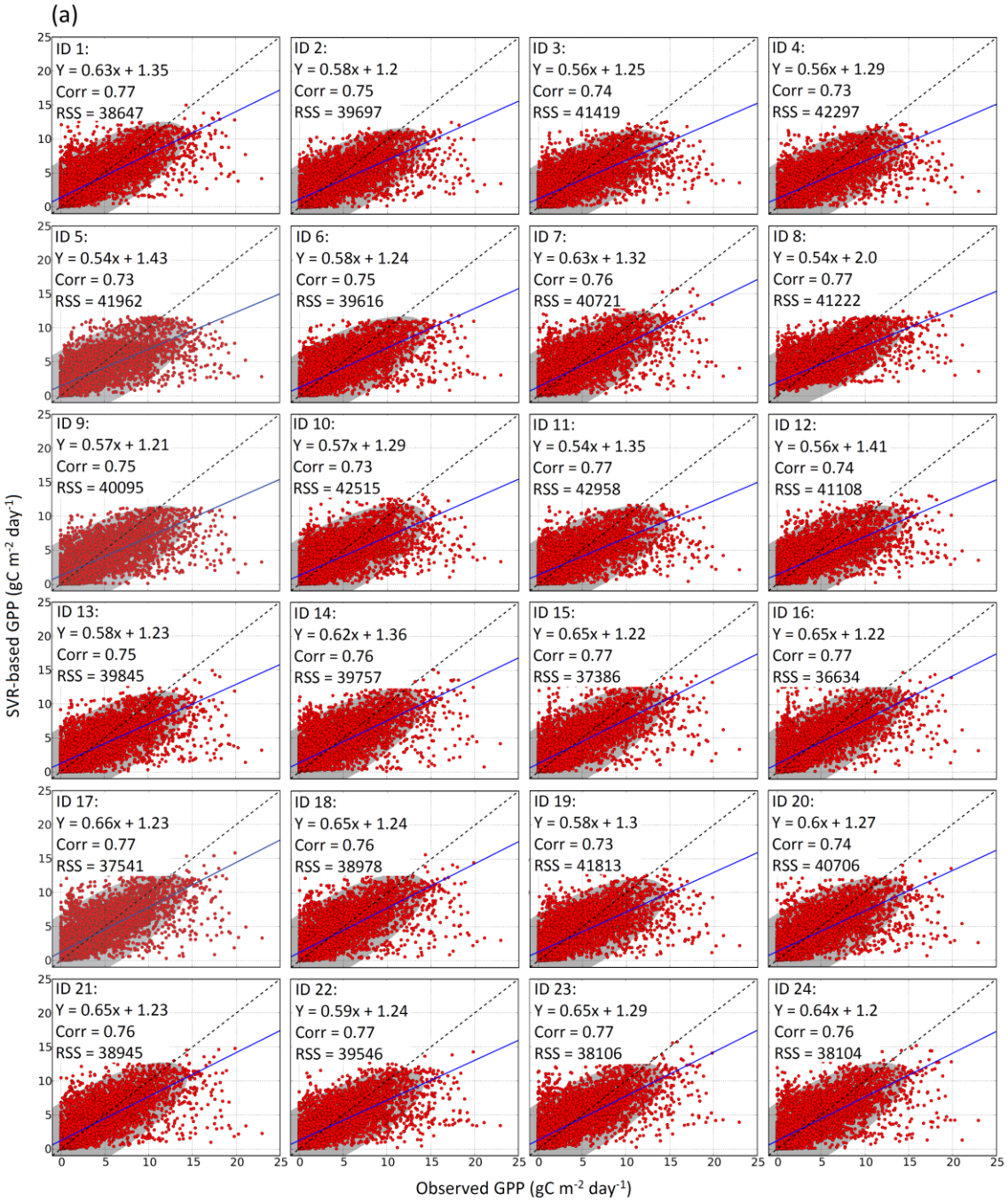

Figure 4.2. Validation of (a) GPP and (b) NEE estimated by the 24 SVR models at the FLUXNET sites. The results from the 24 models constructed from combinations of 10 inputs (SRAD, daytime LST, daily LST, EVI, NDVI, LAI, FPAR, GR43, NDVI43, and EVI43) are shown with regression, Pearson coefficient (Corr., $p < 0.01$), residual sum of squares (RSS), and 95% confidence ellipse.

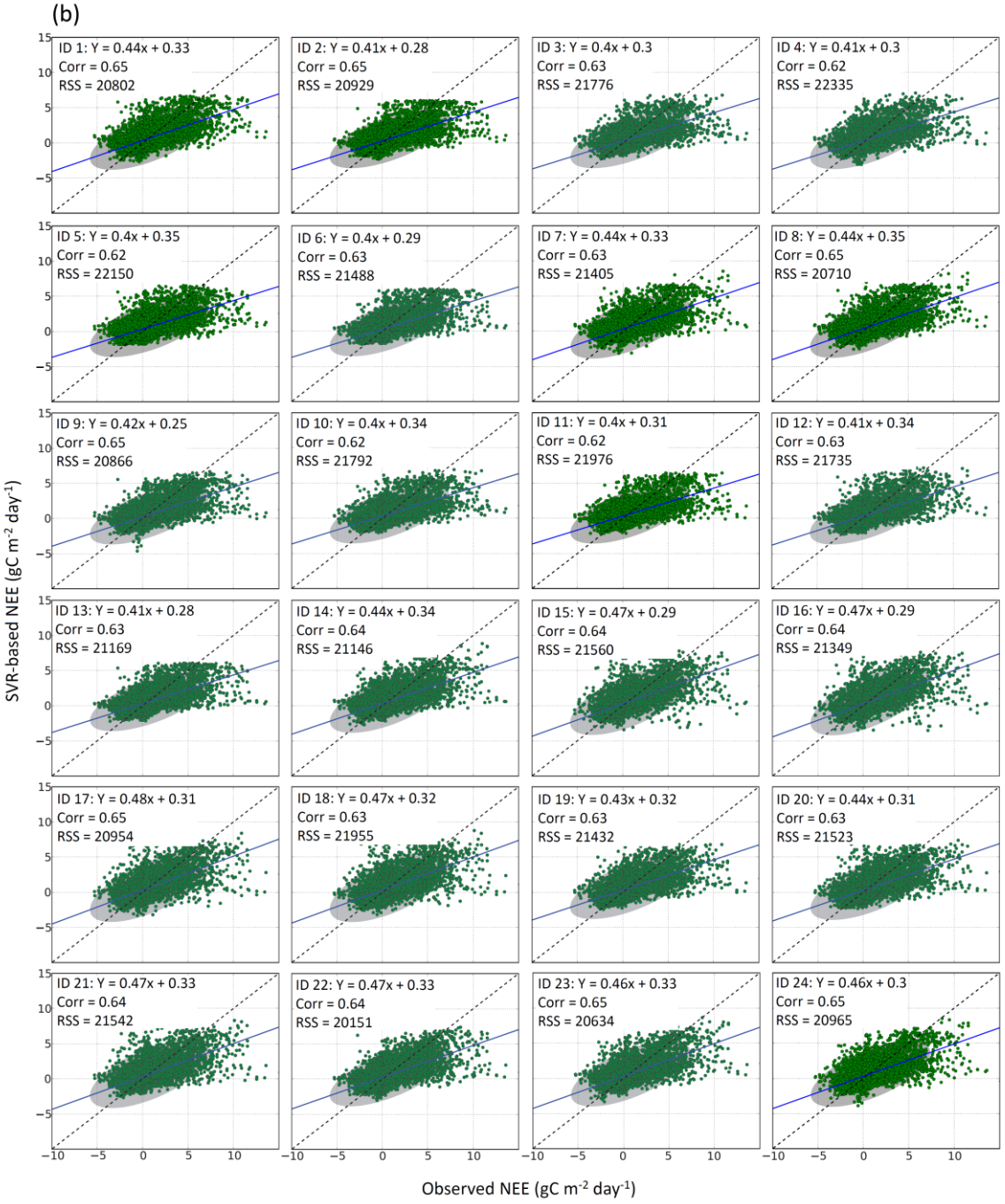

Figure 4.2.continued

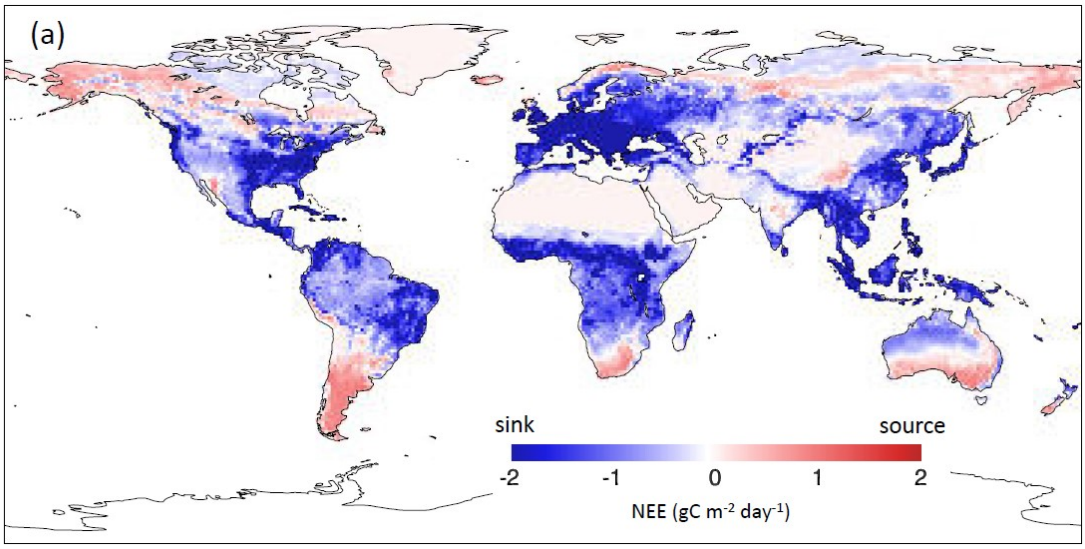

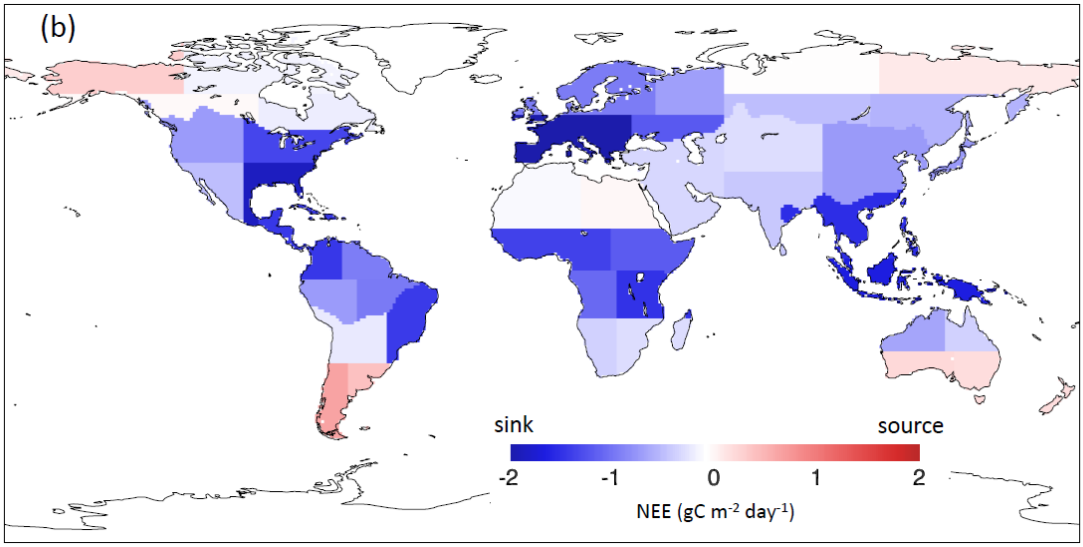

Figure 4.3. SVR-based global NEE on June 2009 with (a) the original 0.25º × 0.25º resolution and (b) tile average configuration.

4.3. Results

4.3.1. Regional seasonal variations and CO_2 budgets of the GOSAT and SVR biosphere fluxes

Seasonal variations (three-month average) of the GOSAT and SVR biosphere fluxes were compared from June 2009 to August 2011 and in most regions of the Northern Hemisphere, the two exhibited similar seasonal variations (Fig. 4.4a). Good agreement

between the two approaches was identified in boreal regions, i.e., northwestern boreal North America (region ID 3), northwestern Europe (region ID 41), and northeastern and southwestern boreal Eurasia (region IDs: 28 and 25, respectively). In temperate regions such as northwestern and northeastern parts of the U.S. (region IDs: 7 and 8, respectively), southwestern Europe (region ID 39), and northeastern Asia (region ID 32), which are characterized by high population densities (including the world's largest cities: New York, London, Madrid, Paris, Beijing, and Tokyo) and active industries, the total surface flux of GOSAT L4A was inclined more towards CO_2 source, by approximately 0.1−1.0 gC m^{-2} day^{-1} compared with the SVR biosphere flux, because of non-negligible fossil fuel emissions. However, better agreement in seasonal variation was identified when only the attribution of biosphere flux was compared between the GOSAT and SVR.

In the sub-tropical and tropical regions, seasonal variations of the GOSAT and SVR biosphere fluxes differed substantially from one another (Fig. 4.4b). For example, in tropical South America (region IDs: 9, 10, and 15), the GOSAT biosphere flux showed seasonal variations pivoted around net CO_2 neutral (NEE = 0 gC m^{-2} day^{-1}), while the SVR biosphere flux showed variations that tended towards CO_2 sink. A similar discrepancy was identified in tropical South Asia (region ID 33) and tropical and sub-tropical Africa (region IDs: 17, 18, 23, and 24). In these regions, the SVR biosphere flux indicated CO_2 source in only a few seasons, even with the range of uncertainty taken into account.

Despite consistent seasonal variations, the CO_2 budgets of the two biosphere fluxes were deviated in boreal and temperate regions (Fig. 4.5a). There were a few boreal regions where opposite CO_2 sink–source trends were indicated by the two estimates (e.g., region IDs: 3, 4, and 27; SVR biosphere flux indicated CO_2 sink and GOSAT biosphere flux CO_2 source). Differences between the total boreal and temperate CO_2 budgets of the two biosphere fluxes were not negligible: -1.2 ± 0.3 Pg C yr^{-1} (GOSAT) and -0.1 ± 0.5 Pg C yr^{-1} (SVR) in boreal

regions, and -2.5 ± 0.8 Pg C yr^{-1} (GOSAT) and -4.6 ± 1.9 Pg C yr^{-1} (SVR) in temperate regions (Fig. 4.5b).

Contrasting seasonal variations in sub-tropical and tropical regions affected the CO_2 budget from the two approaches considerably. As illustrated in Figure 4.5a, the GOSAT biosphere flux yielded CO_2 budgets in sub-tropical and tropical regions close to neutral, e.g., 0.19 ± 0.12 Pg C yr^{-1} (northeastern South Africa: region ID 24) and -0.17 ± 0.16 Pg C yr^{-1} (southeastern temperate Asia: region ID 30). However, budgets from the SVR biosphere flux indicated large net sinks in most sub-tropical and tropical regions. In particular, the sink found in southwestern tropical Africa (region ID 17: 2.7 ± 1.0 Pg C yr^{-1}) was several times greater than that of the GOSAT biosphere flux. Thus, the total sub-tropical and tropical CO_2 budgets estimated by the two approaches were substantially different: -0.2 ± 0.7 Pg C yr^{-1} (GOSAT) and -7.4 ± 0.8 Pg C yr^{-1} (SVR) in the sub-tropical region, and 0.3 ± 0.6 Pg C yr^{-1} (GOSAT) and -11.2 ± 0.6 Pg C yr^{-1} (SVR) in the tropical region (Fig. 4.5b). We identified that these large differences in sub-tropical and tropical CO_2 budgets accounted for 83% of the difference in global CO_2 budget: -3.7 ± 2.7 Pg C yr^{-1} (GOSAT) and -26.7 ± 4.2 Pg C yr^{-1} (SVR).

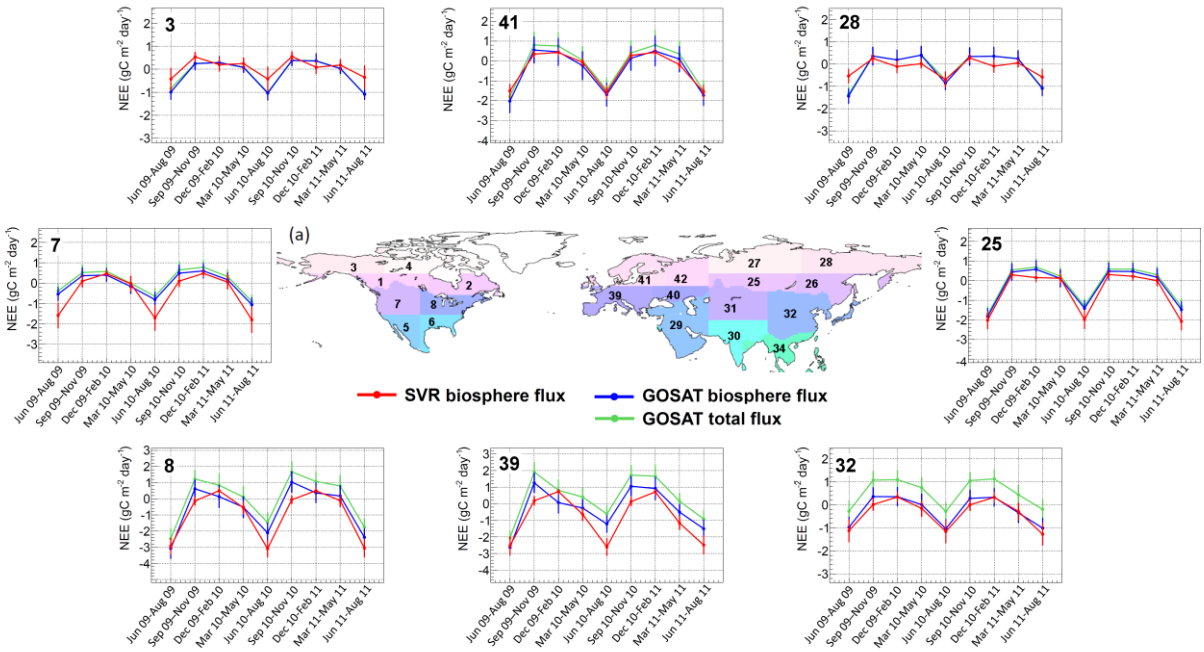

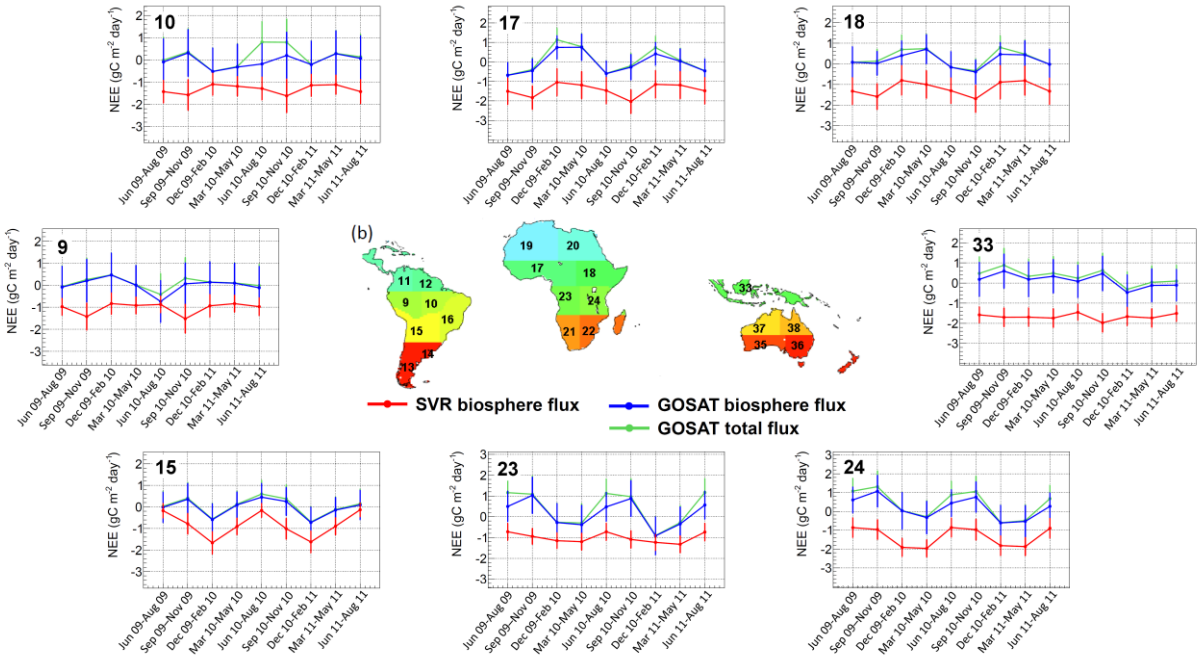

Figure 4.4. Three-monthly average seasonal variations of regional NEEs from the bottom-up (SVR) and top-down (GOSAT biosphere flux) approaches. The eight regional NEEs were each selected from (a) boreal and temperate regions (region IDs: 3, 7, 8, 25, 28, 32, 29, and 41) and (b) sub-tropical and tropical regions (region IDs: 9, 10, 15, 17, 18, 23, 24, and 33).

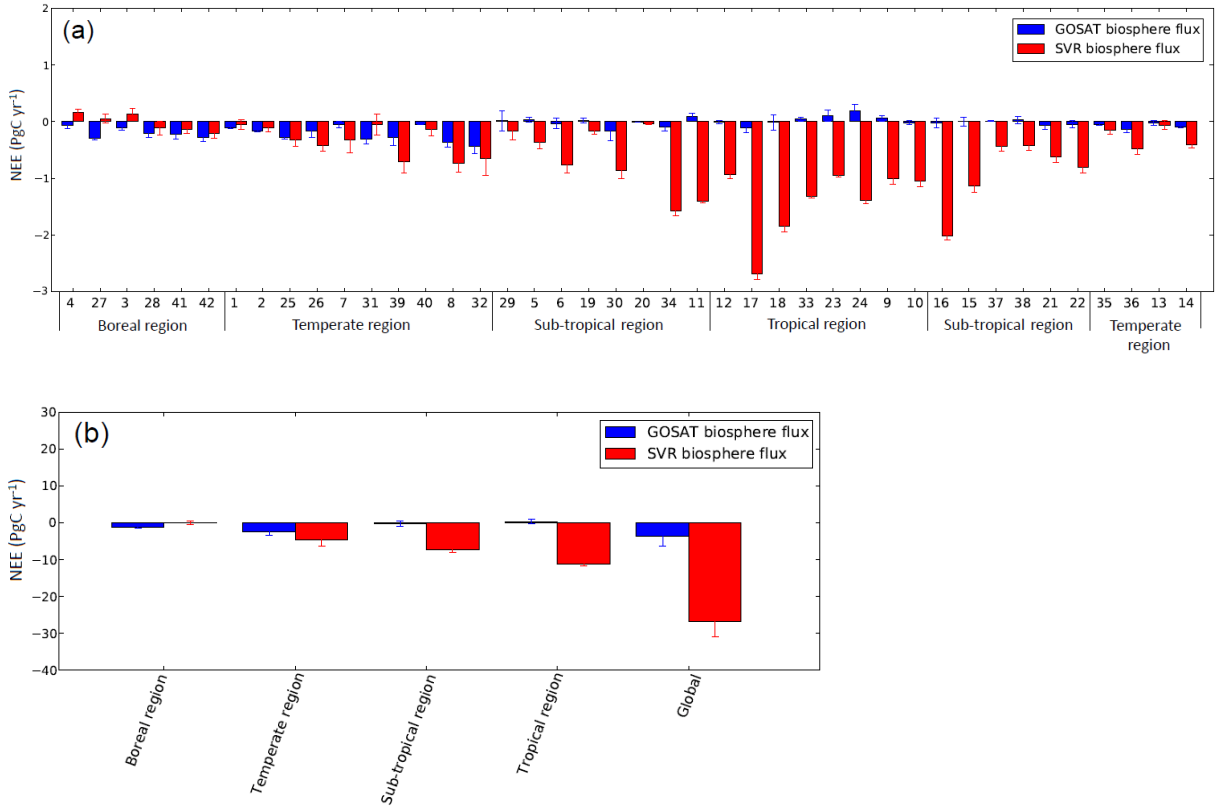

Figure 4.5. Mean budgets of the SVR and GOSAT biosphere fluxes for June 2009–October 2011. The estimates are shown (a) for 42 terrestrial regions and (b) for major terrestrial regions (boreal, temperate, sub-tropical, and tropical regions) and the globe.

3.2. Response to contrasting spring temperature anomalies

Because the seasonal variations in boreal and temperate regions was reasonably consistent, we further investigated the GOSAT and SVR biosphere fluxes by analyzing the responses of the fluxes to the contrasting spring temperature anomalies in North America and boreal Eurasia. The 2009–2010 El Niño event induced higher temperatures across mid-northern regions of North America and lower temperatures across southwestern regions of boreal Eurasia in spring 2010 (JMA, 2011) (Fig. 4.6a). However, the 2010–2011 La Niña event caused converse anomalies in 2011, i.e., lower spring temperatures in North America and higher spring temperatures in boreal Eurasia (JMA, 2012). Correspondingly, the MODIS NDVI indicated that vegetation in those regions was influenced by the spring temperature anomalies. The 2010 spring temperature anomalies induced early growth in North America and late growth in boreal Eurasia, and the 2011 spring temperature anomalies induced the opposite trends of vegetation growth (Fig. 4.6b). These spring temperature anomalies and their corresponding influence on vegetation are expected to influence seasonal variations of surface CO_2 flux because of the strong relationship between vegetation activities and CO_2 fluxes.

The GOSAT biosphere flux showed clear indication of the positive response to the contrasting spring temperature anomalies (Fig. 4.7a and 4.7b). In the event of the higher 2010 spring temperature in North America, the GOSAT biosphere flux shifted toward CO_2 sink (0.18–0.22 gC m^{-2} day^{-1}) during March–June. Similarly, under the effects of the cooler 2011 spring temperature, it tended towards CO_2 source (~0.12 gC m^{-2} day^{-1}) during the same period. In the case of the contrasting spring temperature anomalies in boreal Eurasia, the GOSAT biosphere flux exhibited converse anomalies to the case in North America, i.e., a sudden shift toward CO_2 source (~0.45 gC m^{-2} day^{-1}) during March–June 2010 and CO_2 sink (~0.4 gC m^{-2}

day^{-1}) during March–June 2011. The a priori biosphere flux (the VISIT model simulation) and biosphere flux from an inversion constrained only by the GV data showed positive responses to the spring temperature anomalies in both regions, but they were associated with weaker variation compared with the GOSAT biosphere flux.

Similar to the GOSAT biosphere flux, the SVR biosphere flux indicated a positive response to the spring temperature anomalies (Fig. 4.8a and 4.8b). The two main inputs to the SVR models, i.e., MODIS LST and NDVI, showed clear contrasting spring anomalies in North America and boreal Eurasia, as illustrated in the spatial distributions in Fig. 4.6. In response to the anomalies identified in those inputs, the SVR-based GPP indicated higher spring CO_2 uptake in 2010 and weaker CO_2 uptake in 2011 in North America, and it showed the opposite pattern in boreal Eurasia. Similar to the LST, NDVI, and SVR-based GPP, the SVR biosphere flux indicated spring anomalies; however, its variations were slightly less profound than the GOSAT biosphere flux.

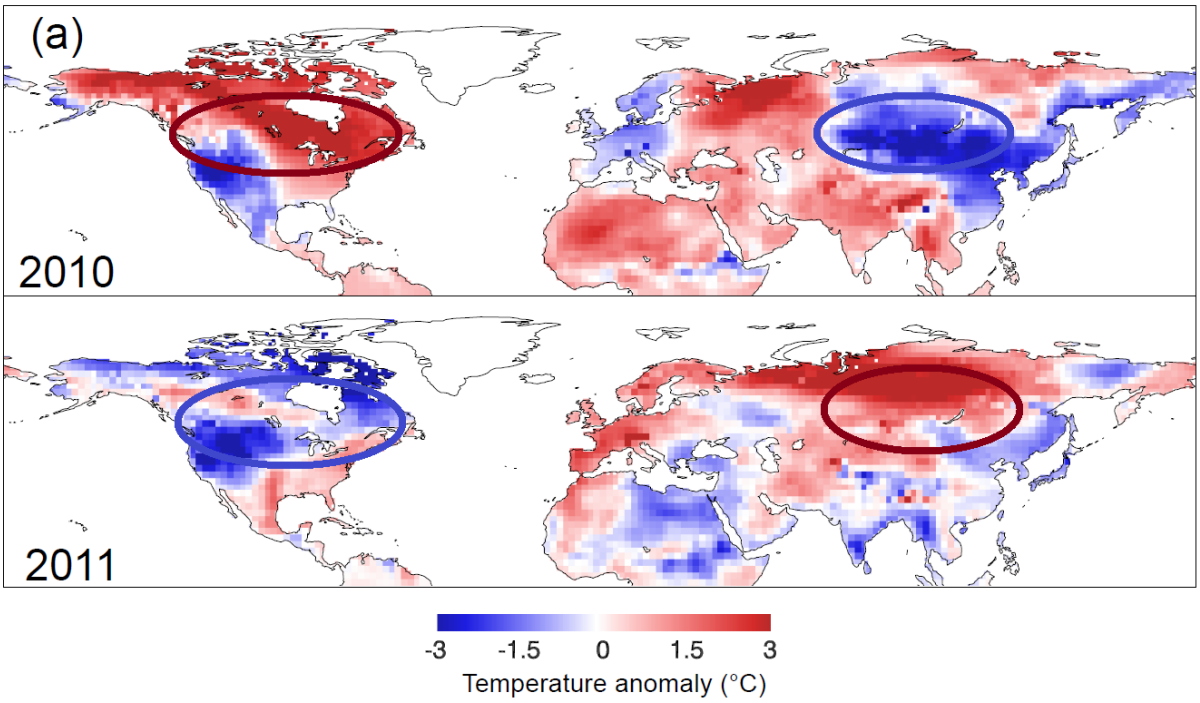

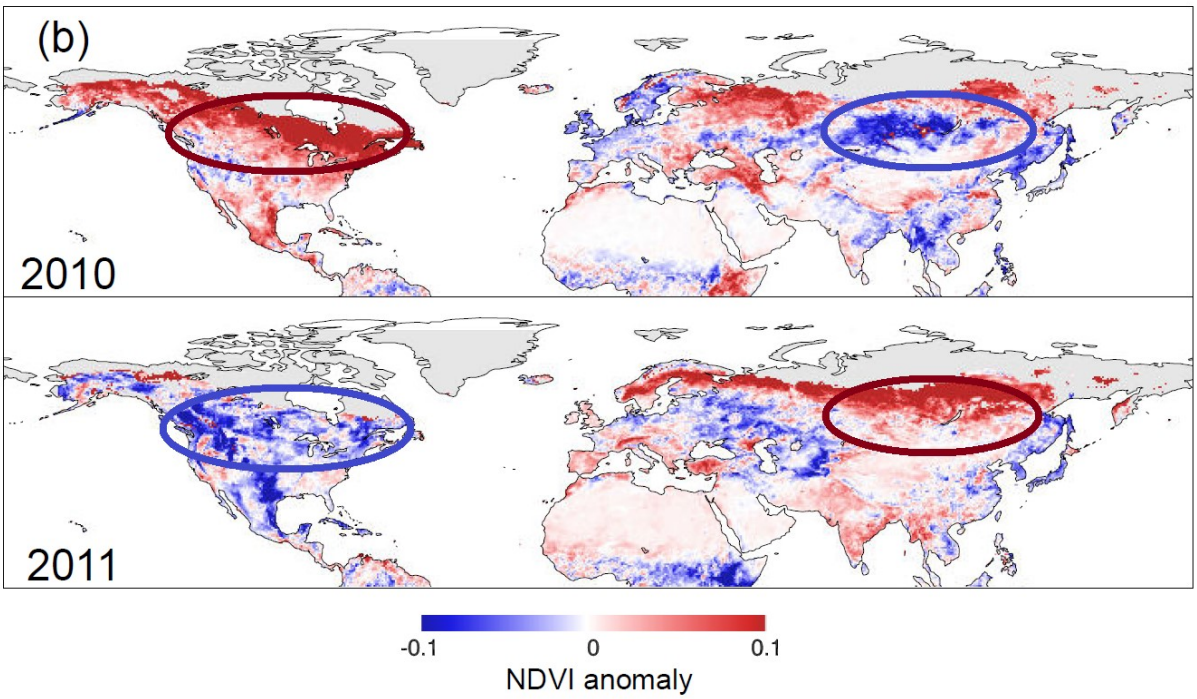

Figure 4.6. Distributions of spring (an average of April–May) (a) air temperature (NCEP/NCAR reanalysis data (Kalnay et al., 1996)) and (b) MODIS NDVI anomalies in the Northern Hemisphere for base period of 2009–2011. For NDVI anomaly, pixels corresponding to LST values of <0 °C were disregarded (gray shading) in order to eliminate unrealistically high NDVI values due to snow cover.

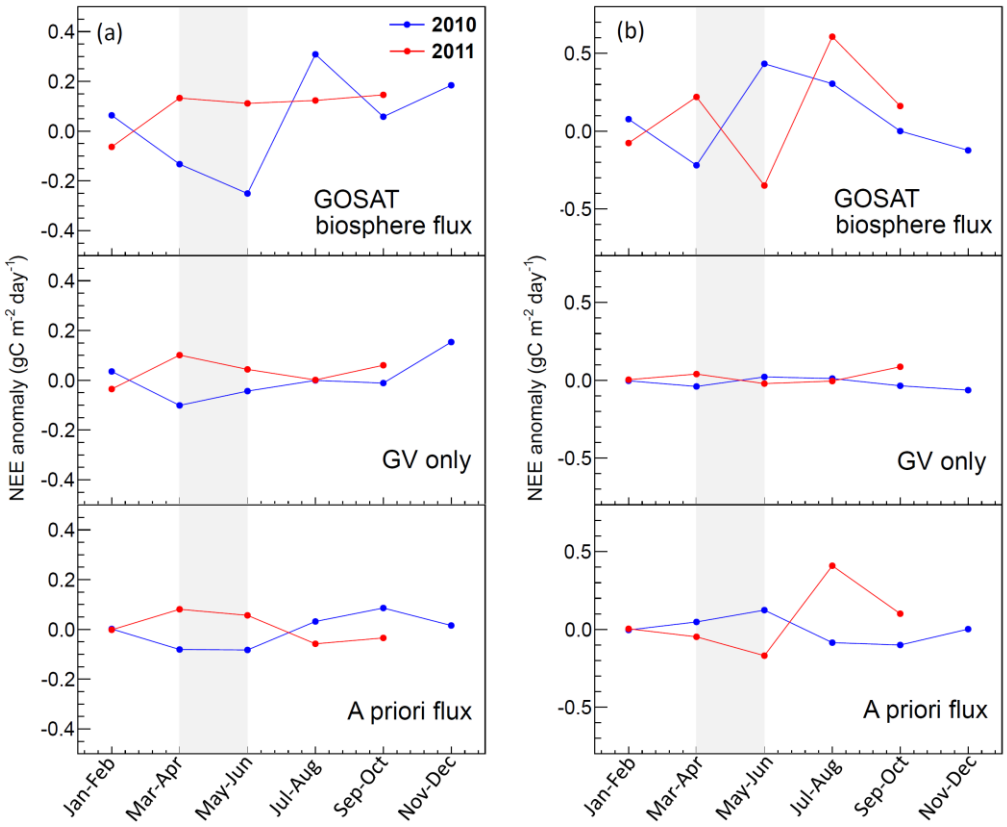

Figure 4.7 Two-monthly average seasonal anomalies of biosphere flux from GOSAT L4A, GV-based inversion (GV only), and a priori flux in (a) North America (a mean of three regional results: region IDs: 1, 2, and 8) and (b) boreal Eurasia (region ID 25). Anomalies refer to base period of 2010–2011.

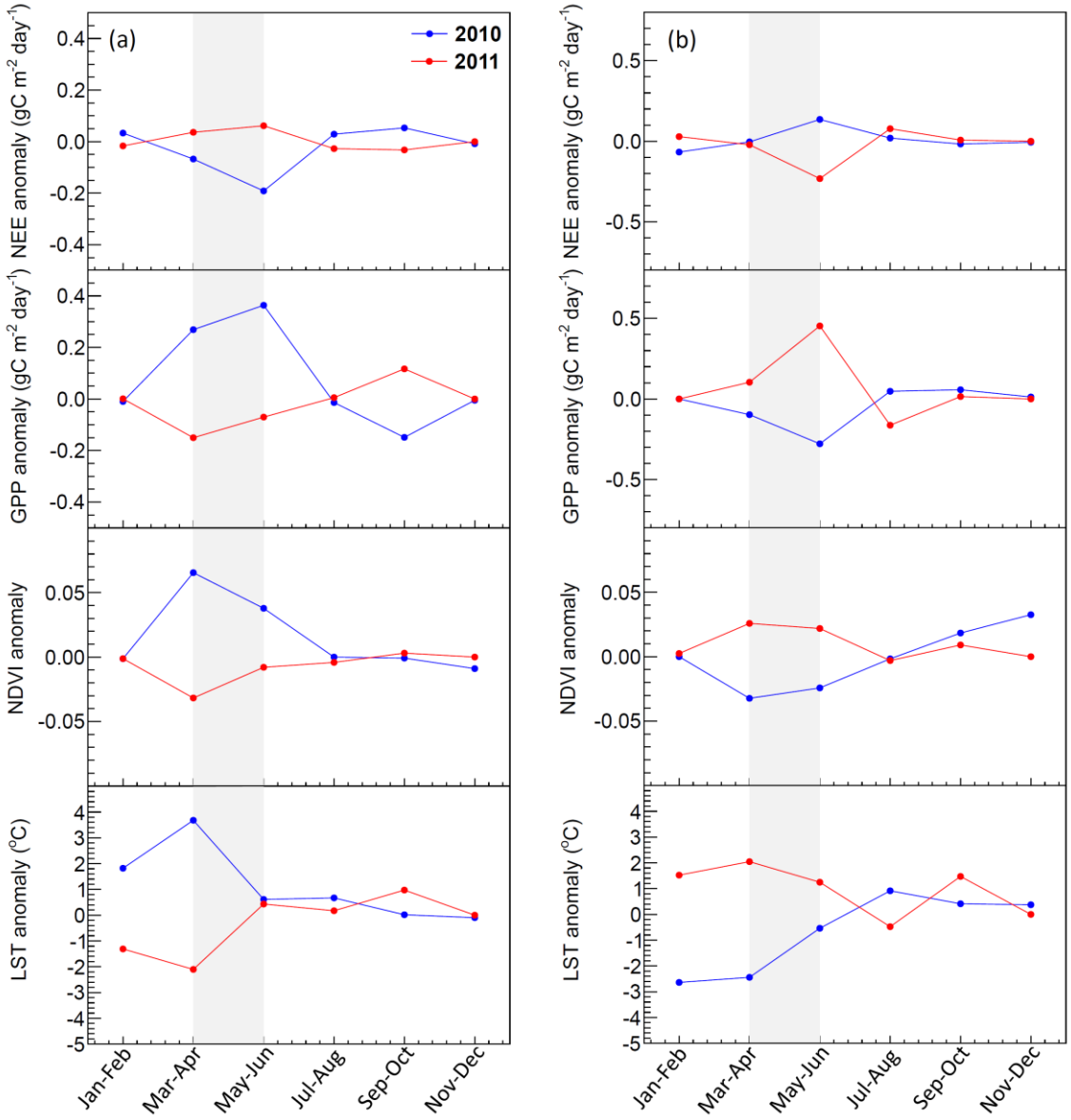

Figure 4.8. Two-monthly average seasonal variations of the SVR biosphere flux, SVR-based GPP, MODIS NDVI, and daytime LST in (a) North America (region IDs: 1, 2, and 8) and (b) boreal Eurasia (region ID 25). Anomalies refer to base period of 2010–2011.

3.3. Trends of annual GPP and NEE in the SVR model, and observations

In order to investigate the reasons for the large CO_2 sink in the tropics produced by the SVR model, the relationship between annual GPP and NEE was examined using annual eddy flux observations from the global compilation of ecological site studies (Luyssaert et al., 2007,

2010). Scatter plots of annual GPP and NEE showed similarities and dissimilarities to the trends of the SVR model, ecosystem models, and ground observations (Fig. 4.9). Linear GPP–NEE correlations were identified in the results of the SVR model and eddy flux observations. The slopes of the linear regressions were reasonably close to one another for the cases of the Arctic region (Fig. 4.9a: -0.18 and -0.35), North America (Fig. 4.9b: -0.32 and -0.30), Europe (Fig. 4.9c: -0.24 and -0.52), and Asia (Fig. 4.9d: -0.19 and -0.20).

The GPP–NEE relationship derived from the SVR models was inconsistent with observations in productive tropical ecosystems (Fig. 4.9e). Below a GPP value of 3000 gC m^{-2} yr^{-1}, the SVR model showed a linear GPP–NEE relationship with a slope similar to the observations (Fig. 4.9e: -0.23 and -0.38, respectively), but it failed to reproduce the observed GPP above that value. Observations above this value of GPP no longer showed a linear GPP–NEE relationship; instead, they showed mixed patterns of sinks, sources, and neutral CO_2. We identified that the observation sites that showed these high values of GPP were located in tropical rainforests (within a latitudinal range of 5N°−3S°).

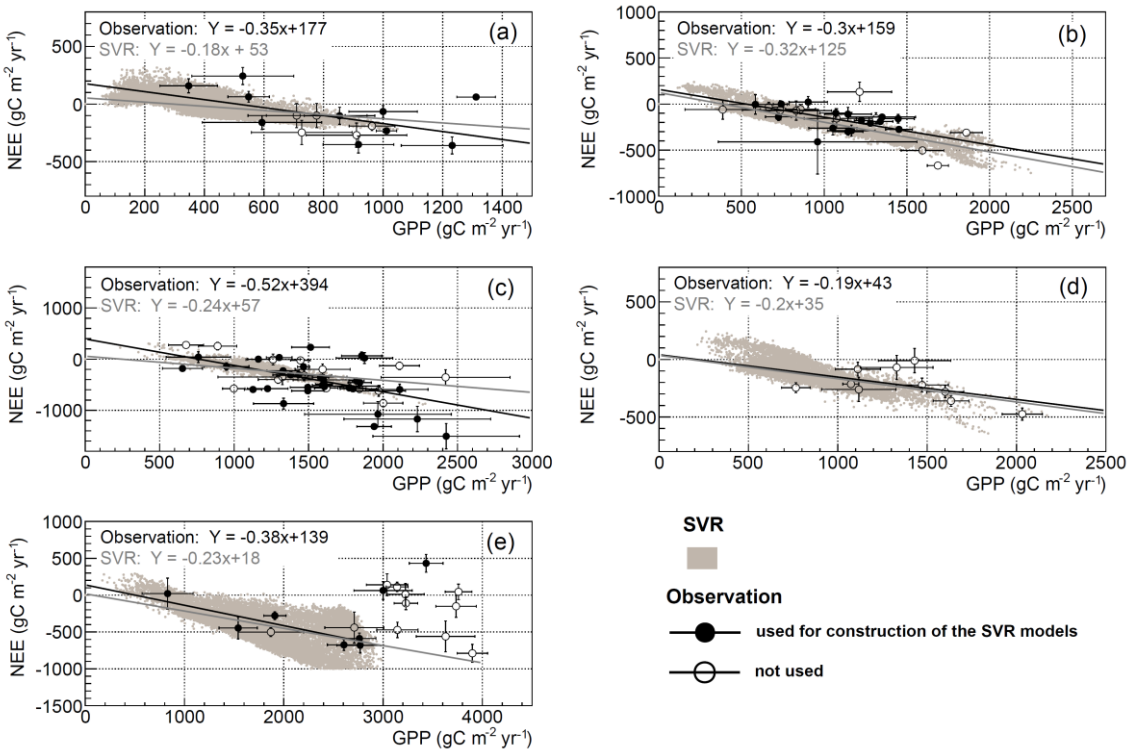

Figure 4.9. Distributions of annual GPP and NEE in (a) the northern high latitudinal region (>60°N), northern mid-latitudinal region (30°–60°N), (b) the U.S. (50°–180W), (c) Europe (50°E–20°W), (d) East Asia (50°−180°E), and (e) the tropical and sub-tropical region (30°N−30°S). Mean annual fluxes (2000−2010) of the SVR models with spatial resolution of 0.5º × 0.5º are shown together with ground observations obtained from the global compilation of ecological site studies version [*Luyssaert et al*., 2007, 2010]. Site data used and not used for the construction of the SVR models are indicated by full and open circles, respectively.

4. Discussion

4.1. Reliability of the data-driven top-down and bottom-up approaches in boreal and temperate regions

The comparison of the data-driven top-down (GOSAT L4A) and bottom-up (SVR) biosphere fluxes revealed agreement in the seasonal variation in boreal and temperate regions across continents, but offsets in net CO_2 budget. This results indicate that the data integration effectively produces similar seasonal patterns, but it is not as effective as to bring close agreement in net CO_2 budget. In order to produce consistent regional net CO_2 budgets between the top-down and bottom-up approaches, ecosystem models may be a better tool than machine-learning models because the former has freedom in parameters for net CO_2 budget refinement, whereas the machine-learning models are strictly constrained by data availability.

Despite offsets in net CO_2 budget, the same responses to the spring temperature anomalies in North America and boreal Eurasia strengthen the reliability of the two data-driven biosphere fluxes in seasonal patterns across boreal and temperate regions. The clearer anomalies found in the GOSAT biosphere flux than the a priori and GV-only biosphere fluxes indicate that GOSAT XCO_2 may be a more sensitive metric for diagnosing seasonal flux anomalies over these regions than either biosphere models or the surface data included in GV (Fig. 4.7). In particular, the successful anomaly detection in boreal Eurasia signifies the effect of GOSAT XCO_2 because, unlike North America, the GV sites are absent in boreal Eurasia. This effect is also illustrated in a posterior CO_2 concentration field (GOSAT L4B). In 2010 and

2011, monthly time series of Siberian tower observations managed by NIES (Azovo (AZV) at N 54°42′18″and E 73°01′45″ and Igrim (IGR) at N 63°11′25″ and E 64°24′56″: *Sasakawa et al*., 2013) and the corresponding data from L4B indicated similar variations (Fig. 4.10). In addition to the anomalies presented here, a significant reduction of summer CO_2 uptake in Eurasia between 2009 and 2010 was indicated by the GOSAT XCO_2 retrievals (Guerlet et al., 2013). Furthermore, consistent with the result of the spring anomalies, a joint inversion of the GOSAT XCO_2 and surface CO_2 data exhibited a stronger signal of reduction of summer CO_2 uptake in western Eurasia compared with a surface-data-only inversion. Work by Basu et al. (2014) also indicated that a feature of the GOSAT XCO_2 retrievals is to induce a larger dynamic seasonal cycle of CO_2 flux.

The successful detection of the spring anomalies in the SVR biosphere flux is attributable to the relevant input parameters (i.e., LST and NDVI). The spring temperature anomalies represented by LST were reflected well in the NDVI (Fig. 4.8). Moreover, influence from the anomalous spring temperatures was also identified in other vegetation parameters used for the construction of the SVR models, i.e., LAI and EVI (validated, but results not shown). Information contained in these parameters led to the successful detection of the spring anomalies in photosynthesis and net biosphere flux. A previous study that analyzed the effect of the low summer radiation in the East Asian ecosystem in 2003 also indicated that the SVR model was capable of detecting an anomalous spatiotemporal pattern of GPP because of distinct negative summer anomalies inherited via the input SRAD data (Saigusa et al., 2010).

The common anomalies identified in the GOSAT and SVR biosphere fluxes suggest that the XCO_2 retrievals used in the GOSAT inversion and the meteorological and vegetation input parameters used in the SVR models are equally effective in producing spatiotemporal variations of biosphere flux. One discrepancy between the two estimates is that the GOSAT biosphere flux yielded a slightly stronger signal of the spring anomalies compared with that of

the SVR biosphere flux in both North America and boreal Eurasia. This tendency could be characteristic of the two data-integrated approaches. At this stage, it is difficult to determine more realistic anomalous signal from one another with the available information.

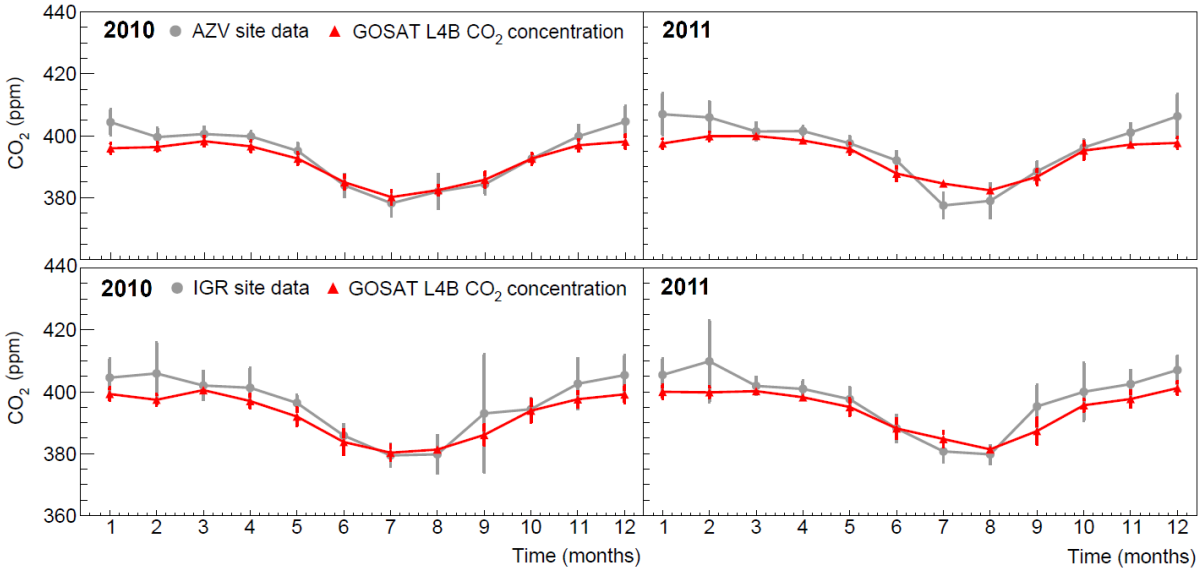

Figure 4.10. Temporal variations of monthly mean of daytime CO_2 concentrations (13:00-17:00 LST) from two Siberian tower observations (AZV and IGR sites) and GOSAT L4B in 2010 and 2011.

4.2. Discrepant biosphere fluxes in sub-tropical and tropical regions

The substantial disagreement in sub-tropical and tropical regions indicates that major discrepancies in CO_2 flux estimations remain in either or both of the top-down and bottom-up approaches. We found that the large gap in global CO_2 budget (~23 Pg C yr^{-1}) was mostly attributable to disagreement in sub-tropical and tropical regions (~19 Pg C yr^{-1}). A previous study has suggested that a potential cause for inconsistent global CO_2 budgets between the top-down and bottom-up approaches was due to CO_2 emissions that were not addressed by the bottom-up approaches, e.g., land use change and crop harvest emissions (Jung et al., 2011). However, this argument does not sufficiently explain the results of the present study, because global patterns of land use change and crop harvest activities do not indicate that CO_2 emissions from those activities are primarily evolved from sub-tropical and tropical regions. A

study based on FAO statistics has revealed considerable transition of land use during the last century in South America and Africa (46 and 107×10^3 km^{-2} yr^{-1}, respectively), but an even higher transition has occurred in Eurasia (159×10^3 km^{-2} yr^{-1}) (Hurtt et al., 2011). Increasing agricultural activities have been reported (frequent cropping and harvesting) during 2000–2011 in the agricultural countries in Africa and South America, but there has been a more profound increase in Asian countries, particularly in China and India (Ray and Foley, 2013).

The difference in availability of integrated data (CO_2 concentration data for the GOSAT inversion and eddy flux data for the SVR model) is a plausible explanation for the discrepant CO_2 budgets. The GOSAT XCO_2 retrievals were widely available across global terrestrial regions (Fig. 4.11a). In regions corresponding to Amazonian, central African, and southeast Asian rainforests, the frequency of XCO_2 retrievals for the study period was lower than for other regions (<100). However, in other sub-tropical and tropical regions, such as Australia, and mid-southern parts of South America and Africa, a large number of retrievals (100−1000) were obtained; as a result, nearly 30 % of the imposed uncertainty was reduced (Takagi et al., 2011). This result implies that despite variations in the XCO_2 retrievals, constraint by the observed CO_2 concentrations is effective for a wide range of sub-tropical and tropical regions. A comparison of five inversion models identified that the GOSAT XCO_2 retrievals induced a common uptake reduction in South America (region IDs: 15 and 16) and a common uptake enhancement in Africa (region IDs: 23 and 24) and tropical Asia (region ID 33) with respect to the results of surface-data-only inversions (Takagi et al., 2014). These common behaviors, regardless of different inversion models, suggest effective constraint by the GOSAT XCO_2 retrievals.

Compared with the GOSAT XCO_2 retrievals, the 144 FLUXNET sites are distributed rather sparsely around the world (Fig. 4.11b). Most of the FLUXNET sites are found in boreal and temperate regions of North America and Europe and only a few sites are found in Eurasia,

South America, Africa, and Australia. However, unlike the CO_2 concentration data in the inversion models (i.e., the GV data and XCO_2 retrievals), eddy flux data do not enforce regional constraints to the SVR model through its design, but instead they constrain CO_2 flux estimates of common biome types (Yang et al., 2008). Thus, despite there being no site located in East Asia, abundant data from boreal and temperate regions of North America and Europe enforce constraints on CO_2 fluxes of the same biome types in East Asia (resulting in the linear GPP–NEE trend that is consistent with observations: Fig. 4.9d). However, this characteristic of the SVR models imposes limitations on CO_2 flux estimates in sub-tropical and tropical regions, because there are only three sites representing the biomes in those regions. As illustrated by the scatter plot of annual GPP and NEE, the SVR model failed to reproduce the transition from the linear GPP–NEE relationship to the mixed relationship in the tropics (Fig. 4.9e). Above the threshold of transition (GPP = 3000 gC m^{-2} yr^{-1}), two site data that were used in the construction of the SVR models indicated a net CO_2 source, but their effects were not reflected in the results of the SVR model. Therefore, a sink–source trend of the SVR biosphere flux was largely constrained by the linear GPP–NEE relationship, regardless of different biomes, and this trend is the reason for the large CO_2 sink in the tropics.

Considering the data coverage difference between the two approaches, we consider that annual flux of the GOSAT biosphere flux is better estimated for sub-tropical and tropical regions than that of the SVR biosphere flux (Fig. 4.4b). Previous estimates of the carbon balance in the tropics have reported nearly neutral CO_2 budgets that are close to the results of the GOSAT biosphere flux: -0.61 ± 0.58 PgC yr^{-1} in Africa (Valentini et al., 2014) and approximately -0.1 PgC yr^{-1} in South America (Gloor et al., 2012). The large tropical sink of CO_2 produced by the SVR model is an artifact induced from the underrepresented biosphere flux due to the limited data coverage for tropical biomes. This issue regarding the tropics is also indicated by uncertainty in the SVR flux. The SVR uncertainty is lower in the tropics than

the temperate regions (0.6 Pg C yr^{-1} in the tropics and 1.9 Pg C yr^{-1} in the temperate region), which implies that all 24 SVR models equivalently produced unrealistically high CO_2 sink in the tropics. In order to improve this limitation in the performance of the SVR model, eddy flux observations need to become openly available because, as discussed before, the model relies heavily on the availability of training data. Furthermore, in addition to meteorological and vegetation parameters, factors relevant to CO_2 emissions, such as forest biomass, soil organic carbon, and disturbance information, might facilitate improvement in the performance of the empirical upscaling (Jung et al., 2011).

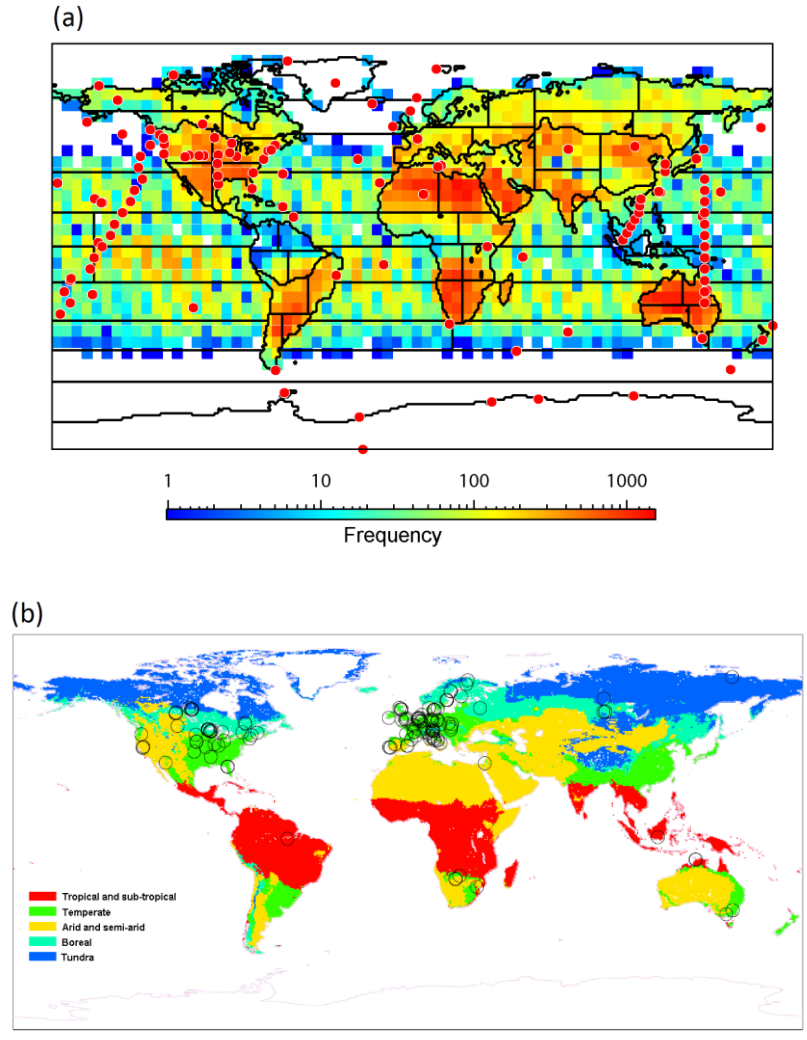

Figure 4.11. (a) Number of GOSAT Level 2 XCO_2 data per each 5° × 5° grid cell over the analyzed period (29 months from Jun 2009–Oct 2011). The overlaid red circles indicate the locations of GV sites chosen for this study (212 sites). Solid line indicates boundaries of the 64 source regions. (b) Global site distribution of FLUXNET data (144 sites) used for the construction of the SVR models. Site

distribution is overlaid on the biome classification map from Reich and Eswaran (2002).

5. Concluding remarks

This study presented the first insight into regional and global correlations of data-driven top-down and bottom-up CO_2 fluxes. From the comparison of biosphere CO_2 fluxes based on the two approaches, it was found that data integration effectively brings agreement in seasonal variation and response to climate anomalies in boreal and temperate regions; however, consistency in net CO_2 budget was not identified. Because of the limited spatial coverage of eddy flux data, seasonal variations in sub-tropical and tropical regions were largely different between the two approaches. The mean global CO_2 budgets by the two approaches from June 2009 to October 2011 were -3.7 ± 2.7 and -26.7 ± 4.2 Pg C yr^{-1}, respectively. The large differences in sub-tropical and tropical CO_2 fluxes were found to be responsible for the disagreement in the global CO_2 budgets.

Because of the global coverage of atmospheric CO_2 concentration data, the GOSAT inversion produces a better estimate of CO_2 flux than the SVR model. The GOSAT biosphere flux tends to yield stronger seasonal variations of CO_2 flux than the surface-data-only inversion and the SVR models, which makes it a useful product for anomaly detection. However, one shortcoming is that its application is limited to recent events because of the short temporal coverage (29 months from June 2009 to October 2011 for the current version). Although the excessively large CO_2 sinks in sub-tropical and tropical regions need to be improved, the empirical CO_2 flux upscaling by the SVR model still has an advantage over the GOSAT inversion because of the longer temporal coverage (2001–2010). Reliable seasonal variations in boreal and temperate regions indicate that long-term trends and anomalous events during the past 11 years over North America and Eurasia can be analyzed with the SVR biosphere flux. Thus, despite issues relating to the global budget, both methods of CO_2 exchange estimation

can be useful in appropriate research subjects and can provide new insights into the understanding of terrestrial CO_2 exchange.

Chapter 5

Summary and Conclusion

Throughout the site scale to global scale applications, this study analyzed effects of the model-data integration in carbon cycle. From the site scale application, is was identified that not only carbon fluxes such as GPP and RE, but also biometric observation such as biomass is an important factor for the estimation of the current and future net carbon exchanges. In other words, partial model-data integrations that are oriented to either carbon flux or biomass are not sufficient to refine net carbon exchange estimation.

Subsequently, this study demonstrated that the multiple data integration can induce plausible variations of frNPP that is difficult to infer from observation. By this supplementation to observation, responses of the cool-temperate forest ecosystem to contrasting climate anomalies were identified with multiple components of carbon cycle (i.e., GPP, fNPP, wNPP, frNPP, litterfall, and SR). Specifically, the negative summer PPFD and accompanying low temperature anomalies in 2003 decreased the GPP, SR, and RE, but did not affect the components of NPP. The positive early spring temperature anomaly in 2002 increased the GPP and wNPP and decreased the frNPP and SR. This result indicated that variation patterns of carbon fluxes cannot always be inferred from the GPP. Factors such as the timing and duration of the climate anomaly and allocation shift between components of the NPP need to be considered when characterizing the impact of anomalous climate events.

As the global scale applications of the model-data integrations, the current status of the global CO_2 budget was investigated via the comparison of the top-down and bottom-up approaches (GOSAT and SVR biosphere fluxes, respectively). Between the two approaches, good agreement in seasonal variation and response to climate anomalies in boreal and

temperate regions; however, consistency in net CO_2 budget was not identified because slight offsets in seasonal variations propagated into budget assessment. In sub-tropical and tropical regions, the coverage of observation data used in the integration was substantially sparse in the bottom-up approach than the top-down approach. As consequence, not only seasonal variations, but also CO_2 budgets in those regions were largely different between the two approaches. Because of this issue in sub-tropical and tropical regions, the two data integration approaches resulted in substantially different global CO_2 budgets: -3.7 ± 2.7 Pg C yr^{-1} by GOSAT and -26.7 ± 4.2 Pg C yr^{-1} by SVR.

As demonstrated in this study, the model-data integration is clearly an effectively tool for understanding carbon cycle. Despite its effectiveness, however, the research community has not been fully taking advantage of the model-data integration. For example, only a few studies were conducted at ecological research sites such as Howland and Harvard forests in the U.S. (e.g., Richarson et al., 2010; Keenan et al., 2011). Particularly before this study, the technique has not yet been applied in ecological research sites in Asia. Furthermore, previous studies focus on conceptual and technical aspects of the model-data integration (e.g., Raupach et al., 2005; Wang et al, 2009; Keenan et al., 2012), and application studies such as done in Chapters 2 and 3 have not been reported before to the author's knowledge. It is important to continue and extend application studies not only for new scientific findings about carbon cycle, but also for motivating the research community to take more advantage of the model-data integration.

As shown in the global scale application in Chapter 4, a limitation of data availability is a stagnant of the data integration approach. Because of sparse ground observations, global carbon flux estimation may be less effective in the bottom-up approach. To improve the current performance of the bottom-up approach, further compilation of ground observation data is necessary.

References

Ahl, D. E., Gower, S. T., Burrows, S. N., et al. (2006), Monitoring spring canopy phenology of a deciduous broadleaf forest using MODIS. Remote Sens. Environ, 104, 1, 88-95.

Alexander, L.V., Zhang, X., Peterson, T.C., et al. (2006) Global observed changes in daily climate extremes of temperature and precipitation, J. Geophys. Res., 111, D05109.

Andren O, Paustian K (1987) Barley straw decomposition in the field: a comparison of models. Ecology 68:1190-1200.

Andres, R. J., Gregg, J. S., Losey, L., et al. (2011), Monthly, global emissions of carbon dioxide from fossil fuel combustion. Tellus, 63B, 309−327.

Asner, G.P., Townsend, A.R., Braswell, B.H., (2000) Satellite observation of El Niño effects on Amazon forest phenology and productivity, Geophys. Res. Lett., 27, 981–84.

Baldocchi, D. (2008), 'Breathing' of the terrestrial biosphere: Lessons learned from a global network of carbon dioxide flux measurement systems, Aust. J. Bot., 56, 1–26.

Basu, S., Krol, M., Butz, A., et al. (2014), The seasonal variation of the CO_2 flux over Tropical Asia estimated from GOSAT, CONTRAIL, and IASI, Geophys. Res. Lett., 41, 1809–1815.

Beer, C., Lucht. W., Schmullius. C., and Shvidenko. A. (2006), Small net carbon dioxide uptake by Russian forests during 1981–1999, Geophys. Res. Lett., 33, L15403.

Black, T. A., Chen, W. J., Barr, A. G., et al. (2000) Increased carbon sequestration by a boreal deciduous forest in years with a warm spring, Geophys. Res. Lett., 27, 1271–1274.

Bonan, G. B., Lawrence, P. J., Oleson, K.W., et al. (2011), Improving canopy processes in the Community Land Model version 4 (CLM4) using global flux fields empirically inferred from FLUXNET data, J. Geophys. Res., 116, G02014.

Bruhwiler, L. M. Michalak, P., A. M., Peters, W., et al. (2005), An improved Kalman Smoother for atmospheric inversions, Atmos. Chem. Phys., 5, 2691–2702.

Campioli, M., Gielen, B., Göckede, M., et al. (2011) Temporal variability of the NPP-GPP ratio at seasonal and interannual time scales in a temperate beech forest, Biogeosciences, 8, 2481-2492.

Chapin, F. S., Matson, P. A., Vitousek, P., (2002) Principles of ecosystem ecology. New York: Springer-Verlag.

Chevallier, F., Fisher, M., Peylin, P., et al. (2005) Inferring CO_2 sources and sinks from satellite observations: Method and application to TOVS data, J. Geophys. Res., 110, D24309.

Chiesi M, Maselli F, Moriondo M, Fibbi L, Bindi M, Running SW (2007) Application of BIOME-BGC to simulate Mediterranean forest processes. Ecol. Model. 206, 179-190.

Chiesi M, Chirici G, Barbati A, Salvati R, Maselli F (2011) Use of BIOME-BGG to simulate Mediterranean forest carbon stocks. iForest 4, 121-127.

Ciais, P., Tans, P.P., Trolier, M., et al. (1995), A large northern hemisphere terrestrial CO_2 sink indicated by the $^{13}C/^{12}C$ ratio of atmospheric CO_2, Science, 269, 1098-1102, 1995.

Ciais, P., Sabine, C., Bala, G., et al. (2013), Carbon and Other Biogeochemical Cycles. In: Climate Change 2013: The Physical Science Basis. Contribution of Working Group I to the Fifth Assessment Report of the Intergovernmental Panel on Climate Change (Stocker, T.F., D. Qin, G.-K. Plattner, M. Tignor, S.K. Allen, J. Boschung, A. Nauels, Y. Xia, V. Bex and P.M. Midgley (eds.)). Cambridge University Press, Cambridge, United Kingdom and New York, NY, USA.

Cox PM, (2001) Description of the "TRIFFID" dynamic global vegetation model. Hadley centre technical note 24 Met Office Hadley Centre Technical Notes.

Cramer, W., Kicklighter, D.W., Bondeau, A., et al. (1999), Comparing global models of terrestrial net primary productivity (NPP): overview and key results. Global Change Biol., 5: 1–15.

Cramer, W., Bondeau, A., Woodward, F. I., et al. (2001), Global response of terrestrial

ecosystem structure and function to CO2 and climate change: results from six dynamic global vegetation models. Global Change Biol., 7: 357–373.

Cristianini, N., and J. Shawe-Taylor (2000), An introduction to Support Vector Machines and other kernel-based learning methods. Cambridge University Press 189 pp.

Davidson, E.A., Savage, K., Bolstad, P., et al. (2002) Belowground carbon allocation in forests estimated from litterfall and IRGA based soil respiration measurements, Agric. For. Met., 113, 39–51.

Detling, J. K., Parton, W. J., Hunt H. W. (1997), An empirical model for estimating CO_2 exchange of Bouteloua gracilis (H.B.K.) Lag. in the shortgrass prairie. Oecologia, 33, 137-147.

Enquist, B.J., Niklas, K.J. (2001) Invariant scaling relations across tree-dominated communities. Nature, 410, 655–660.

Farquhar, G.D., Von Caemmerer, S., Berry, J.A. (1980) A biochemical model of photosynthetic CO_2 assimilation in leaves of C3 species, Planta, 149, 79–90.

Foley, J.A., Botta, A., Coe, M.T., Costa, M.H. (2002) El Niño–Southern oscillation and the climate, ecosystems and rivers of Amazonia, Global Biogeochem. Cy., 16, 1132.

Friedlingstein, P., Joel, G., Field, C.B., Fung, I.Y. (1999) Toward an allocation scheme for global terrestrial carbon models. Global Change Biol., 5, 755–770.

Friedlingstein P, Cox P, Betts R, et al. (2006) Climate-carbon cycle feedback analysis: results from the C4MIP model intercomparison. J Climate 19:3337–3353.

Frouin, R., Franz, B. A., Werdell P. J. (2003), The SeaWiFS PAR product. p. 46–50. In Algorithm Updates for the Fourth SeaWiFS Data Reprocessing, ed. by S. B. Hooker and E. R. Firestone, NASA/TM-2003-206892, 22.

Frouin, R. and H. Murakami (2007), Estimating photosynthetically available radiation at the ocean surface from ADEOS-II Global Imager data. J. Oceanogr., 63, 493–503.

Giardina, C.P., Ryan, M.G., Binkley, D. Fownes, J.H. (2003) Primary production and carbon allocation in relation to nutrient supply in a tropical experimental forest, Global Change Biol., 9, 1438–1450.

Gloor, M., Gatti L., Brienen R., et al. (2012), The carbon balance of South America: a review of the status, decadal trends and main determinants, Biogeosciences, 9, 5407-5430.

Gough, C.M., Vogel, C.S., Schmid, H.P., et al. (2008) Multi-year convergence of biometric and meteorological estimates of forest carbon storage, Agr. For. Meteorol., 148, 158–170.

Gower, S.T., Vogt, K.A., Grier, C.C. (1992) Carbon dynamics of Rocky Mountain Douglas-fir: influence of water and nutrient availability, Ecol. Monogr., 62, 43–65.

Guerlet S., Basu S., Butz A., et al. (2013), Reduced carbon uptake during the 2010 Northern Hemisphere summer from GOSAT, Geophys. Res. Lett., 40, 2378–2383.

Gurney, K. R., Law, M. L., Denning, A. S., et al. (2004), Transcom 3 inversion intercomparison: Model mean results for the estimation of seasonal carbon sources and sinks, Global Biogeochem. Cycles, 18, GB1010.

Harazono, Y., Chikamoto, K., Kikkawa, S., et al. (2009), Applications of MODIS visible bands index, greenery ratio to estimate CO_2 budget of a rice paddy in Japan, J. Agric. Meteorol., 65, 365–374.

Harris, I., Jones, P. D., Osborn, T. J., Lister, D. H. (2014) Updated high-resolution grids of monthly climatic observations - the CRUTS3.10 dataset, Int. J. Climat., 34: 623–642.

Haynes, B.E., Gower, S.T. (1995) Belowground carbon allocation in unfertilized and fertilized red pine plantations in northern Wisconsin, Tree Physiol., 15, 317–325.

Hirata R, Hirano T, Saigusa N, Fujinuma Y, Inukai K, Kitamori Y, Takahashi Y, Yamamoto S (2007) Seasonal and interannual variations in carbon dioxide exchange of a temperate larch forest. Agric For Meteorol 147:110-124

Hirata R, Saigusa N, Yamamoto S, Ohtani Y, Ide R, Asanuma J, Gamo M, Hirano T, Kondo H,

Kosugi Y, Li SG, Nakai Y, Takagi K, Tani M, Wang H (2008) Spatial distribution of carbon balance in forest ecosystems across East Asia. Agric For Meteorol 148:761-775.

Houghton, J.T., Ding, Y., Griggs, D.J., et al. Eds., (2001) Climate Change 2001: The Scientific Basis. Cambridge University Press, 944 pp.

Huete, A. R., Didan, K., Miura, T., et al. (2002), Overview of the radiometric and biophysical performance of the MODIS vegetation indices. Remote Sens. Environ., 83, 195−213.

Huntington, T.G. (2006) Evidence for intensification of the global water cycle: review and synthesis, J. Hydrol., 319, 83–95.

Huntzinger, D.N., Post, W. M., Wei, Y., et al. (2012) North American Carbon Program (NACP) regional interim synthesis: Terrestrial biospheric model intercomparison. Ecol. Model., 232, 144-157.

Hurtt, G. C., Chini, L. P., Frolking, S., et al. (2011), Harmonization of land-use scenarios for the period 1500-2100: 600 years of global gridded annual land-use transitions, wood harvest, and resulting secondary lands. Climatic Change, 109, 117−161.

Ichii, K., Kondo, M., Lee, Y. H., et al. (2013) Site-level model-data synthesis of terrestrial carbon fluxes in the CarboEastAsia eddy-covariance observation network: Toward future modeling efforts, J. For. Res., 18, 13-20.

Ichii K, Suzuki T, Kato T, et al. (2010) Multi-model analysis of terrestrial carbon cycles in Japan: Limitations and implications of model calibration using eddy flux observations. Biogeosciences 7, 2061-2080.

IPCC (2007) The Physical Science Basis: Summary for Policymakers. Intergovernment, Panel on Climate Change Secretariat, Geneva.

IPCC (2013) Climate Change 2013: The Physical Science Basis. Contribution of Working Group I to the Fifth Assessment Report of the Intergovernmental Panel on Climate Change [Stocker, T.F., D. Qin, G.-K. Plattner, M. Tignor, S.K. Allen, J. Boschung, A.

Nauels, Y. Xia, V. Bex and P.M. Midgley (eds.)]. Cambridge University Press, Cambridge, United Kingdom and New York, NY, USA, 1535 pp.

Ise T, Litton CM, Giardina CP, Ito A (2010) Comparison of modeling approaches for carbon partitioning: Impact on estimates of global net primary production and equilibrium biomass of woody vegetation from MODIS GPP. J Geophys Res 115 G04025.

Ito A, Saigusa N, Murayama D, Yamamoto S (2005) Modeling of gross and net carbon dioxide exchange over a cool-temperate deciduous broad-leaved forest in Japan: Analysis of seasonal and interannual change. Agric For Meteorol 134:122-134

Ito A. (2008) The regional carbon budget of East Asia simulated with a terrestrial ecosystem model and validated using AsiaFlux data. Agric For Meteorol 148 (5) 738-747.

Ito, A. (2010), Changing ecophysiological processes and carbon budget in East Asian ecosystems under near-future changes in climate: implications for long-term monitoring from a process-based model. J. Plant Res., 123, 577−588.

Ito A, Ichii K, Kato T (2010) Spatial and temporal patterns of soil respiration over the Japanese Archipelago: A model intercomparison study. Eco Res 25:1033-1044

Jackson, R.B., Mooney, H.A., Schulze, E.-D. (1997) A global budget for fine root biomass, surface area, and nutrient contents, Proc. Nat. Acad. Sci., 94, 7362–7366.

Japan Meteorological Agency (JMA), (2011), Climate Change Monitoring Report 2010, 1-3-4 Otemachi, Chiyoda-ku, Tokyo 100-8122, Japan, http://www.jma.go.jp/jma/en/NMHS/indexe_ccmr.html.

Japan Meteorological Agency (JMA), (2012), Climate Change Monitoring Report 2011, 1-3-4 Otemachi, Chiyoda-ku, Tokyo 100-8122, Japan, http://www.jma.go.jp/jma/en/NMHS/indexe_ccmr.html.

Janssens, I. A. Dieleman, W., Luyssaert, S., et al. (2010) Reduction of forest soil respiration in response to nitrogen deposition, Nature Geoscience, 3, 315-322.

Jarvis, P.G. (1976) The interpretation of the variations in water potential and stomata conductance found in canopies in the field, Philos. T. R. Soc. B., 273, 593-610.

Joos F., Prentice I. C., Sitch S., et al. (2001), Global warming feedbacks on terrestrial carbon uptake under the Intergovernmental Panel on Climate Change (IPCC) Emission Scenarios, Global Biogeochem. Cycles 15(4), 891–907.

Jung, M., et al. (2007), Uncertainties of modeling gross primary productivity over Europe: A systematic study on the effects of using different drivers and terrestrial biosphere models, Global Biogeochem. Cycles, 21, GB4021.

Jia, S., Akiyama, T. (2005) A precise, unified method for estimating carbon storage in cool-temperate deciduous forest ecosystems, Agric. For. Met., 134, 70-80.

Jiang, F., Wang, H. W., Chen, J. M., et al. (2013) Nested atmospheric inversion for the terrestrial carbon sources and sinks in China, Biogeosciences, 10, 5311-5324.

Jung, M., Reichstein, M., and Bondeau, A., (2009), Towards global empirical upscaling of FLUXNET eddy covariance observations: validation of a model tree ensemble approach using a biosphere model, Biogeosciences, 6, 2001-2013.

Jung, M., Reichstein, M., Margolis, H. A., et al. (2011), Global patterns of land-atmosphere fluxes of carbon dioxide, latent heat, and sensible heat derived from eddy covariance, satellite, and meteorological observations, J. Geophys. Res., 116, 0148-0227.

Kalnay, E., Kanamitsu, M., Kistler, R., et al. (19969 The NCEP/NCAR 40-year reanalysis project, B. Am. Meteorol. Soc.,77, 437–471.

Kawamura, K., Hashimoto, Y., Sakai, T., Akiyama, T. (2001) Effects of phenological changes of canopy leaf on the spatial and seasonal variations of understory light environment in a cool-temperate deciduous broadleaved forest (in Japanese with English summary), J. Jpn. For. Soc., 83, 231–237.

Keenan, T. F., Carbone, M. S., Reichstein, M., Richardson, A. D. (2011) The model–data fusion

pitfall: assuming certainty in an uncertain world. Oecologia, 167, 587–597.

Keenan, T.F., Davidson E., Moffat A.M., et al. (2012) Using model-data fusion to interpret past trends, and quantify uncertainties in future projections, of terrestrial ecosystem carbon cycling. Global Change Biol., 18: 2555–2569.

Kindermann, G. E., McCallum, I., Fritz, S., et al. (2008), A global forest growing stock, biomass and carbon map based on FAO statistics, Silva Fennica, 42, 387–396.

Kondo, M., Ichii, K., Ueyama, M., et al. (2013) The role of carbon flux and biometric observations in constraining a terrestrial ecosystem model: a case study in disturbed forests in East Asia, Eco. Res., 28, 5, 893-905.

Krinner, G., Viovy, N., de Noblet-Ducoudre, et al. (2005) A dynamic global vegetation model for studies of the coupled atmosphere-biosphere system, Global Biogeochem. Cy., 19, GB1015.

Kuze, A., Suto, H., Shiomi, K., et al. (2012), Level 1 algorithms for TANSO on GOSAT: processing and on-orbit calibrations. Atmos. Meas. Tech., 5, 2447-2467.

Law, B. E., Thornton, P. E., Irvine, J., et al. (2001) Carbon storage and fluxes in ponderosa pine forests at different developmental stages. Global Change Biol 7:755–777.

Law, R. M., Rayner, P. J., Denning, A. S., (1996), Variations in modelled atmospheric transport of carbon dioxide and the consequences for CO_2 inversions, Global Biogeochem. Cy., 10, 783-796.

Le Quéré C., Raupach, M. R., Canadell, J. G., et al. (2009), Trends in the sources and sinks of carbon dioxide. Nature Geosci., 2, 831-836.

Lee, K.H., Jose, S. (2003) Soil respiration, fine root production, and microbial biomass in cottonwood and loblolly pine plantations along a nitrogen fertilization gradient, Forest Ecol. Manag., 185, 263-273.

Leuschner, C., Moser, G., Bertsch, C., et al. (2007) Large altitudinal increase in the tree

root/shoot ratio in tropical mountain forests of Ecuador, Basic Appl. Ecol., 8, 219–230.

Levenberg, K. (1944). A Method for the Solution of Certain Non-Linear Problems in Least Squares, Q. Appl. Math., 2, 164–168.

Li, W., Zhang, P., Ye, J., et al. (2011) Impact of two different types of El Nino events on the Amazon climate and ecosystem productivity, J. Plant Ecol., 4, 91-99.

Lieth, H. (1975) Modeling the primary productivity of the world. In: Primary productivity of the biosphere. (eds Lieth H, Whittaker RH) pp 237–263., Springer-Verlag.

Litton, C.M., Raich, J.W., Ryan, M.G. (2007) Carbon allocation in forest ecosystems, Global Change Biol., 13, 2089-2109.

Lloyd, J., Taylor, J.A. (1994) On the temperature dependence of soil respiration, Funct. Ecol., **8**, 315–323.

Luyssaert, S., Inglima, I., Jung ,M., et al. (2007), CO_2 balance of boreal, temperate, and tropical forests derived from a global database. Global Change Biol., 13, 2509–2537.

Luyssaert, S., Ciais, P., Piao, S. L., et al. (2010), The European carbon balance. Part 3: forests. Global Change Biol., 16, 1429–1450.

Maksyutov, S., Patra, P. K., Onishi, R., et al. (2008), NIES/FRCGC global atmospheric tracer transport model: description, validation, and surface sources and sinks inversion, J. Earth Simulator, 9, 3–18.

Maksyutov, S., Takagi, H., Valsala V. K., et al. (2013), Regional CO_2 flux estimates for 2009–2010 based on GOSAT and ground-based CO_2 observations, Atmos. Chem. Phys., 13, 9351-9373.

Maier, C.A., Kress, L.W. (2000) Soil CO_2 evolution and root respiration in 11 year-old loblolly pine (Pinustaeda) plantations as affected by moisture and nutrient availability, Can. J. For. Res., 30, 347-359.

Min, S.-K., Zhang, X., Zwiers, F.W., and Hegerl, C. (2010) Human contribution to

more-intense precipitation extremes, Nature, 470, 378–81.

Malhi, Y., Doughty, C., and Galbraith, D. (2011) The allocation of ecosystem net primary productivity in tropical forests, Philos. T. R. Soc. B., 366, 3225-3245.

Mitchell S, Beven K, Freer J (2009) Multiple sources of predictive uncertainty in modeled estimates of net ecosystem CO_2 exchange. Ecol Model 220:3259-3270

Mitchell SR, Beven KJ, Freer JE, Law BE (2011) Processes influencing model-data mismatch in drought-stressed, fire-disturbed eddy flux sites. J Geophys Res 116 G02008.

Mitchell TD, Jones PD (2005) An improved method of constructing a database of monthly climate observations and associated high-resolution grids. Int J Climatol 25:693-712

Mizoguchi Y, Ohtani Y, Takanashi S, Iwata H, Yasuda Y, Nakai Y (2011) Seasonal and interannual variation in net ecosystem production of an evergreen needleleaf forest in Japan. J For Res 17:283-295.

Mo, W., Lee, M.-S., Uchida, M., et al. (2005) Seasonal and annual variations in soil respiration in a cool-temperate deciduous broad-leaved forest in Japan, Agric. For. Met., 134, 81-94.

Morgenstern, K., Black, T.A., Humphreys, E.R., et al. (2004) Sensitivity and uncertainty of the carbon balance of a Pacific Northwest Douglas-fir forest during an El Nino/La Nina cycle, Agric. For. Met., 123, 201-219.

Muraoka, H., Koizumi, H. (2005) Photosynthetic and structural characteristics of canopy and shrub trees in a cool-temperate deciduous broadleaved forest: implication to the ecosystem carbon gain, Agric. For. Meteorol., 134, 39–59.

Myneni, R. B., Hoffman, S., Knyazikhin, Y., et al. (2002), Global products of vegetation leaf area and fraction absorbed PAR from year one of MODIS data. Remote Sens. Environ., 83, 214-231.

Nasahara, K. N., Muraoka, H., Nagai, S., Mikami, H. (2008) Vertical integration of leaf area index in a Japanese deciduous broad-leaved forest, Agric. For. Met., 148, 1136-1146.

Nakatsuka, Y. and Maksyutov, S., (2009), Optimization of the seasonal cycles of simulated CO_2 flux by fitting simulated atmospheric CO_2 to observed vertical profiles, Biogeosciences, 6, 2733–2741.

Nemani, R.R., Keeling, C.D., Hashimoto, H., et al. (2003) Climate-driven increases in global terrestrial net primary production from 1982 to 1999, Science, 300, 1560-1563.

Noormets, A., Chen, J., and Crow. T. (2007) Age-Dependent Changes in Ecosystem Carbon Fluxes in Managed Forests in Northern Wisconsin, USA. Ecosystems, 10, 187-203.

Oda, T., and Maksyutov S. (2011), A very high-resolution (1 km × 1 km) global fossil fuel CO_2 emission inventory derived using a point source database and satellite observations of nighttime lights. Atmos. Chem. Phys., 11, 543−556.

Ohtsuka, T., Akiyama, T., Hashimoto, Y., et al. (2005) Biometric based estimates of net primary production (NPP) in a cool-temperate deciduous forest stand beneath a flux tower, Agric. For. Met., 134, 27-38.

Ohtsuka, T., Mo, W., Satomura, T. et al. (2007) Biometric based carbon flux measurements and net ecosystem production (NEP) in a temperate deciduous broad-leaved forest beneath a flux tower, Ecosystems, 10, 324-334.

Ohtsuka, T., Saigusa, N., Koizumi, H. (2009) On linking multiyear biometric measurements of tree growth with eddy covariance-based net ecosystem production, Global Change Biol., 15, 1015-1024.

Olson, R. J., Johnson, K. R., Zheng, D. L., et al. (2001), Global and Regional Ecosystem Modeling: Databases of Model Drivers and Validation Measurements, Oak Ridge National Laboratory.

Onogi, K., Tsutsui, J., Koide, H, et al. (2007), The JRA-25 Reanalysis, J. Meteorol. Soc. Jap., 85, 369–432, 2007.

Pan, Y.D., J.M. Melillo, A.D. McGuire, et al. (1998) Modeled responses of terrestrial

ecosystems to elevated atmospheric CO_2: A comparison of simulations by the biogeochemistry models of the Vegetation/Ecosystem Modeling and Analysis Project (VEMAP). Oecologia 114:389-404.

Papale, D. and Valentini, R. (2003), A new assessment of European forests carbon exchanges by eddy fluxes and artificial neural network spatialization. Global Change Biol., 9, 525–535.

Patra, P. K., Maksyutov, S., and Nakazawa, T., (2005), Analysis of atmospheric CO_2 growth rates at Mauna Loa using inverse model derived CO_2 fluxes, Tellus B, 57, 357–365.

Patra, P. K., Canadell, J. G., Houghton, R. A., et al. (2013), The carbon budget of South Asia, Biogeosciences, 10, 513-527.

Peters, W., Jacobson, A. R., Sweeney, C., et al. (2007), An atmospheric perspective on North American carbon dioxide exchange: CarbonTracker, Proc. Natl. Acad. Sci. USA, 104, 18925–18930.

Peylin, P., Law, R. M., Gurney, K. R., et al. (2013), Global atmospheric carbon budget: Results from an ensemble of atmospheric CO_2 inversions. Biogeosciences, 10, 6699-6720.

Piao, S. L., Ito, A., Li, S. G., et al. (2012), The carbon budget of terrestrial ecosystems in East Asia over the last two decades. Biogeosciences, 9, 3571-3586.

Piao, S., Sitch, S., Ciais, P., et al. (2013), Evaluation of terrestrial carbon cycle models for their response to climate variability and to CO_2 trends. Global Change Biol., 19, 2117–2132.

Pietsch SA, Hasenauer H, Thornton PE (2005) BGC-model parameters for tree species growing in central European forests. Forest Ecol Manag 211:264-295.

Raich, J.W., Russell, A.E., Kitayama, K., et al. (2006) Temperature influences carbon accumulation in moist tropical forests, Ecology, 87, 76–87.

Raupach, M.R., Rayner, P.J., Barrett, D.J., et al. (2005), Model–data synthesis in terrestrial carbon observation: methods, data requirements and data uncertainty specifications.

Global Change Biol., 11: 378–397.

Ray, D. K., and Foley, J. A. (2013), Increasing global crop harvest frequency: recent trends and future directions, Environ. Res. Lett., 8, 044041.

Richardson, A.D., Williams, M., Hollinger, D.Y., et al. (2010) Estimating parameters of a forest ecosystem C model with measurements of stocks and fluxes as joint constraints. Oecologia, 164, 25–40.

Roderstein, M., Hertel, D., Leuschner, C. (2005) Above- and below-ground litter production in three tropical montane forests in southern Ecuador, J. Trop. Ecol., 21, 483–492.

Ryan, M.G., Binkley, D., Fownes, J.H., et al. (2004) An experimental test of the causes of forest growth decline with stand age, Ecological Monogr., 74, 393–414.

Saigusa, N., Yamamoto, S., Murayama, S., et al. (2002) Gross primary production and net ecosystem production of a cool-temperate deciduous forest estimated by the eddy covariance method, Agric. For. Met., 112, 203-215.

Saigusa, N. Yamamoto, S. Murayama, S., Kondo, H. (2005) Inter-annual variability of carbon budget components in an AsiaFlux forest site estimated by long-term flux measurements, Agric. For. Met., 134, 4-16.

Saigusa, N., Ichii, K., Murakami, H., et al. (2010) Impact of meteorological anomalies in the 2003 summer on Gross Primary Productivity in East Asia, Biogeosciences, 7, 641-655.

Saito, M., Maksyutov, S., Hirata, R., et al. (2009), An empirical model simulating diurnal and seasonal CO_2 flux for diverse vegetation types and climate conditions, Biogeosciences, 6, 585-599.

Santaren D, Peylin P, Viovy N, Ciais P (2007) Optimizing a process-based ecosystem model with eddy-covariance flux measurements: A pine forest in southern France. Global Biogeochem Cycles, 21, GB2013.

Sato, H., Ito, A., Kohyama, T. (2007), SEIB-DGVM: A new dynamic global vegetation model

using a spatially explicit individual based approach. Ecol. Model., 200, 279–307.

Satomura, T., Hashimoto, Y., Koizumi, H., et al. (2006) Seasonal patterns of fine root demography in a cool-temperate deciduous forest in central Japan, Eco. Res., 21, 741-753.

Schaaf, C. B., Gao, F., Strahler, A. H., et al. (2002), First operational BRDF, albedo and nadir reflectance products from MODIS, Remote Sens. Environ., 83, 135–148.

Schimel, D., Melillo, J., Tian, H., et al. (2000) Contribution of increasing CO2 and climate to carbon storage by ecosystems of the United States. Science, 287, 2004-2006.

Scurlock, J. M. O., Cramer, W., Olson, R. J., et al. (1999), Terrestrial NPP: toward a consistent data set for global model evaluation, Ecol. Appl., 9, 913–919.

Schwalm, C. R., Williams, C. A., Schaefer, K., et al. (2010) A model-data intercomparison of CO_2 exchange across North America: Results from the North American Carbon Program site synthesis. J. Geophys. Res., 115, G00H05.

Sitch, S., Smith, B., Prentice, I. C., et al. (2003) Evaluation of ecosystem dynamics, plant geography and terrestrial carbon cycling in the LPJ Dynamic Vegetation Model. Global. Change Biol., 9, 161–185.

Sitch, S., Huntingford, C., Gedney N., et al. (2008), Evaluation of the terrestrial carbon cycle, future plant geography and climate-carbon cycle feedbacks using five Dynamic Global Vegetation Models (DGVMs), Global Change Biol., 14: 2015–2039.

Takagi, H., Saeki, T., Oda, T., et al. (2011), On the Benefit of GOSAT Observations to the Estimation of Regional CO_2 Fluxes, Sola, 7, 161-164.

Takagi, H., Houweling, S., Andres, R. J., et al. (2014), Influence of differences in current GOSAT X_{CO2} retrievals on surface flux estimation, Geophys. Res. Lett., 41, 2598–2605.

Taguchi, S. (1996), A three-dimensional model of atmospheric CO_2 transport based on analyzed winds: Model description and simulation results for TRANSCOM. J. Geophys. Res., 101, 15099–15109.

Takahashi, T., Sutherland, S. C., and Kozyr, A., (2011), Global Ocean Surface Water Partial Pressure of CO_2 Database: Measurements Performed During 1957–2010 (Version 2010), ORNL/CDIAC-159, NDP-088(V2010), Carbon Dioxide Information Analysis Center, Oak Ridge National Laboratory, US Department of Energy, Oak Ridge, Tennessee.

Tanabe H, Nakano T, Mimura M, Abe Y, Mariko S (2003) Biomass and net primary production of a Pinus densiflora forest established on a lava flow of Mt.Fuji. central Japan. J. For. Res., 8, 247-252.

Tans, P. P., Conway, T. J. and Nakazawa, T., (1989), Latitudinal distribution of the sources and sinks of atmospheric carbon dioxide derived from surface observations and an atmospheric transport model, J. Geophys. Res., 94, 5151-5172.

Tatarinov FA, Cienciala E (2006) Application of BIOME-BGC model to managed forests. 1. Sensitivity analysis. Forest Ecol Manag **237**:267–379

Thornton, P.E., Law, B.E., Gholz, H.L., et al. (2002) Modeling and measuring the effects of disturbance history and climate on carbon and water budgets in evergreen needleleaf forests, Agric. For. Met., 113, 185-222.

Ueyama M, Ichii K, Hirata R, Takagi K, Asanuma J, Machimura T, Nakai Y, Ohta T, Saigusa N, Takahashi Y, Hirano T (2010) Simulating carbon and water cycles of larch forests in East Asia by the Biome-BGC model with AsiaFlux data. Biogeosciences 7:959-977

Ueyama M, Kai A, Ichii K, Hamotani K, Kosugi Y, Monji N (2011) The sensitivity of carbon sequestration to harvesting and climate conditions in a temperate cypress forest. Ecol Model 222:3216-3225

Ueyama M, Hirata R, Mano M, Hamotani K, Harazono Y, Hirano T, Miyata A, Takagi K, Takahashi Y (2012) Influences of various calculation options on heat, water and carbon fluxes determined by open- and closed-path eddy covariance methods. Tellus B 64 19048

Ueyama M., Ichii, K., Iwata, H., et al. (2013), Upscaling terrestrial carbon dioxide fluxes in Alaska with satellite remote sensing and support vector regression. in press, J. Geophys. Res.,.

Unger, M., Homeier, J., Leuschner, C. (2012) Effects of soil chemistry on tropical forest biomass and productivity at different elevations in the equatorial Andes, Oecologia, 170, 263–274.

Vaganov, E.A., Hughes, M.K., Kirdyanov, A.V., et al. (1999) Influence of snowfall and melt timing on tree growth in subarctic Eurasia, Nature, 400, 149–151.

Valentini, R., Arneth, A., Bombelli, A., et al. (2014), A full greenhouse gases budget of Africa: synthesis, uncertainties, and vulnerabilities, Biogeosciences, 11, 381-407.

Valsala, V., and Maksyutov, S. (2010), Simulation and assimilation of global ocean pCO_2 and air-sea CO_2 fluxes using ship observations of surface ocean pCO_2 in a simplified biogeochemical offline model. Tellus, 62B, 821−840.

van der Werf, G. R., Randerson, J. T., Giglio, L., et al. (2010), Global fire emissions and the contribution of deforestation, savanna, forest, agricultural, and peat fires (1997−2009). Atmos. Chem. Phys., 10, 11707−11735.

Wan, Z., Zhang, Y., Zhang, Q., et al. (2002), Validation of the land-surface temperature products retrieved from Terra Moderate Resolution Imaging Spectroradiometer data. Remote Sens. Environ., 83, 163−180.

Wang H. M., Saigusa N., Zu Y. G., et al. (2008) Carbon fluxes and their response to environmental variables in a Dahurian larch forest ecosystem in northeast China. J. For.

Res., 19, 1-10.

Wang W, Zu Y, Wang H, Matsuura Y, Sasa K, Koike T (2005) Plant biomass and productivity of Larix gmelinii forest ecosystems in Northern China: Intra- and Inter- species comparison. Eurasian Journal of Forest Research 8:21-41

Wang W, Dungan J, Hashimoto H, Michaelis AR, Milesi C, Ichii K, Nemani RR (2011) Diagnosing and assessing uncertainties of terrestrial ecosystem models in a multi-model ensemble experiment: 1. Primary production. Global Change Biol 17:1367-1378

Wang W, Dungan J, Hashimoto H, Michaelis AR, Milesi C, Ichii K, Nemani RR (2011) Diagnosing and assessing uncertainties of terrestrial ecosystem models in a multi-model ensemble experiment: 2 Carbon balance. Global Change Biol 17:1350-1366

Wang, Y. P., Trudinger, C. M., Enting, I. G. (2009) A review of applications of model–data fusion to studies of terrestrial carbon fluxes at different scales, Agric. For. Meteorol., 149, 1829-1842.

White, M.A., Thornton, P.E., Running, S.W., Nemani, R.R. (2000) Parameterization and sensitivity analysis of the BIOME-BGC terrestrial ecosystem process model: net primary production controls, Earth Interact, 4, 1–85.

Williams M, Schwarz PA, Law BE, Irvine J, Kurpius MR (2005) An improved analysis of forest carbon dynamics using data assimilation. Global Change Biol 11:89–105

Xiao, J., Zhuang, Q., Baldocchi, D. D., et al. (2008), Estimation of net ecosystem carbon exchange for the conterminous United States by combining MODIS and AmeriFlux data, Agric. For. Meteorol., 148, 1827-1847.

Yang, F., White, M. A., Michaelis, A. R., et al. (2006), Prediction of continental-scale evapotranspiration by combining MODIS and AmeriFlux data through support vector

machine, IEEE Trans. Geosci. Remote Sens. 44, 11, 3452-3461

Yang, F., Ichii, K., White, M. A., et al. (2007), Developing a continental-scale measure of gross primary production by combining MODIS and AmeriFlux data through Support Vector Machine approach, Remote Sens. Environ., 110, 109-122.

Yang, F., Zhu, A.-X., Ichii, K., et al. (2008), Assessing the representativeness of the AmeriFlux network using MODIS and GOES data, J. Geophys. Res., 113, G04036.

Yokota, T., Aoki, T., Eguchi, N., et al. (2008), Data retrieval algorithms of the SWIR bands of the TANSO-FTS sensor aboard GOSAT, J. Remote Sens. Soc. Jpn. , 28, 152– 160.

Yone Y, Oguma H, Yamagata Y, Fujinuma Y (2005) Development of measurement system for evaluating forest Ecosystems -Measurement method of over-ground biomass growth by using airborne laser survey. Phyton 45:517-524.

Zach, A., Horna, V., Leuschner, C., and Zimmermann, R. (2010) Patterns of wood carbon dioxide efflux across an 2,000-m elevation transect in an Andean moist forest, Oecologia 162:127-137.

Zaks, D. P. M., Ramankutty, N., Barford, C. C., Foley, J. A. (2007) From Miami to Madison: Investigating the relationship between climate and terrestrial net primary production. Global Biogeochem. Cy., 21, GB3004.

Zhang, Y., Rossow, W. B., Lacis, A. A., et al. (2004) Calculation of radiative fluxes from the surface to top of atmosphere based on ISCCP and other global data sets: refinements of the radiative transfer model and the input data, J. Geophys. Res., 109.

Acknowledgements

The author is grateful to Dr. Kazuhito Ichii of Japan Agency for Marine-Earth Science and Technology for providing valuable advices in modelling and analyses throughout years. The model-data integration analysis was initiated and supported by the Environment Research and Technology Development Funds (RFa-1007 and RFa-1201) of the Ministry of the Environment of Japan that were obtained by Dr. Ichii. The author is in debt to Dr. Takashi Hirano of Hokkaido University for helpful comments in finalizing this thesis.

Data used in the analyses are outcomes of efforts from scientists over the world. The authors acknowledge all members of the GOSAT project. The GOSAT project is a joint effort promoted by the Japan Aerospace Exploration Agency (JAXA), National Institute for Environmental Studies (NIES), and Ministry of the Environment (MOE), Japan. The PAR and radiation data used in this research were developed in a collaborative study between JAXA and NIES. This dataset is one of the JAXA Satellite Monitoring for Environmental Studies (JASMES) datasets derived from a cooperative research effort conducted by JAXA and NIES. The author acknowledges the FLUXNET community and the following networks in particular: AmeriFlux (U.S. Department of Energy, Biological and Environmental Research, Terrestrial Carbon Program (DE-FG02-04ER63917 and DE-FG02-04ER63911)), AfriFlux, AsiaFlux, CarboAfrica, CarboEuropeIP, CarboItaly, CarboMont, ChinaFlux, Fluxnet-Canada (supported by CFCAS, NSERC, BIOCAP, Environment Canada, and NRCan), GreenGrass, KoFlux, LBA, NECC, OzFlux, TCOS-Siberia, and USCCC. We acknowledge the financial support for the eddy covariance data harmonization provided by CarboEuropeIP, FAO-GTOS-TCO, iLEAPS, the Max Planck Institute for Biogeochemistry, National Science Foundation, University of Tuscia, Université Laval, Environment Canada, and U.S. Department of Energy. In addition, we are grateful for the database development and technical support from the Berkeley Water

Center, Lawrence Berkeley National Laboratory, Microsoft Research eScience, Oak Ridge National Laboratory, University of California - Berkeley, and University of Virginia. The author acknowledge Dr. Sebastiaan Luyssaert for graciously providing the global compilation of ecological site studies. The biome classification map used in this study was provided through courtesy of Dr. Paul Reich.

Publications

1. Kondo M., Ichii K., Takagi H., Sasakawa M., Comparison of the data-driven top-down and bottom-up global terrestrial exchanges: empirical eddy flux upscaling and GOSAT CO_2 inversion, Journal of Geophysical Research – Biogeosciences, 120, doi:10.1002/2014JG002866

2. Kondo M., Ichii K., Ueyama M. (2015) Impact of anomalous climates on carbon allocation to biomass production of leaves, woody components, and fine roots in a cool-temperate deciduous forest, Agricultural and Forest Meteorology, 201, 38-50.

3. Ichii K., Kondo M., Okabe Y., Ueyama M., Kobayashi H., Lee S.-J., Saigusa N., Zhu Z., Myneni R.B. (2013) Recent changes in terrestrial gross primary productivity in Asia from 1982 to 2011, Remote Sensing, 5, 6043-6062 (AVHRR 30yrs Special Issue).

4. Kondo M., Ichii K., Ueyama M., Hirata R., Mizoguchi Y., Saigusa N. (2013) Role of carbon flux and pool observations to constrain terrestrial ecosystem model: a case study in disturbed forests in East Asia. Ecological Research, 28, 893-905.

5. Ichii K., Kondo M., Lee Y. H., Wang S. Q., Kim J., Ueyama M., Lim H. J., Shi H., Suzuki T., Ito A., Kwon H., Ju W., Huang M., Sasai T., Asanuma J., Han S. J., Hirano T., Hirata R., Kato T., Li S. G., Li Y. N., Maeda T., Miyata A., Matsuura Y., Maruyama S., Nakai Y., Ohta T., Saitoh T. M., Saigusa N., Takagi K., Tang Y. H., Wang H. M., Yu G. R., Zhang Y. P., Zhao F. H. (2013) Site-level model-data synthesis of terrestrial carbon fluxes in the CarboEastAsia eddy-covariance observation network: Toward future modeling efforts. Journal of Forest

Research (CarboEastAsia special issue), 18, 13-20.